F. W. KLAIBER
T. L. THOMAS
D. Y. LEE
FEBRUARY 1979

FINAL REPORT

FATIGUE BEHAVIOR OF AIR-ENTRAINED CONCRETE: PHASE II

HR-197
ISU-ERI-AMES 79110
ERI Project 1324

In cooperation with the
Highway Division
Iowa Department of Transportation

ENGINEERING RESEARCH INSTITUTE
IOWA STATE UNIVERSITY
AMES, IOWA 50010 USA

The opinions, findings, and conclusions expressed in this publication are those of the authors and not necessarily those of the Highway Division of the Iowa Department of Transportation.

ENGINEERING RESEARCH

ENGINEERING RESEARCH
ENGINEERING RESEARCH
ENGINEERING RESEARCH
ENGINEERING RESEARCH

FINAL REPORT

FATIGUE BEHAVIOR OF AIR-ENTRAINED CONCRETE PHASE II

F. W. Klaiber
T. L. Thomas
D. Y. Lee

February 1979

Submitted to the
Highway Division,
Iowa Department of Transportation
HR-197

ISU-ERI-AMES 79110
ERI Project 1324

DEPARTMENT OF CIVIL ENGINEERING
ENGINEERING RESEARCH INSTITUTE
IOWA STATE UNIVERSITY AMES

TABLE OF CONTENTS

LIST OF FIGURES

LIST OF TABLES

1. INTRODUCTION

1.1. Fatigue of Concrete in Pavement

When a material fails under a number of repeated loads, each smaller than the ultimate static strength, a fatigue failure is said to have taken place. Many studies have been made to characterize the fatigue behavior of various engineering materials. The results of some of these studies have proved invaluable in the evaluation and prediction of the fatigue strength of structural materials. Considerable time and effort have gone into the evaluation of the fatigue behavior of metals. These early studies were motivated by practical considerations: the first fatigue tests were performed on materials that had been observed to fail after repeated loading of a magnitude less than that required for failure under the application of a single load. Mine-hoist chains (1829), railway axles (1852), and steam engine parts were among the first structural components to be recognized as exhibiting fatigue behavior.

Since concrete is usually subjected to static loading rather than cyclic loading, need for knowledge of the fatigue behavior of concrete has lagged behind that of metals. One notable exception to this, however, is in the area of highway and airfield pavement design. Due to the fact that the fatigue behavior of concrete must be understood in the design of pavements and reinforced concrete bridges, highway engineers have provided the motivation for concrete fatigue studies since the 1920s.

Results from fatigue studies are usually presented in the form of an S-N curve (stress versus log of the number of cycles to failure). If there is a break in the curve and the curve becomes asymptotic to a line

parallel to the horizontal axis, the stress at which this occurs is called the endurance or fatigue limit. Most metals have an endurance limit; however, tests on concrete up to 10 million cycles of load application have failed to establish an endurance limit [6].* It is therefore important to quote fatigue strength for a specified number of cycles when discussing the fatigue properties of concrete. Fatigue strength is defined as the stress causing failure after a stated number of cycles of loading. Fatigue life is the number of cycles of stress that a specimen can withstand without failure.

The fatigue of concrete is associated with the formation and propagation of microcracks at the aggregate-cement matrix interface and in the cement matrix itself [6,7,14,38,45]. The mechanism of fatigue fracture of concrete is essentially identical to the mechanism of fracture under static and sustained loading [7]. Fatigue fracture involves microcracking similar to, but more extensive than, the microcracking that accompanies static failure. For instance, Bennett [6] found that the total length of surface cracks visible on a concrete specimen subjected to 100,000 cycles of a stress equal to 75% of the static strength was typically 35% greater than the length measured after a single loading to 95% of the static strength.

Most research into the fatigue strength of concrete involves the repeated application of a constant stress until failure (constant stress fatigue).

Highway concrete slabs are subjected to many repetitions of traffic loads during their service lives; thus, the importance of fatigue in

*Numbers in brackets denote references, listed alphabetically in section 8.

concrete pavement is self-evident. Since the flexural stresses in concrete pavement slabs are critical, fatigue due to flexural stress is used for concrete pavement design. Fatigue tests in compression, although useful for many design applications, do not provide information useful to the designer of pavements. Loading schemes that subject concrete specimens to flexural loading more realistically duplicate conditions encountered in the field.

The first fatigue tests using concrete flexure specimens were carried out by Féret in 1906 [33]. These tests were part of a broader study that included plain and reinforced concrete, mortar beams and cubes and cylinders. Because of more recent and complete research, the findings and conclusions of this study are of historical value only. In 1907, Van Ornum [28] utilized reinforced concrete beams in a flexural fatigue study. The beams had 2 1/2 percent steel and were subjected to progressive loading. This investigation determined a fatigue limit of 50 percent of the modulus of rupture and showed that, as the applied loading increased above the fatigue limit, the number of repetitions of loading necessary to cause failure decreases rapidly.

The first investigations of significant consequence on flexural fatigue of concrete were carried out almost simultaneously by the Illinois Department of Highways (1921-23) and Purdue University (1922-24). The Illinois tests (reported by Clemmer [9] and Older [34,35]) and the Purdue tests (reported by Hatt [13]) served as a basis for the development of the 1933 Portland Cement Association (PCA) design curve for fatigue strength of concrete pavements.

The Illinois tests were undertaken after Illinois highway officials observed pavement failures in several cases occurring at loads below the static ultimate strength of the slab. Therefore, the laboratory study at the University of Illinois was devised to simulate the loading on the corner of a pavement slab, which is the most critical loading.

Clemmer designed a unique testing machine in which 6 in. × 6 in. × 36 in. concrete beams were cantilevered out from a central hub. Load was applied by rotating a pair of rubber-tired wheels about the central hub. Blocks were placed between the cantilevered beams to form a smooth circular track. Load applied by the wheels could be varied by placing dead weight in two weight boxes located on the axle between the two wheels. Test beams were subjected to 40 load applications per minute.

Four series of beams with different loading histories were tested in this investigation. In this study the following conclusions were made:

- The endurance limit for concrete in flexure is 51-54 percent of the static failure stress.
- The repeated application of a load less than 50 percent of the modulus of rupture increases the strength of the concrete at the stressed section.
- The number of cycles to failure increases with the richness of the mix and decreases rapidly with increases of stress above 50 percent of the modulus of rupture.

The fatigue tests of Hatt at Purdue were also motivated by the interest in highway pavement failures. Hatt felt the Illinois test's rate of loading was too fast and that without rest periods it did not duplicate actual highway conditions. The Purdue tests had complete reversals

of stress applied at 10 cycles per minute and the tests were shut down overnight and on weekends. The fatigue strength of fatigue specimens was compared to unfatigued companion modulus of rupture beams. From the Purdue study [33] the following conclusions were drawn:

- There is no definite fatigue limit for 28-day-old concrete; for concrete 4 months old the fatigue limit is 50-55 percent of the modulus of rupture; a fatigue limit of 54-55 percent of the modulus of rupture exists for concrete over 6 months old.
- There is a recovery in stiffness resulting from the overnight rest periods.
- Cycling test specimens below their endurance limit was found to strengthen the member.

The next significant study of the fatigue of plain concrete was reported by Kesler [18] in 1953. Since fatigue investigations are by nature time consuming, Kesler wanted to determine the effect of speed of testing on the flexural fatigue life of plain concrete. The specimens used were 64 inches long, supported on a span of 60 inches, and loaded at one-third points. Two different strengths of concrete (3600 psi, 4600 psi) were tested at rates of 70, 230, and 440 cycles per minute. The average S-N curves for all beams tested, regardless of strength or speed of testing, were very close together, indicating that for the range of 70 to 440 cpm the speed of testing has a negligible effect. This finding is important since time can be saved by conducting fatigue tests at higher speeds. Even though these tests were conducted to a maximum of 10 million cycles, there was no indication that an endurance limit exists.

During the period 1954-56 Kesler [31] conducted fatigue tests that studied the effect the range of stress had on fatigue life. Specimens, 6 in. × 6 in. × 64 in., supported on a span of 60 inches, and loaded at the one-third points, were also used in this study. Four series were tested with the ratio, R, of minimum applied stress to maximum applied stress varying from 0.13 to 0.75. The tests indicated that, as R increases, the value of the fatigue strength, at 10 million cycles, also increases from 56 percent of the modulus of rupture for R = 0.0 up to 85 percent of the modulus of rupture for R = 0.75. Again no fatigue limit was indicated.

In 1966 Hilsdorf and Kesler [15] conducted a much more comprehensive fatigue study. It was felt that previous studies with loads between constant minimum and maximum values and no rest periods did not represent actual loading conditions. The first phase of the Kesler investigation studied the effect a rest period had on fatigue life. Each specimen was loaded 4500 cycles and then rested for a period of 1, 5, 10, 20, or 27 minutes; during the rest period the minimum load was maintained. The rest period effect was more noticeable for specimens that required a greater number of cycles to failure. The fatigue strength increased as length of rest period increased up to 5 minutes; the differences were negligible for tests having rest periods of 5, 10, 20, or 27 minutes.

Kesler's second phase, which consisted of two parts, studied the effect of variable loading on the fatigue life of plain concrete. In part one, the maximum stress level was changed only once during the test. In part two, the maximum stress level was changed periodically between two stress levels. It was determined that the sequence of the applied loads

affects the fatigue strength of concrete. A relatively low number of cycles at high loads increased the fatigue strength of concrete that was subsequently loaded at a lower load as compared to the fatigue strength of a specimen that had not been previously loaded. This increase in fatigue life can be attributed to the fact that concrete exhibits two opposing effects when loaded: consolidation with consequent strengthening and microcracking with consequent weakening. The controlling effect will depend on the relative magnitude and method of application of the loads. As the load was changed periodically between two stress levels, it was found that the fatigue life decreased with increased higher stress and also with increased number of cycles at the higher stress.

A commonly used theory for cumulative damage of concrete structures under repeated loads, known as Miner's hypothesis [29], was checked and found to give unconservative values of fatigue strength at high loads and overly conservative values for low loads. A procedure was presented to adjust Miner's hypothesis so it could be safely used for design.

In 1972, Ballinger [5] conducted a two-phase fatigue study that was very similar to Kesler's 1966 investigation. One series of tests was conducted between set values of minimum and maximum stress. In the second series of tests, specimens were subjected to two different levels of cyclic loads; the level of load was changed just once during the test. Ballinger's tests indicate that the initial portion of the S-log N line is not straight but curves downward from 100% to intersect the linear portion. This low-cycle region exists up to about 70 cycles and it is felt that factors other than simple fatigue affect failure in this region.

Ballinger's other conclusions vary somewhat from those of Kesler. In Ballinger's opinion Miner's rule adequately reflects cumulative damage effects; also the order in which cyclic loads of different magnitudes are applied has no effect on the fatigue life.

In general, the information on fatigue of concrete is scarce. However, it has been suggested that the various factors that affect static strength of conrete may also affect fatigue in a similar manner; among these are aggregate type and quality, moisture condition, rate of loading, age of concrete at testing, type of loading, concrete strength, curing conditions, specimen size, and air entrainment [19,32,33,36].

In Kesler's fatigue study conducted in the early 1950s [18], specimens of two different compressive strengths (3600 and 4600 psi) were tested. At the end of the tests, the results were compared and it was shown that the fatigue lives of the specimens of different compressive strengths were not significantly different. Therefore Kesler concluded that the compressive strength, and thus the water-cement ratio, had no effect on the fatigue strength of plain concrete.

No information could be found on the effect of aggregate types on flexural fatigue of concrete.

1.2. Air-entrained Concrete in Pavement

The use of admixtures that cause the entrainment of air in concrete is considered by many to be one of the most important developments in concrete technology in the last few decades. The principal application has been to pavement concrete. Entrained air benefits concrete mainly in two ways: (1) improved resistance of the concrete to freezing and

thawing and (2) improvement of the workability and decrease in segregation of freshly mixed concrete. Air bubbles present in the cement paste of unhardened concrete can come from several sources [24]: (1) air originally present in intergranular spaces in the cement and aggregate, (2) air originally present within the particles of cement and aggregate but expelled from the particles before hardening of the concrete by inward movement of water under hydraulic and capillary potential, (3) air originally dissolved in the mixing water, and (4) air in-folded and mechanically enveloped within the concrete during mixing and placing. These are the only sources of air bubbles in concrete, whether or not an air-entraining agent is used [24]. An air-entraining agent makes use of the fourth method of supplying air bubbles to a plastic concrete mix. Air-entraining agents reduce the surface tension at air-water interfaces within the cement paste, which reduces the rate of dissolution of air in the bubbles and the tendency of bubbles to join together to form larger bubbles. Thus, air-entraining agents produce a uniform distribution of very small air bubbles within the cement paste matrix. It is this distribution of bubbles that accounts for the increased freeze-thaw durability as well as the decreased compressive and tensile strengths of air-entrained concrete. These and other effects of the air-void system in concrete have been well documented [24,25,26,27].

Today air-entrained concrete is recommended for all structures under conditions of severe exposure and for all pavements regardless of climatic conditions [16,22,40,44]. Depending on the maximum size of aggregate, the usual recommended entrained air content varies from 5% for a 2-in. aggregate to 8% for a 1/2-in. aggregate [41]. For pavement concrete the specified air content in Iowa is $6 \pm 1\frac{1}{2}\%$ [39].

In recent years, because of the greatly increased use of de-icing chemicals, it has been found necesary to incorporate higher levels of air in concrete to assure freedom from deterioration due to frost action (in certain instances, air content of 8 or 9% has been recommended for use in structures such as highway bridge decks). Furthermore, there is reason to suspect that, because of the contractor's concern for achieving the desired workability and meeting minimum air content requirements, the actual air content in field-placed concrete could, in some cases, be higher than recommended.

1.3. Fatigue Behavior of Air-entrained Concrete

The effects of air content on most concrete properties such as compressive strength, workability, durability, and creep are quite well understood. For example, it is known that, for normal levels of air content, if there is no change in water-cement ratio, the strength will be reduced by 3 to 5% for each percent air added. However, knowledge of the effect of air content on the flexural fatigue strength of plain concrete is nearly nonexistent. In view of recent nationwide interest in economical pavement design, data must be collected on the effects of all additives and variables on the fatigue strength of concrete.

A literature search of the past 70 years produced only two reported studies on the fatigue strength of air-entrained concrete. One of the studies was carried out in 1943 by Purdue University for the Kentucky Department of Highways [11]. It involved flexural fatigue testing of beam specimens in which one of the variables was air entrainment. The

fatigue life of the air-entrained concrete was slightly greater than non-air-entrained groups. This finding is only of limited interest, however, since the different groups that were compared contained different cements, and the variable of air content was not singled out for comparison. Also, the load histories of the test beams varied, making a comparison of fatigue lives difficult. In the second study, Antrim and McLaughlin [4] performed axial compression fatigue tests on two types of concrete, one air-entrained and the other containing only natural air. This study resulted in two major conclusions:

1. The fatigue behavior of non-air-entrained plain concrete and air-entrained plain concrete in compression are not significantly different. However, there is an indication that air-entrained concrete exhibits longer fatigue life at low stress ratios (less than about 77% of static compressive strength) and shorter fatigue life at higher stress levels.

2. There is considerably less variation present among fatigue test data for air-entrained plain concrete than there is for non-air-entrained concrete.

This study is of interest because an air-entrained concrete was included, although at only one air-content level. However, the failure of highway pavements is essentially a tensile failure, and this study involved loading of specimens in compression; thus, an assumption of the behavior of concrete pavement based on the results of this study would be a dangerous extrapolation of the findings.

1.4. Rigid Pavement Thickness Design

The factors that must be considered in the thickness design of concrete pavements are the effects of traffic, climate, subgrade conditions, and the properties of concrete [10,40]. Pavement designs have evolved

from analytical equations, laboratory research, road tests, field surveys of actual pavement performance, and development of semi-empirical equations.

The first concrete pavement in the United States was built in Bellefontaine, Ohio, in 1892. The pavement was built on the courthouse square and had a special grid pattern designed to provide safe footing for the horses that were expected to use the pavement.

The first mile of rural highway pavement in the United States, built primarily for automobiles, was constructed in Wayne County, Michigan, in 1909. To check their design, the Detroit Public Works Department conducted one of the first road tests. A twenty-foot pole fitted with a set of steel shoes on one end and a heavy iron-rimmed wheel mounted on the other was revolved around a circular track consisting of sections of brick, granite, creosote block, ceder block, and concrete. The report of this test stated, "the concrete section laid under the specifications of the commissioners of Wayne County, Michigan, showed by far the best resistance to the severe test to which pavements were put" [37].

In 1922 and 1923 the state of Illinois constructed the Bates Test Road [34] containing different materials and different designs to provide the Illinois Division of Highways with information on the best pavement type and design. In this test World War I army trucks were driven over the 63 test sections. Of the 22 brick, 17 asphalt, and 24 concrete sections tested, one brick, 3 asphalt, and 10 concrete sections satisfactorily withstood the imposed loads. Until 1922, most concrete pavements had been built with no joints and with a thickened center section in an attempt to stop the formation of longitudinal cracks which developed

in most of the 16-foot to 18-foot wide pavements of that time. Results of this test led highway officials to use a longitudinal center joint to eliminate cracking. Results were also used by Older to develop an equation relating pavement thickness to traffic loading based on the theory of cantilever beams.

In the mid 1920s, H. M. Westergaard [42,43] of the University of Illinois published several theoretical papers concerned with determination of stresses and deflections in concrete pavements. Three loading cases were considered: load applied in the interior of the slab, at the free edge, and at corners. Westergaard presented equations that related load, subgrade reaction, concrete thickness, and modulus of elasticity to the stresses in a concrete slab. Westergaard's equations were used by engineers for many years for pavement thickness design.

The Bureau of Public Roads conducted tests on concrete pavements at Arlington, Virginia, during the early 1930s. In these tests, measurements of stresses, deflections, and subgrade pressures were made to check the Westergaard equations. As a result of these tests, slight modifications were made by Westergaard, Kelly, Spangler, and Pickett on the original Westergaard equations to provide closer agreement with actual measurements [10].

By the 1940s it was common practice to construct pavements with thickened-edge cross sections. The Arlington tests showed that thickened-edge cross sections produced a pavement in which the stresses in the slab were approximately equal for all positions of the load. The cross section had a uniform thickness in the interior and an edge thickness of about 1.67 times the interior thickness; the edge thickness was reduced at a uniform rate in a distance of 2 to 2-1/2 feet.

One of the most comprehensive road tests was conducted by the American Association of State Highway Officials (AASHO), currently known as the American Association of State Highway and Transportion Officials (AASHTO), and reported in 1962 [37]. Air-entrained concrete pavements were subjected to traffic loads in four major traffic loops and in a light traffic loop. A control loop was subjected to a variety of non-traffic tests. The three variables in the test pavements were pavement thickness, depth of subbase, and the presence or absence of distributed steel reinforcement. Each pavement test section was subjected to only one axle spacing and weight. The results of the AASHO road test indicate that thin subbases (3 in.-4 in.) perform as well as thicker ones (6 in.-9 in.). Properly jointed plain pavements, where there is adequate load transfer across joints, perform as well as reinforced pavements.

Virtually all modern rigid pavement design methods recognize the importance of the fatigue life of concrete and, in design, consider not only the anticipated weights but also the number of heavy axle loads that will be applied during the pavement design life. These methods, for example, the AASHTO Interim Design Procedure [1] used by most highway departments in this country, and the Road Note 29 design procedure [3] used in the United Kingdom are also based on road test data. The major input of both methods is the total number of equivalent 18-kip single axle loads applied during the design life. The PCA design procedure evaluates the accumulated fatigue effects of all heavy axle load applications during the pavement life to prevent slab cracking.

The 1966 PCA design procedure [10,40] in use today is based on theoretical analyses of concrete pavement behavior, model and full scale tests, full scale test roads that are loaded by controlled test traffic, and observations of pavements in normal service. This procedure is the only one that makes the direct use of the fatigue S-N curve in the form of a table (stress ratios vs. allowable load repetitions) in design. The 1966 PCA curve can be expressed as follows:

$$SR = .972 - .0828 \log N$$

where

SR = stress ratio

= ratio of flexural stress to modulus of rupture

and

N = number of allowable load repetitions.

In summarizing the preceding discussions on concrete fatigue and rigid pavement design, the following can be concluded:

- Concrete, used in pavement slabs, is subjected to fatigue failure.
- Concrete pavement performance and distress is a function of load repetitions; therefore, load repetitions have a direct influence on the thickness requirements of a concrete pavement.
- Virtually all modern rigid pavement design methods take into consideration the fatigue strength (fatigue life and load repetitions) of concrete.

2. PURPOSE AND SCOPE

While all of the modern pavement design procedures recognize the importance of fatigue life of concrete and while air entrainment is being used for all concrete pavements, design curves currently being used in the design of Portland cement concrete pavements do not reflect the effect of air entrainment. The basic fatigue data, on which concrete pavement designs have been based for the past 40 to 50 years, were derived in early 1920s, 20 years before the introduction and 40 years before the widespread use of air-entrained concrete. No data are available on the fatigue behavior of air-entrained concrete in flexure.

In light of the extensive use of air entrainment and the growing interest in economy and efficiency of design, it becomes self-evident that, in order to properly design concrete pavements, a study of the effects of air entrainment on the fatigue behavior of concrete in flexure was urgently needed. The purpose of Phase I of that study was to evaluate the effects of air entrainment on the fatigue strength of plain concrete and establish preliminary fatigue curves for air-entrained concrete to be used in concrete pavement design.

The scope of Phase I included flexural fatigue testings of concretes at five levels of air entrainment, prepared with crushed limestone, Type I Portland cement, and at a water-cement ratio of 0.41. Based upon the results of Phase I, it has been concluded that flexural fatigue strength decreases as air content increases.

Concrete pavements being poured today are done so with different aggregate types and various air content and water-cement ratios. In

order to produce an efficient and economical design, one must know what effects these factors have on the flexural fatigue of concrete. The purpose of Phase II of this study is to determine the effects of varying water-cement ratios, varying air contents, and different aggregate types on the flexural fatigue of concrete and to establish design curves to be used in rigid pavement design.

The scope of Phase II includes the flexural fatigue testing of ten series of plain concrete. All batches were prepared with Type I Portland cement. The variables include air content, water-cement ratio, and coarse and fine aggregate types. Table 1 indicates the combinations of the variables utilized in this study; I indicates work completed in Phase I, and II indicates work completed in Phase II. In this table "target" air contents are listed; as will be shown later, in some cases there was variation between the nominal and actual air contents.

Table 1. Material combination - Phase I and II.

Coarse Aggregate	Gravel			Limestone							
Fine Aggregate	Hallett Sand			Hallett Sand					Bellevue Sand		
% Air / W/C	2	6	10	2	4	6	8	10	2	6	10
.32				II		II		II			
.41				I[b]	I	I	I	I			
.43	II[a]	II	II			II				II	
.60				II		II					

[a]Phase II

[b]Phase I

The results of Phase I of this investigation have been reported in Reference 21. The results of Phase II are presented in this report. Data from Phase I have been re-analyzed and are also presented here for comparison with the results of Phase II. Pavement design tables and graphs combining results from both phases are presented in this report for completeness and easy reference.

3. MATERIALS AND PROCEDURES

3.1. Testing Program

The objective of this study was to determine the effects of varying air content, varying water-cement ratios, and different aggregate types on the flexural fatigue of concrete. The test program originally proposed was to study nine series. Two different water-cement ratios (low and high) with crushed limestone as the coarse aggregate and three levels of entrained air (low, normal and high) comprised six series while a normal water-cement ratio with gravel as the coarse aggregate and three levels of entrained air (low, normal and high) comprised the remaining three series. From Phase I it had been determined that three levels of air content would be sufficient to demonstrate the effect these variables had on fatigue. Phase I of this study [21] tested concrete made with limestone at a normal water-cement ratio involving air content as the only variable. In Phase II, concrete made with river gravel at a water-cement ratio of 0.43 was tested in order to compare the effects of gravel versus limestone on the flexural fatigue strength. Concrete at a high water-cement ratio with a high air content was not considered to be a usuable mix, thus this series was replaced with one made with a coarse high quality sand to determine what effect fine aggregate had on fatigue strength. A tenth series was added to serve as a control to check the reproducibility of a series from Phase I. For the material combinations, see Table 2. Series designations are also given in Table 2. Each series has a three part designation that includes in order the following: Plastic air content, coarse and fine aggregates used, and water cement ratio times one hundred. In the aggregate part, the two letters employed have the following meaning:

Table 2. Material, air content, and water-cement ratio combinations - Phase II.

Coarse Aggregate	Gravel			Alden Limestone					
Fine Aggregate	Hallet Sand			Hallett Sand			Bellevue Sand		
Air, % / W/C	2*	6	10	2*	6	10	2*	6	10
0.32				3.1-LH-32	5.9-LH-32	9.5-LH-32			
0.43	3.9-GH-43	6.9-GH-43	14.2-GH-43		6.7-LH-43			5.5-LB-43	
0.60				4.2-LH-60	6.2-LH-60				

*Non Air-Entrained

L = Crushed limestone

G = Gravel

H = Hallet sand

B = Bellevue sand

L = Crushed Limestone

G = Gravel

H = Hallett Sand

B = Bellevue Sand

The age variable was reduced by testing all series at an age of 28 to 56 days and by determining the flexural strength of the fatigue beam each time. This meant that one series was mixed and poured approximately once each month. After the initial 28-day period when the first series was being cured, fatigue testing proceeded continuously. The second series was poured when testing began on the first series. While the first series was being tested, the second series was being cured. At the end of the 28-day curing period for the second series, testing of the first series was completed, the third series was poured, and testing of the second series began. This cycle continued until testing of all ten series was completed.

Beams for fatigue testing were 6 in. × 6 in. × 36 in. A modulus of rupture test was performed on the first 18 inches of the beam (Figure 1.) and a fatigue test was performed on the remaining unstressed portion (Figure 1). This technique provided a modulus of rupture value for each fatigue specimen, thus eliminating beam to beam variations. After the modulus of rupture test, and prior to the fatigue test, each beam was sealed in a plastic bag to maintain a constant saturated moisture content. Previous studies [36] indicate that if specimens are allowed to air dry during fatigue testing the scatter of data will increase. This is believed to be due to differential strains generated by moisture gradients within the beam.

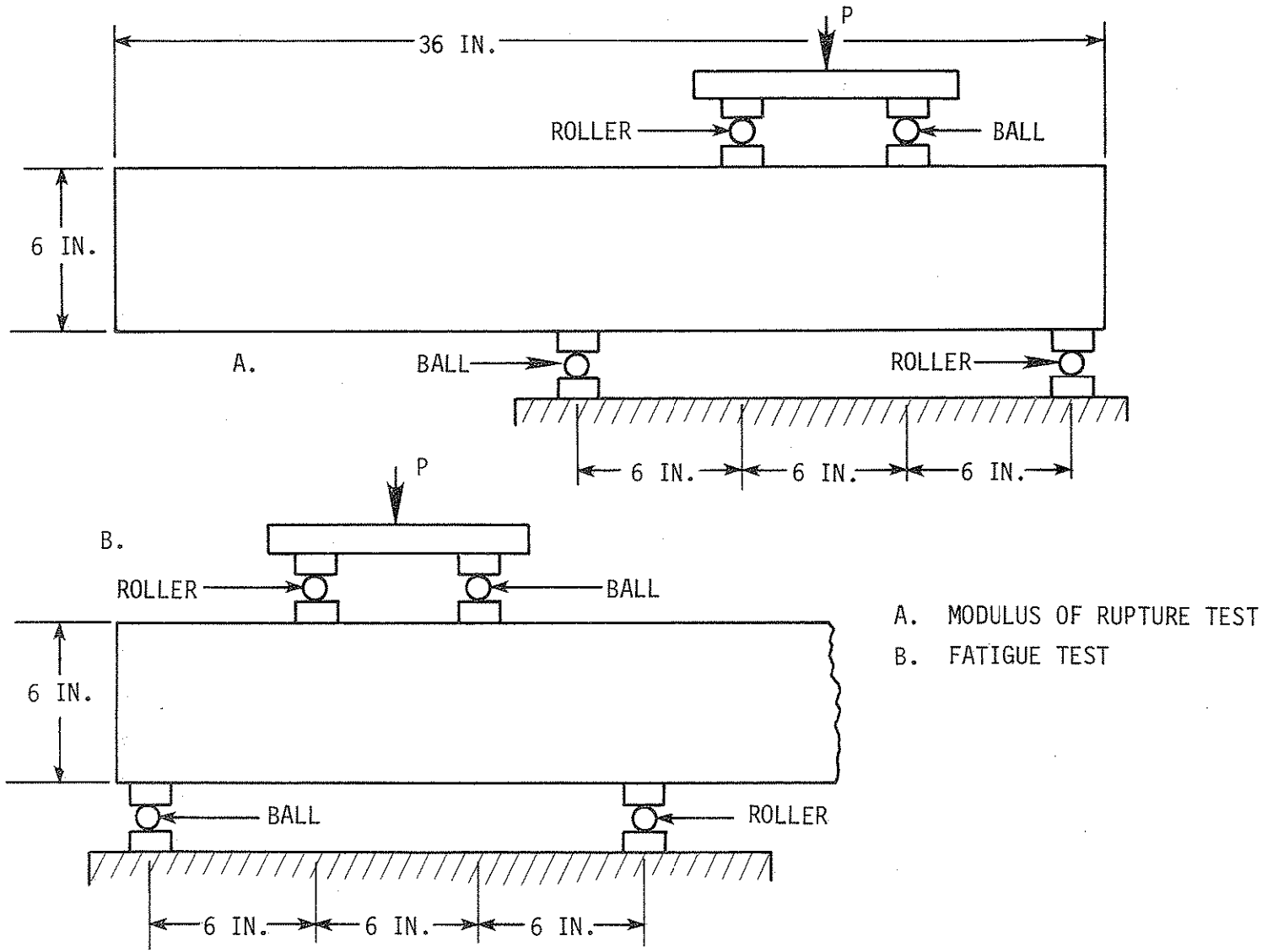

Figure 1. Schematic diagram of loading arrangements.

The stress level for fatigue testing of each specimen was determined by taking a percentage of the modulus of rupture for that specimen. This stress level was then converted to an equivalent load to be applied to the beam. The equivalent load was applied to the beam until failure occurred. Load was varied from a nominal 100 pounds (stress less than 10 psi) to a predetermined percentage of the modulus of rupture stress. The bottom fiber was in tension throughout the test. Fatigue tests were conducted at four stress levels corresponding to 90%, 80%, 70%, and 60% of the modulus of rupture. Six specimens were tested at each stress level [20,23]. All tests were run at a frequency of 5 hertz.

In addition to the main fatigue test program, five other investigations were carried out. The subjects of the additional investigations are:

1. modulus of rupture tests
2. compressive strength tests
3. determination of modulus of elasticity
4. high pressure air tests
5. concrete voids structure by scanning electron microscopy and mercury penetration porosimetry

3.2. Materials

The concrete used for the test specimens was a modified Iowa Department of Transportation (DOT) C-3 mix. A standard Iowa DOT C-3 mix contains a minimum of 604 pounds of cement per cubic yard and has a water-cement ratio of 0.43. Since one of the variables studied was the water-cement ratio, it was necessary to change the cement content in order to

produce a workable mix. Trial batches were run for each mix design to assure the proper air content and a slump between 1 and 3 inches.

Two types of coarse aggregates were used in this study. The gravel came from the Boggess Materials Company near Emmetsburg, Iowa, and had a saturated-surface-dry specific gravity of 2.68 and water absorption of 1.25%. The crushed limestone came from the Alden Quarry near Alden, Iowa, and had a saturated-surface-dry specific gravity of 2.53 and an absorption of 2.54%.

Two types of fine aggregates were used. The Hallett sand (Hallett Construction Co., Ames) was used in 14 out of 15 of the concrete pours (Phase I and II). This sand had a saturated-surface-dry specific gravity of 2.64 and an absorption of 1.15%. Bellevue Sand (from the Bellevue Sand Company near Belleuve, Iowa) was utilized in one of the Phase II series. Use of this sand was suggested by engineers of the Iowa DOT. Bellevue Sand is a coarse sand with a saturated-surface-dry specific gravity of 2.63 and a water absorption of 0.90%. All fine and coarse aggregates utilized in this investigation came from state approved stockpiles. For further information regarding aggregate gradation and specifications, see Tables A.1 and A.2 of Appendix A.

The Type I Portland cement used in the concrete batches was obtained from the Marquette Cement Corporation in Des Moines, Iowa. In order to guarantee uniformity, care was taken to assure that all of the cement utilized was taken from one batch at the cement plant. Chemical and physical properties of the cement are given in Table A.3 of Appendix A. Comparison of the cement properties of Table A.3 with those listed in Table A.3 of reference 21 (Phase I), indicates that there are no significant differences between the two cements utilized in Phase I and Phase II.

Upon recommendation of the engineers at the Iowa DOT, the air-entraining agent used in this investigation was Ad-Aire, a vinsol resin made by the Carter Waters Company of Kansas City, Missouri. Before each concrete pour, trial batches were run to determine the amount of air-entraining agent to be used to produce a specific air content.

A water reducing agent was used in the concretes with a water-cement ratio of 0.32 to produce a workable mix. Plastocrete 161, manufactured by the Sika Chemical Company of Lyndhurst, New Jersey, was the water reducer recommended by the engineers of the Iowa DOT. Plastocrete 161 is a polymer-type, non-air-entraining, water-reducing, strength-producing admixture which conforms to ASTM C 494 Type A (water-reducing admixture).

3.3. Mixing Procedures and Quality Control

A total of ten series of fatigue specimens were poured in Phase II. Prior to each pour, trial batches consisting of the desired aggregates and water-cement ratio were run to develop a mix with the desired air content and slump. Each pour consisted of approximately thirty 6 in. × 6 in. × 36 in. flexural fatigue beams and ten cylinders 6 in. in diameter and 12 in. long. Approximately 1.1 cubic yards of concrete were required for each series.

Since proper control and unformity of the mix was of utmost importance, all mixing was done in the laboratory. At the beginning of the project, all materials were obtained and stockpiled in the laboratory for use throughout the project. A mixer of one cubic yard capacity could not be located, so a concrete mixing truck was rented on the day of each pour. Before the batch quantities were charged into the mixer, the mixing drum was inspected to determine if it contained any leftover concrete

or mixing water from a previous job which would alter the desired mix. Batch quantities (see Table A-4 of Appendix A), which had previously been weighed out and corrected for moisture content, were than charged into the empty concrete mixer. According to Iowa DOT specifications [39], the concrete was mixed 70 revolutions; at the end of the mixing, slump tests and plastic air content tests were run to check the acceptability of the concrete. If the concrete was acceptable, it was transferred to the beam forms by wheelbarrow. If the concrete was unacceptable, the batch was adjusted (keeping the water-cement ratio constant) until it fell within the acceptable limits. The beams were then vibrated according to ASTM C 192 with a 1 in. diameter pencil vibrator which operated at 10,500 vibrations per minute. As the concrete was being placed in the beam forms, cylinders for compressive strength tests and modulus of elasticity tests were being cast in waxed cardboard cylinder molds 6 in. in diameter by 12 in. long.

The beams were then finished and covered with wet burlap and a heavy polyethylene sheet to maintain a moist condition for proper curing.

The burlap was kept wet and after a period of 48 to 72 hours the forms were stripped and the beams were moved to large metal curing tanks where they were cured under water until they were tested. The sequence from mixing to curing is shown in Figure 2.

The slump tests were run according to ASTM C 143; air content tests were run according to ASTM C 231. Three air meters of the pressure type from the Iowa DOT were used throughout the project. The air meters were calibrated prior to the beginning of the study and used exclusively in the study. For consistency, the same operators ran the air tests throughout the study.

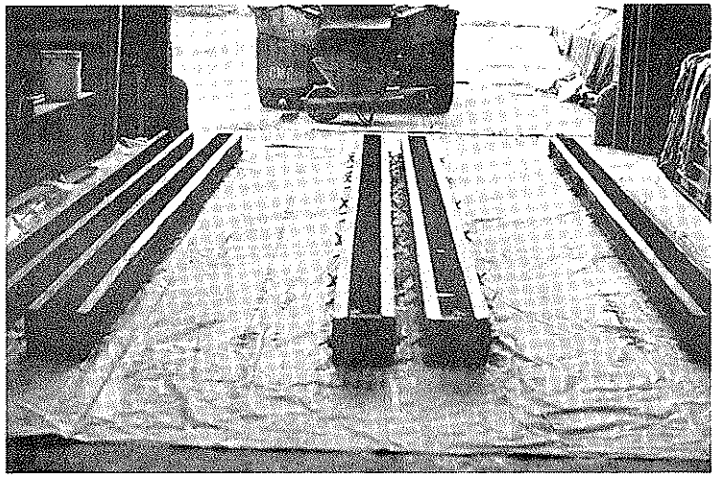

(a) Concrete mixing truck and empty forms.

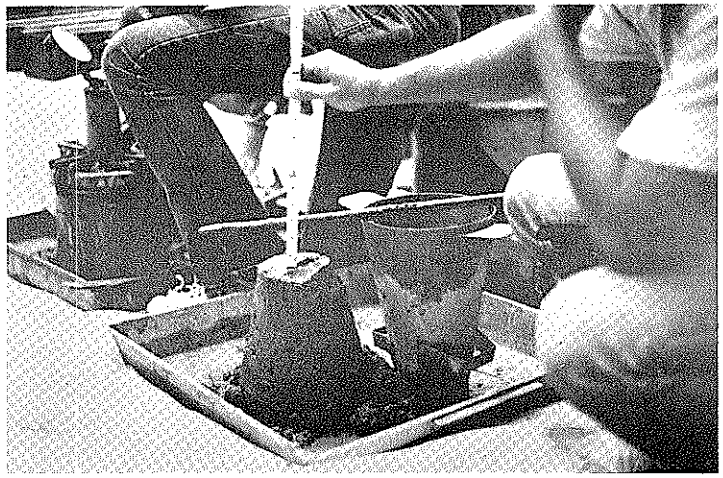

(b) Slump and air tests.

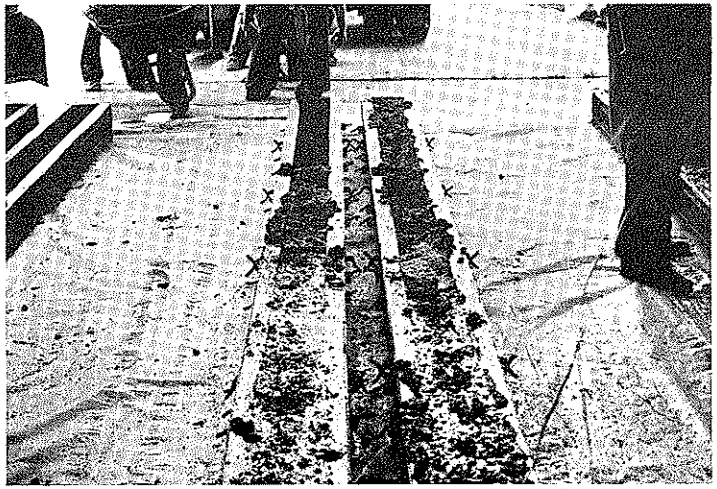

(c) Concrete forms being filled and vibrated.

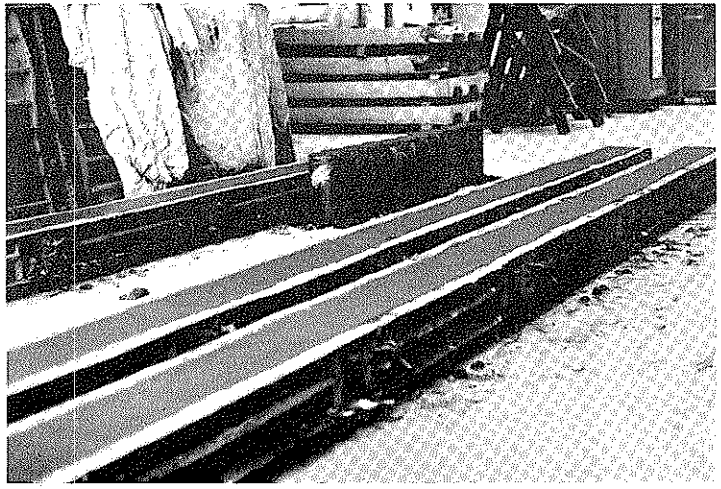

(d) Finished beams.

Figure 2. Sequence showing steps in preparing fatigue specimens.

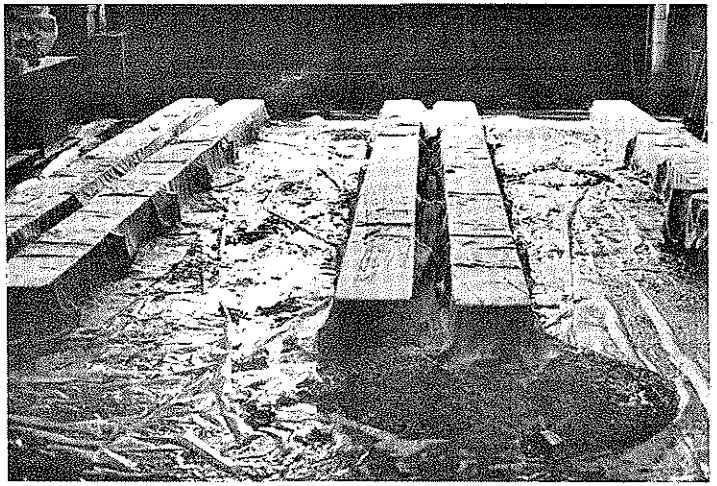

(e) Beams covered with wet burlap.

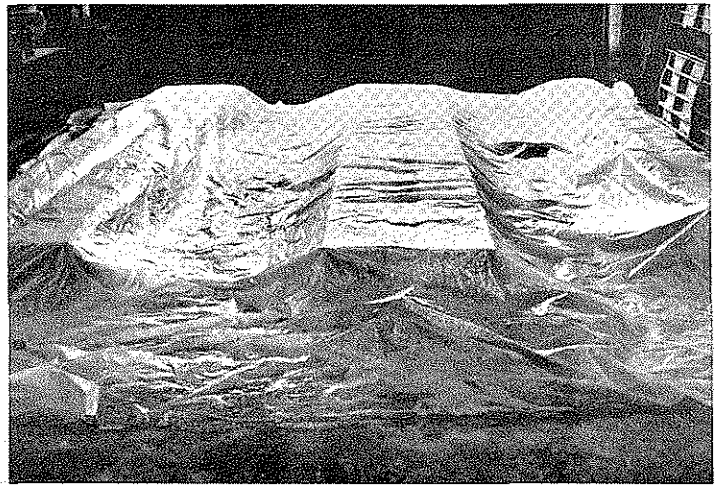

(f) Beams covered with polyethylene sheet.

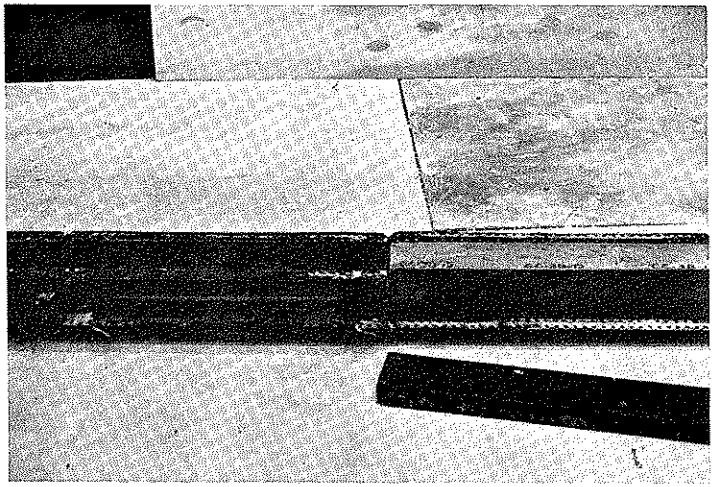

(g) Forms being stripped.

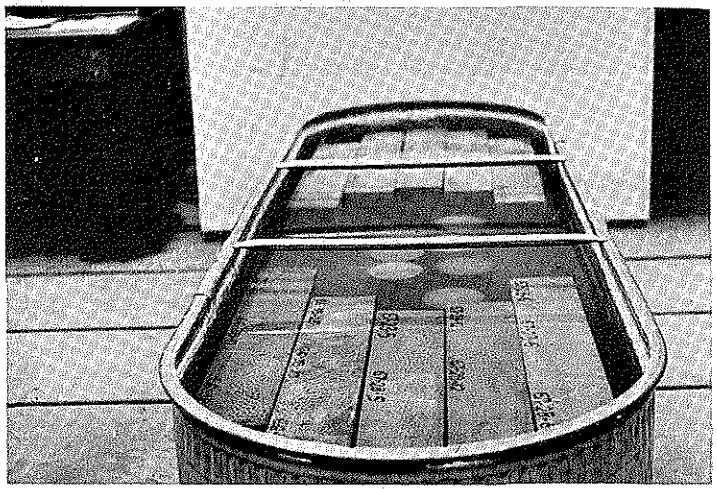

(h) Beams in curing tank.

Figure 2. (Continued). Sequence showing steps in preparing fatigue specimens.

3.4. Equipment

At the end of the 28-day curing period, compression tests were run on the 6-inch diameter by 12-inch concrete cylinders using a 400,000 pound capacity Baldwin-Satec Universal Testing Machine. Modulus of elasticity tests were conducted on the same machine using a Tinius Olsen concrete Cylinder Compressometer following ASTM standard C 469.

The modulus of rupture of each specimen was determined under one-third point loading, utilizing a concrete beam tester, Model S6, made by the American Beam Tester Company.

For the fatigue testing, an Instron Model 1211 dynamic cycler was used. A load frame was constructed so that flexural one-third point loading, at the same geometry as the modulus of rupture test, could be applied. The Instron has a $\pm$ 20,000 pound capacity and the load can be applied at a frequency of 5 to 35 cycles/second. Near the end of the study, a Materials Test System, MTS, fatigue machine became available for use. It too had a load fixture constructed for applying flexural one-third point loading at the same spacings as the modulus of rupture machine. The MTS has a capacity of $\pm$ 110,000 pounds and can apply the load at a frequency of 0.00001 to 990 hertz. Testing machines utilized in this study are shown in Figure 3.

During this investigation all of the machines were calibrated. Strain gages were attached to an aluminum beam that was loaded at one-third points in the same manner as the concrete test specimens. Strains due to static loading in the 400^{k} universal test machine, the beam tester, the Instron, and the MTS were measured using a Vishay strain indicator. For dynamic

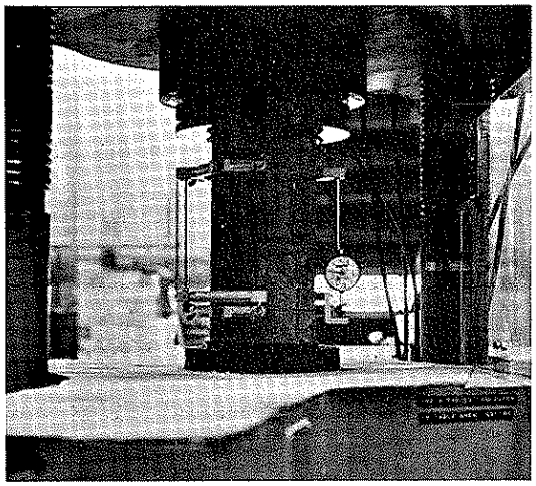

(a) 400^{k} machine with compressometer.

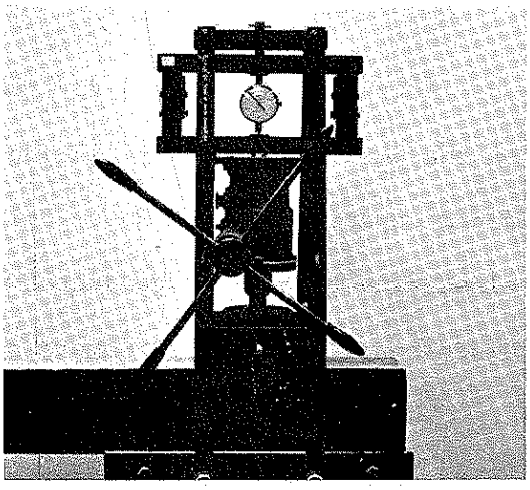

(b) Modulus of rupture machine with beam.

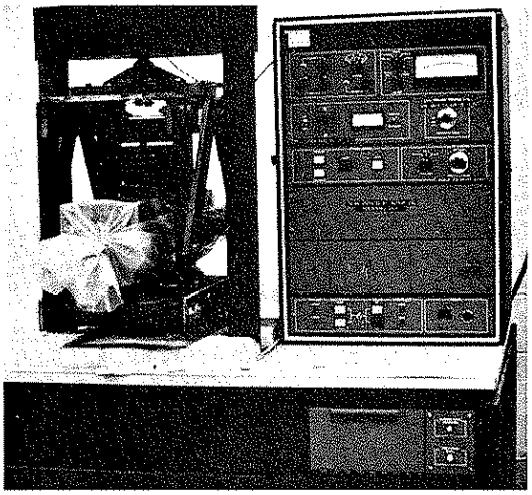

(c) Instron Dynamic cycler.

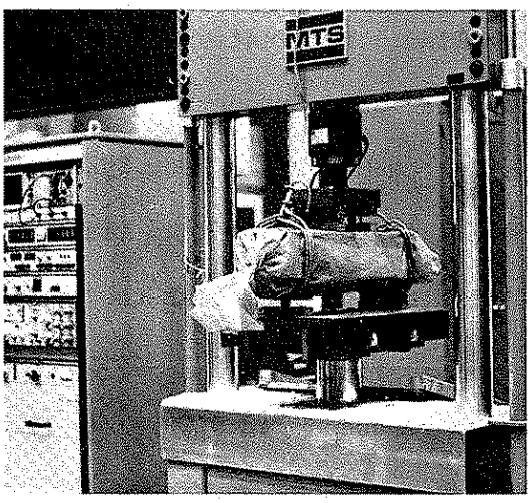

(d) MTS fatigue machine.

Figure 3. Test machines utilized.

loading in the Instron and MTS, a Sanborn Model 850 Dynamic Recorder was used to record the loads. All loads delivered were within acceptable limits of the load setting.

The high pressure air content was determined by the Materials Laboratory of the Iowa Department of Transportation. Four-inch diameter cores were drilled from sections of tested fatigue beams, oven dried at 300^{o}F for 72 hours, and then cooled for 3 hours. After weighing, the cores were soaked in water for 48 hours. The cores were then weighed in water, removed and patted dry with a cloth, and weighed again in air to determine absorption. The cores were placed in the high pressure air meter, and pressure of approximately 5000 psi was applied. Air content was then computed from dial readings based on Boyle's Law. For more details of the procedure see Test Method No. Iowa 407-A, April 1971, Iowa Department of Transportation, Materials Department.

Microstructures of hardened concrete were studied using a JEOL USM-U3 scanning electron microscope and a micromeritics model 905-1 mercury porosimeter.

4. RESULTS AND DISCUSSION

4.1. Physical Properties

This section presents the experimentally determined physical properties of the ten series of concrete tested in this study (Phase II). A summary of the concrete properties for the various series is presented in Table 3. The modulus of elasticity is the average of three tests. The slump is the average of two measurements; the 28-day compressive strength if the average of four compression tests, and the modulus of rupture value is the average of all beams tested in each series. Percent air in this table and elsewhere in this report refers to plastic air content unless stated otherwise.

4.1.1. Modulus of Elasticity

The modulus of elasticity tests were made using a standard concrete cylinder compressometer with a dial gage attachment following the procedure given by ASTM C 469. As may be seen in Figure 4, an increase in the amount of entrained air decreases the modulus of elasticity for Series LH-32 and Series GH-43. For Series LH-60 there is a slight increase. The equations of the lines in this figure are:

Series: LH-32

$$E_c = - 0.1791 \text{ (PA)} + 5.0877$$

Correlation Coefficient, $r = - 0.9988$

Series: GH-43

$$E_c = - 0.2301 \text{ (PA)} + 6.0506$$

Correlation Coefficient, $r = - 0.9787$

Table 3. Summary of concrete properties.

Series	Air Content, %	Slump, in.	Unit Weight, pcf	Modulus of Rupture, psi	Compressive Strength, 28-day, psi	Modulus of Elasticity, psi
3.1-LH-32	3.1	1	147.0	783	7375	4.55 (10^6)
5.9-LH-32	5.9	1 1/2	144.6	660	6520	4.00 (10^6)
9.5-LH-32	9.5	3 1/2	135.0	550	4300	3.40 (10^6)
3.9-GH-43	3.9	1 3/4	149.0	840	5200	4.95 (10^6)
6.9-GH-43	6.9	4 1/4	145.2	735	4730	4.75 (10^6)
14.2-GH-43	14.2	5 3/4	136.0	430	1905	2.70 (10^6)
6.7-LH-43	6.7	5 1/2	137.5	527	2966	3.25 (10^6)
5.5-LB-43	5.5	2 1/2	142.8	664	5625	4.10 (10^6)
4.2-LH-60	4.2	2	143.5	625	3880	3.25 (10^6)
6.2-LH-60	6.2	2 1/2	140.8	570	3560	3.35 (10^6)

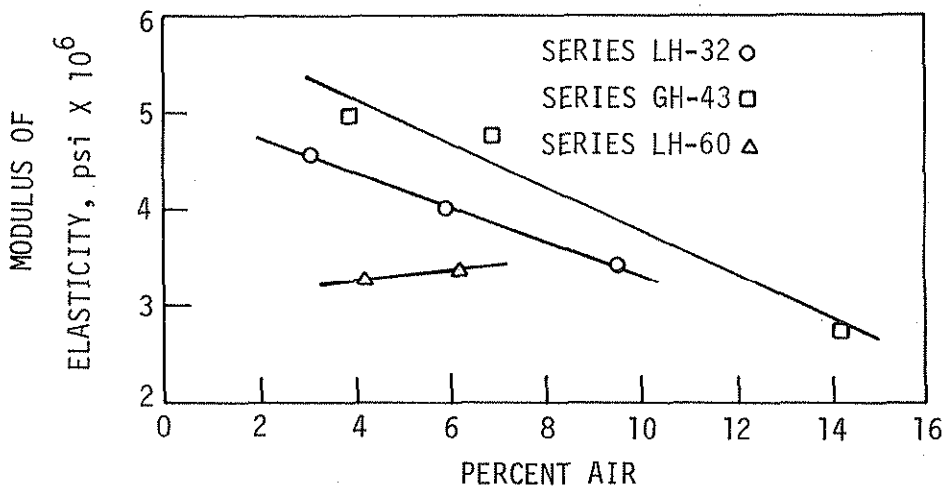

Figure 4. Modulus of elasticity versus percent air.

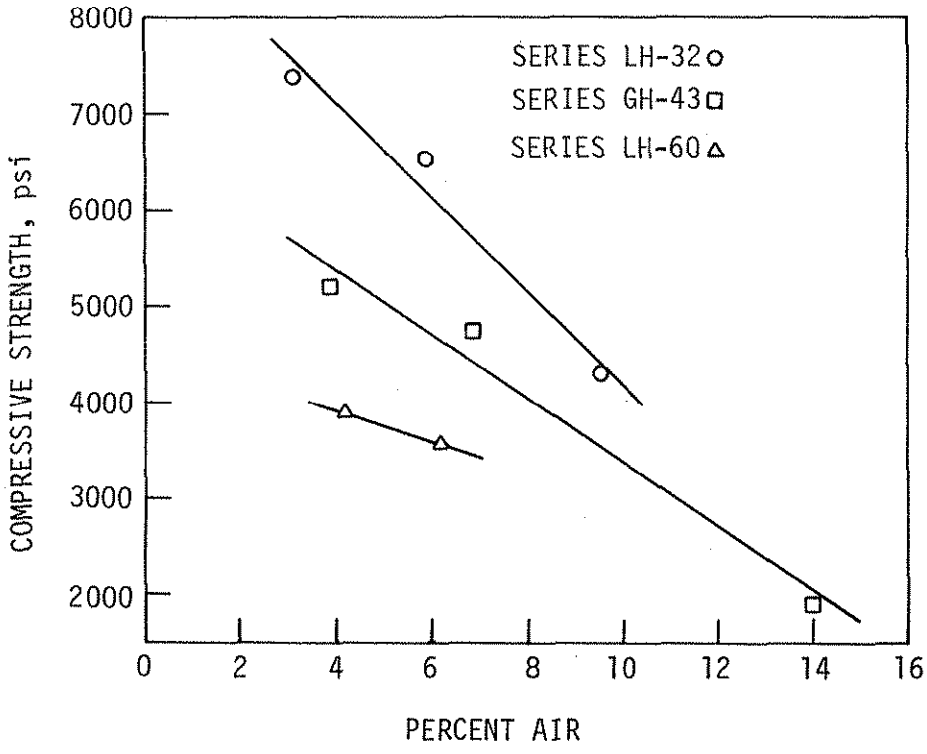

Figure 5. 28-day compressive strength versus percent air.

Series: LH-60

$E_c = 0.0500\ (PA) + 3.0400$

(No correlation coefficient given as there are only 2 data points.)

where:

E_c = modulus of elasticity in 10^6 psi

PA = percent air in the concrete

4.1.2. Compressive Strength

The 28-day compressive strength tests were conducted according to ASTM C 39-72. The results of these tests are shown in Figure 5.

As these tests indicate, the compressive strength decreases as the water-cement ratio increases. For a constant water-cement ratio, the compressive strength decreases linearly as the air content increases. The equations of the lines are:

Series: LH-32

$f'_c = -\ 486.8\ (PA) + 9067.1$

Correlation Coefficient, $r = -\ 0.9840$

Series: GH-43

$f'_c = -\ 332.4\ (PA) + 6715.1$

Correlation Coefficient, $r = -\ 0.9880$

Series: LH-60

$f'_c = -\ 160.0\ (PA) + 4552.0$

(No correlation coefficient is given as there are only two data points.)

where:

f'_c = 28-day compressive strength in psi

PA = percent air in the concrete

4.1.3. Modulus of rupture

The modulus of rupture stresses, determined according to ASTM C 78-75, were obtained from tests on one end of the fatigue specimens. Other fatigue studies have determined an average modulus of rupture stress from testing a few specimens and used the average modulus of rupture stress for all tests. However, in this investigation a companion modulus of rupture test was conducted for each fatigue specimen (see Figure 1), giving the most accurate estimate of the modulus of rupture for the fatigue tests.

The results of the modulus of rupture tests are plotted in Figure 6; these tests indicate that as the air content increases, the modulus of rupture decreases. For series LH-32, GH-43, and LH-60, the modulus of rupture decreased approximately as the cubic root, square root, and fourth root of the percent air, respectively. The equations of the curves according to a log-log regression analysis are:

Series: LH-32

$$f_r = 1125.30\ (PA)^{-0.3126}$$

Correlation Coefficient = -0.9945

Series: GH-43

$$f_r = 1829.80\ (PA)^{-0.5279}$$

Correlation Coefficient = -0.9647

Series: LH-60

$$f_r = 877.59\ (PA)^{-0.2385}$$

(No correlation coefficient is given as there are only two data points.)

where:

f_r = modulus of rupture in psi

PA = percent air in the concrete

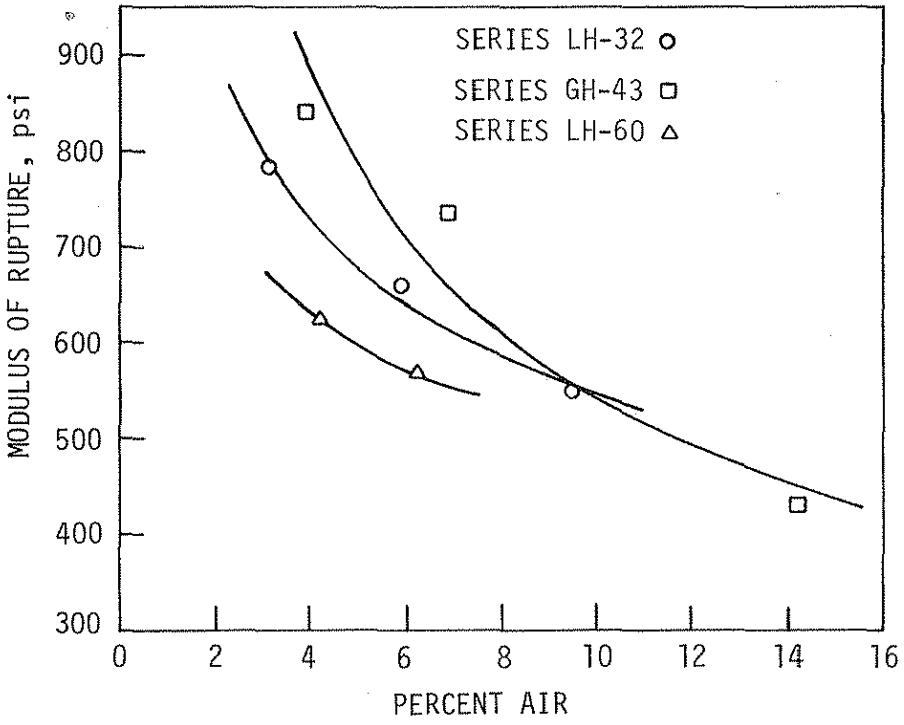

Figure 6. Modulus of rupture versus percent air.

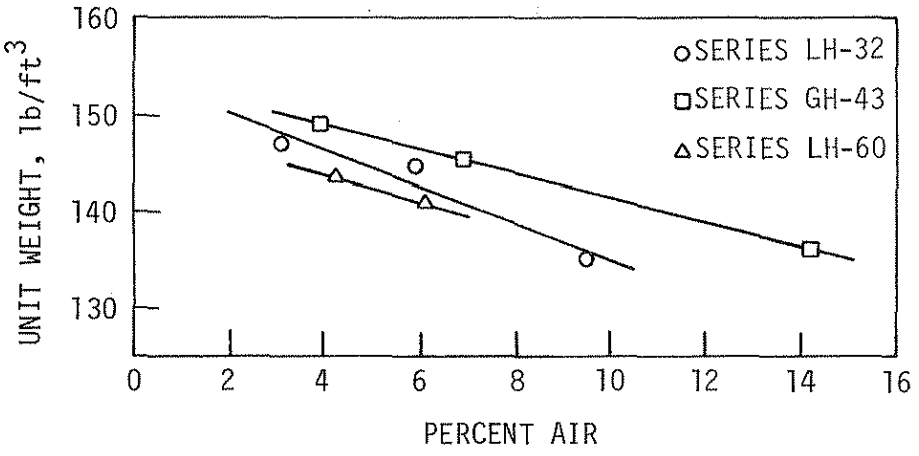

Figure 7. Unit weight versus percent air.

The modulus of rupture strengths in this investigation are probably somewhat higher than can be expected in the field because of the better control over the mix and the continuous curing until the time of the test.

4.1.4. Unit weight

At the time of the pour, the unit weight of each batch was determined. In each series, there is a linear decrease in unit weight as the percent of air increases. Approximately, there is a loss of 1 - 2 pcf for each percent air increase. A plot of the results is shown in Figure 7; equations of the curves are:

Series: LH-32

$Y = -1.9119\ (PA) + 153.9902$

Correlation Coefficient, $r = -0.9660$

Series: GH-43

$Y = -1.2618\ (PA) + 153.9149$

Correlation Coefficient, $r = -0.9999$

Series: LH-60

$Y = -1.3500\ (PA) + 149.1700$

(No correlation coefficient is given as there are only two data points.)

where:

Y = unit weight in pcf

PA = percent air in the concrete

4.1.5. Air Content

As previously noted, the air content used to compare the changes in modulus of elasticity, compressive strength, modulus of rupture, and unit weight was the plastic air content, which was determined by the

pressure method (ASTM C 231). The air content of the hardened concrete was determined by the high pressure air method.

The results of the high pressure air tests are compared to the plastic air contents in Table 3. As may be noted, depending upon the series, the high pressure air content may be higher or lower than the plastic air content. The equation for the relationship is:

$$HA = 0.9968\ (PA) + 0.033$$

where:

HA = high pressure air content, percent

PA = plastic air content, percent

Correlation Coefficient = 0.9777

4.1.6. Fatigue Tests

The fatigue specimens were tested in flexure with the load applied at the one-third points, the same spacings as in the modulus of rupture tests. Ten different concretes were tested in Phase II with various combinations of materials and levels of air content.

The concrete test specimens within each series were tested at stress levels corresponding to 60, 70, 80 and 90 percent of the modulus of rupture. At least five specimens, but more typically six specimens, were tested at each stress level for each series. A total of 239 flexural specimens were tested in Phase II. The modulus of rupture strength, the maximum load applied as a percentage of modulus of rupture, and the number of load applications to failure for each specimen are given in Tables B-1 through B-10 of Appendix B. As has been previously noted, each series has a three-part designation. In these tables there is a decimal point after the water-cement ratio designation. The number that

comes after the decimal point is the identification of the individual beams within a given series. Specimens that did not fail are so indicated in these tables. In all but a few cases, specimens that did not fail were run a minimum of 2 million cycles.

Table 4. Comparison of plastic air content and high pressure air content.

Series	Plastic Air Content, %	High Pressure Air Content, %			
		Individual Tests			Average
3.1-LH-32	3.1	3.1	3.0	6.3	4.1
5.9-LH-32	5.9	6.0	6.7	6.1	6.3
9.5-LH-32	9.5	9.2	8.7	9.4	9.1
3.9-GH-43	3.9	---	---	---	---*
6.9-GH-43	6.9	5.9	6.4	5.4	5.9
14.2-GH-43	14.2	14.9	13.6	15.3	14.6
6.7-LH-43	6.7	7.1	7.1	6.9	7.0
5.5-LB-43	5.5	4.5	4.8	5.1	4.8
4.2-LH-60	4.2	3.0	4.6	3.2	3.6
6.2-LH-60	6.2	6.0	5.9	8.9	6.9

*Data not available

As stated before, the specimens were tested at four different stress levels. A constant minimum stress corresponding to less than 10 psi was maintained on the specimens so that the bottom fiber was always in tension. Figure 8 shows the failure surfaces of several test specimens comparing the failure surfaces at similar air contents when different coarse aggregates and water-cement ratios are used. A difference in failure surfaces (Figure 8b) may be seen between concretes made with different coarse aggregate types at similar air contents as well as between concretes with different air contents (Figures 8a, b and c) using the same coarse aggregate. At similar air contents (Figure 8b), concrete made with limestone seems to fail through the aggregate while the concrete made with gravel tends to fail around the aggregate. This result is in agreement with the findings of other researchers in that an aggregate with a rougher surface texture provides a better bond between the aggregate particles and the cement paste [2,17,32].

Inspection of the failure surfaces for each aggregate type shows increasing numbers of failures around the aggregate, as compared to through the aggregate, as the air content is increased. This indicates that high percentages of air weaken the bond between the cement paste matrix and the aggregate.

The fatigue data have been plotted on S-N curves (S, stress, vs., log N, no. of cycles to failure) for each of the ten series. The curves shown in Figures 9 to 18 are the result of a log-log regression analysis program, CENSOR, which has the capability of considering and assigning values for the number of cycles to failure to specimens that did not fail. A discussion of the regression analysis of the data and the equations of the curves are given in Appendix C.

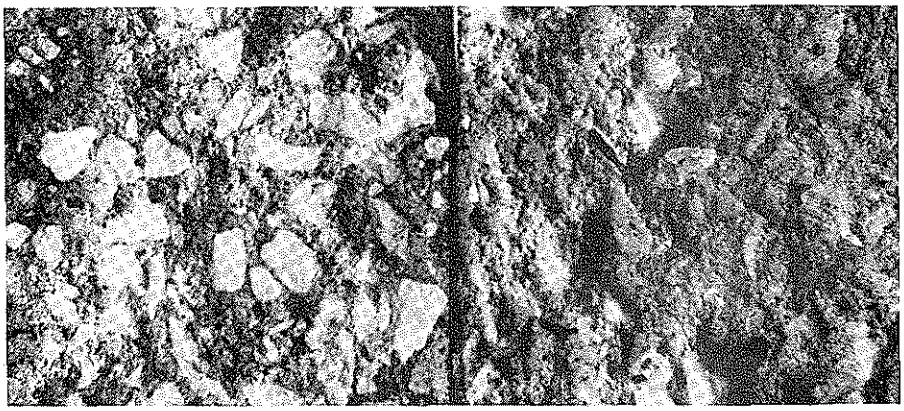

(a)

Series 9.5-LH-32 Series 14.2-GH-43

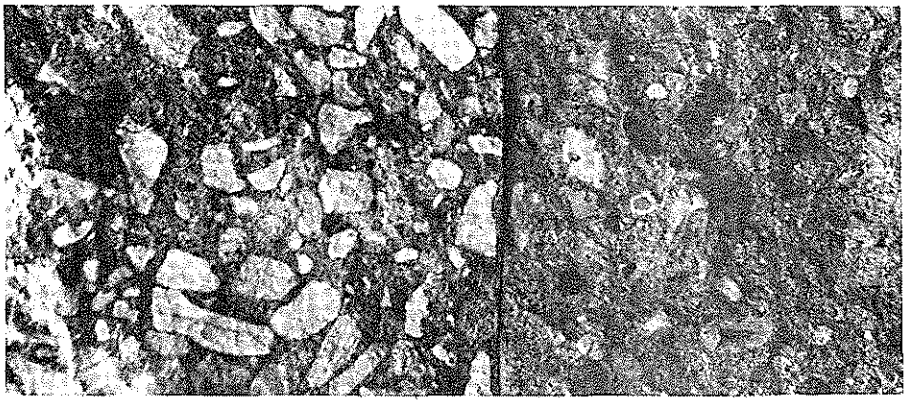

(b)

Series 6.7-LH-43 Series 6.9-GH-43

(c)

Series 3.1-LH-32 Series 3.9-GH-43

Figure 8. Failure surfaces of test specimens:
(a) high air content,
(b) medium air content,
(c) low air content.

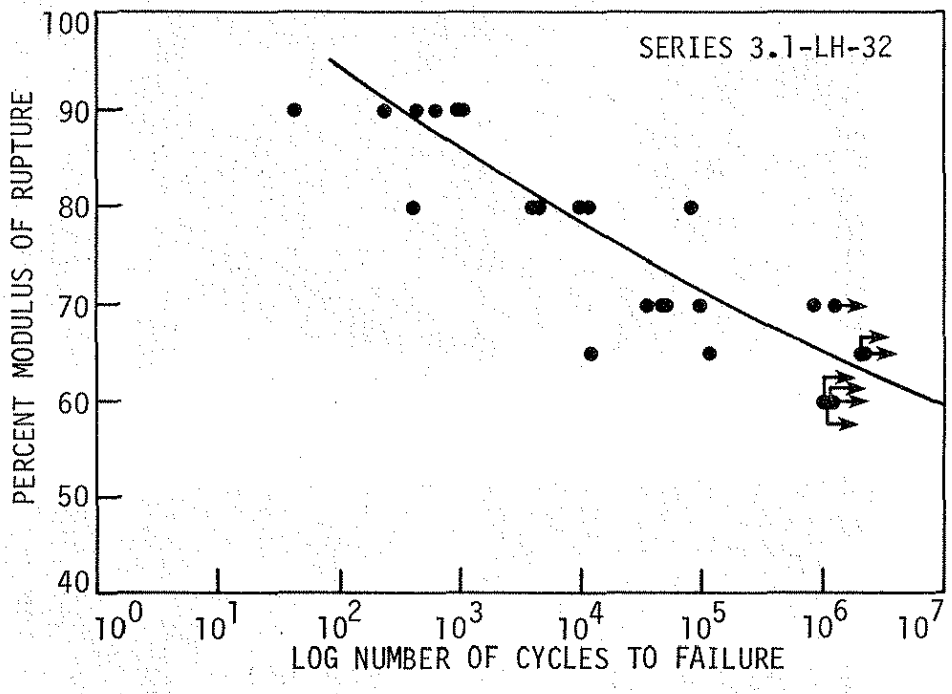

Figure 9. S-N curve for Series 3.1-LH-32.

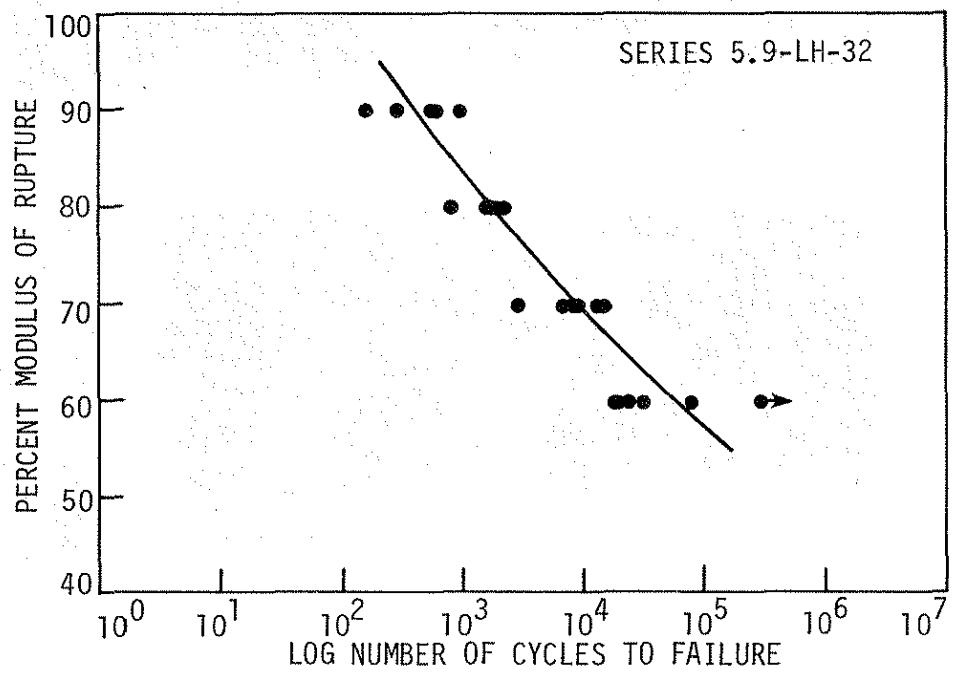

Figure 10. S-N curve for Series 5.9-LH-32.

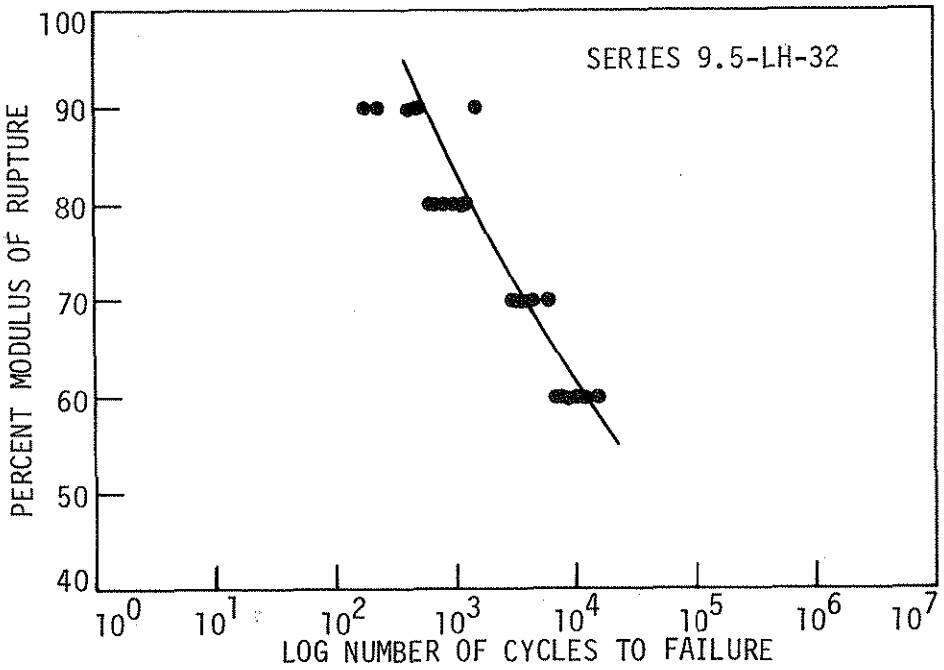

Figure 11. S-N curve for Series 9.5-LH-32.

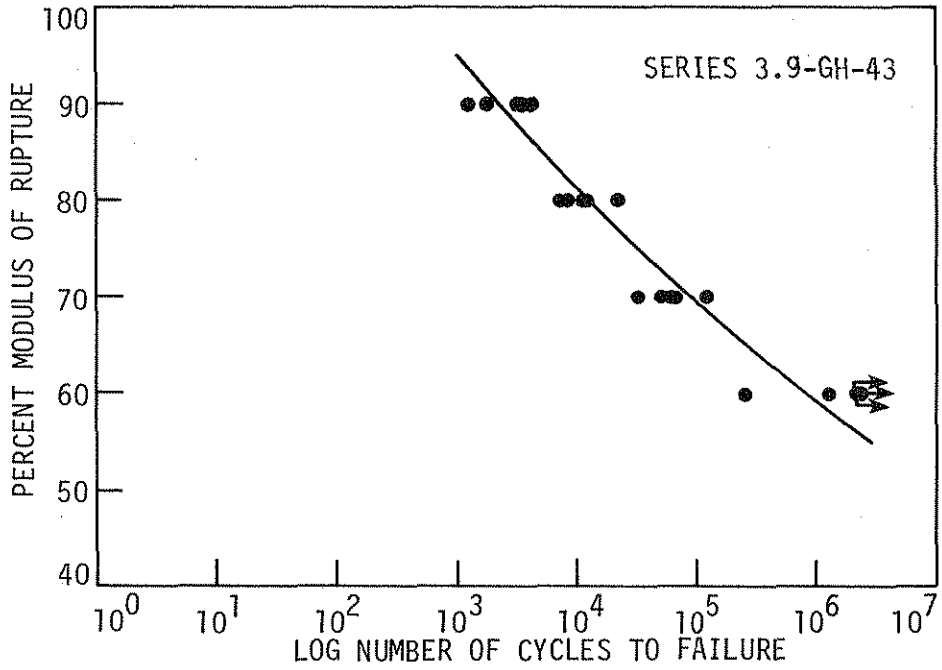

Figure 12. S-N curve for Series 3.9-GH-43.

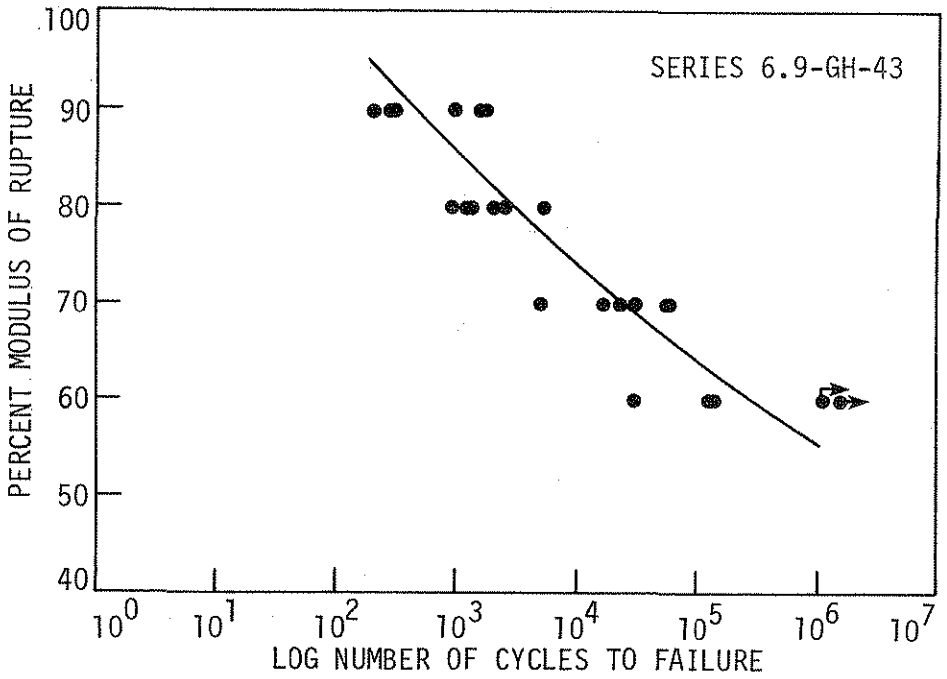

Figure 13. S-N curve for Series 6.9-GH-43.

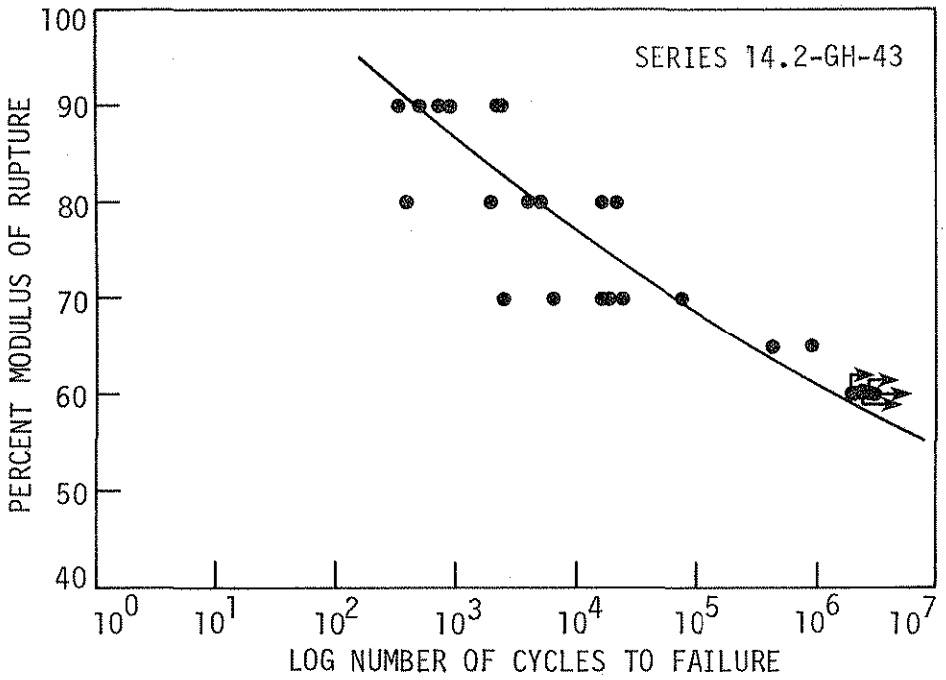

Figure 14. S-N curve for Series 14.2-GH-43.

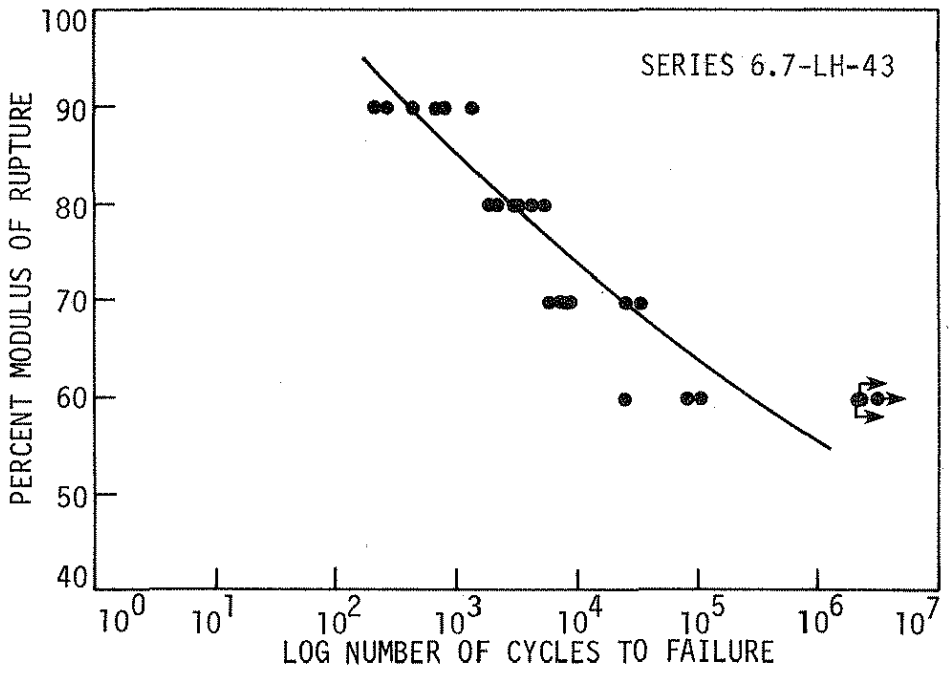

Figure 15. S-N curve for Series 6.7-LH-43.

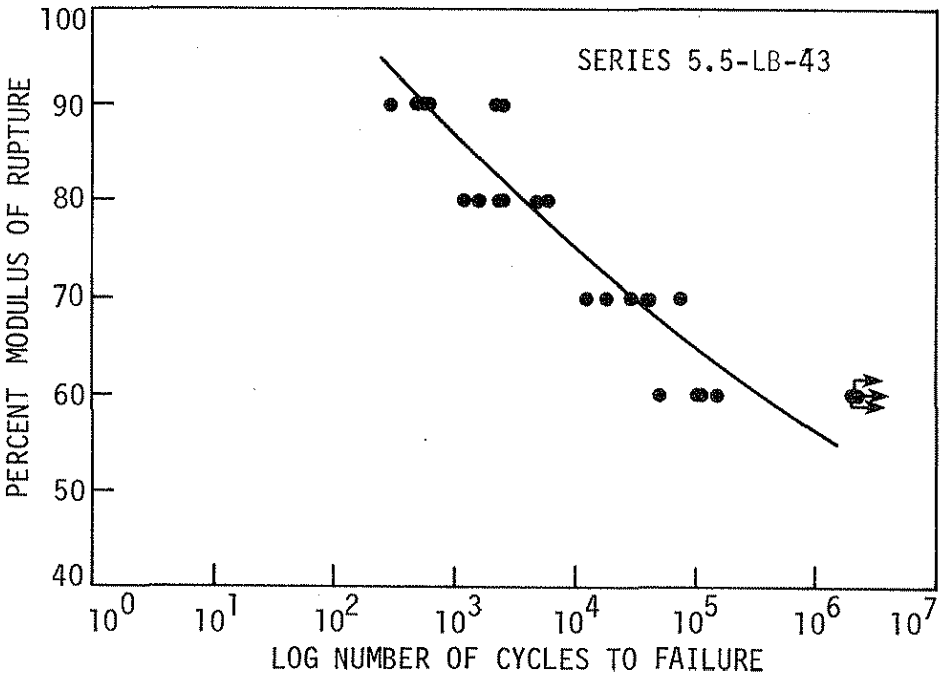

Figure 16. S-N curve for Series 5.5-LB-43.

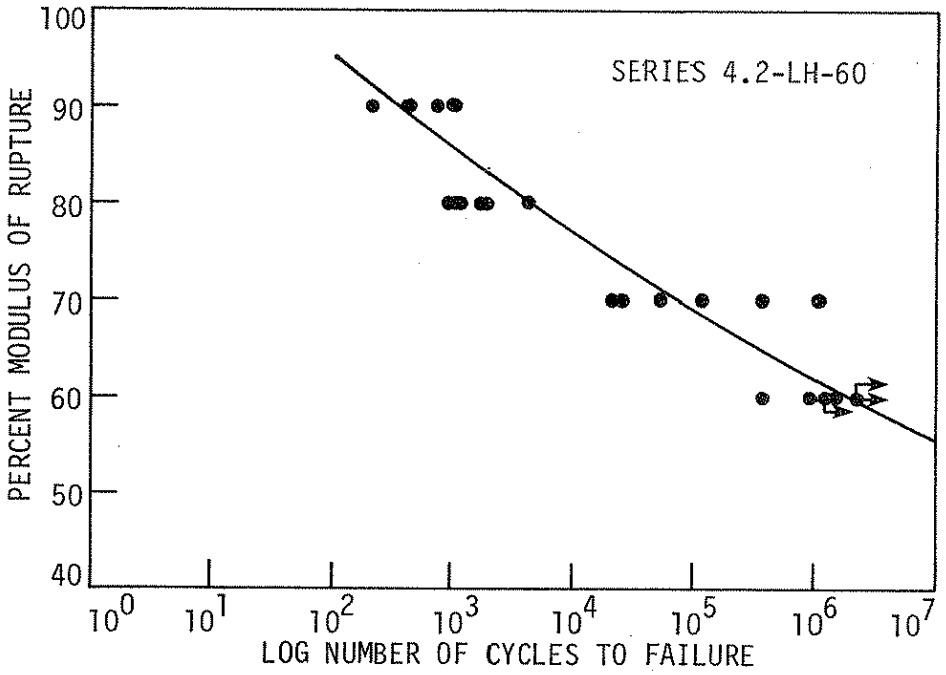

Figure 17. S-N curve for Series 4.2-LH-60.

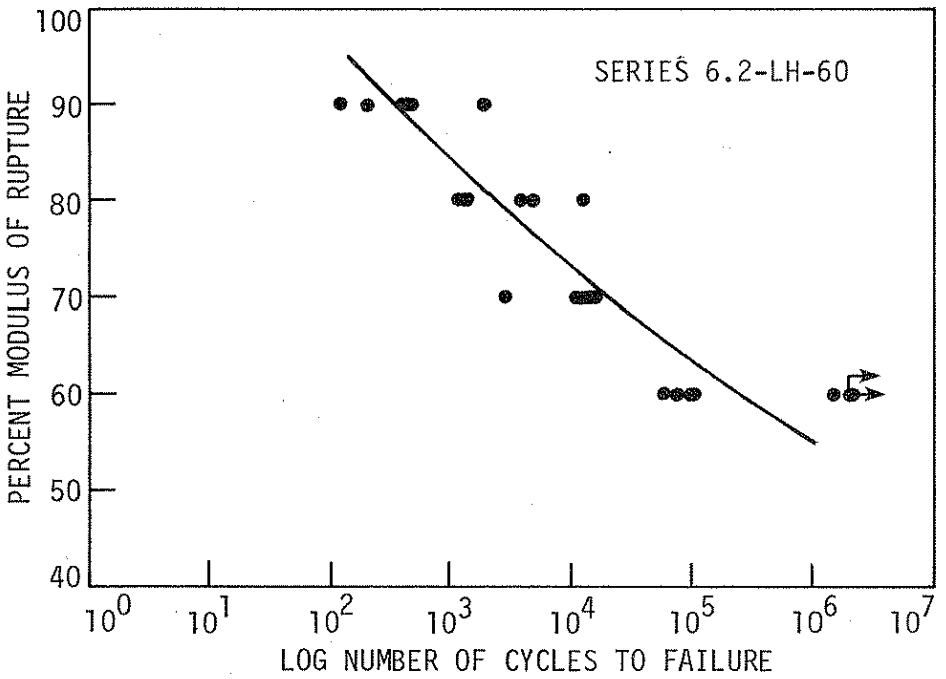

Figure 18. S-N curve for Series 6.2-LH-60.

For comparison, curves representing concretes with identical water-cement ratios and aggregate types are shown in composite plots in Figures 19 to 22.

To obtain a more accurate and comprehensive analysis, fatigue data from Phase I of this study were re-analyzed utilizing the computer program CENSOR. As has been previously stated, CENSOR makes it possible to take into account unfailed specimens more accurately. In Phase I the only variable was air content; all concrete was made with Alden Limestone, Hallett Sand with a water-cement ratio of 0.41. This combination of materials except for the slight difference in water-cement ratio is the same as Series LH-43 of Phase II. Utilizing data from Phases I and II, comparison of fatigue life can thus be made for gravel vs. limestone at similar water-cement ratios when the aggregate is kept constant.

The results of the log-log regression analysis for Series LH-41 (Phase I) are shown in Figures 23 to 27 and a composite plot is presented in Figure 28. Equations for the curves are given in Appendix C.

By studying the composite plots (Figures 19, 20, 21, 22, and 28), it is readily apparent that flexural fatigue life decreases as the air content increases regardless of the aggregate or water-cement ratio. One exception to this general trend is the behavior of Series 14.2-GH-43 near the lower stress levels. Series 14.2-GH-43 had a high air content (14.2%) and a low modulus of rupture (430 psi). None of the specimens in Series 14.2-GH-43 failed when loaded at the 60% level; each of the unfailed specimens was loaded a minimum of 2 million cycles. This behavior and the method of analysis (CENSOR), in the opinion of the authors, are the reasons for the characteristics of fatigue curve found for Series 14.2-GH-43.

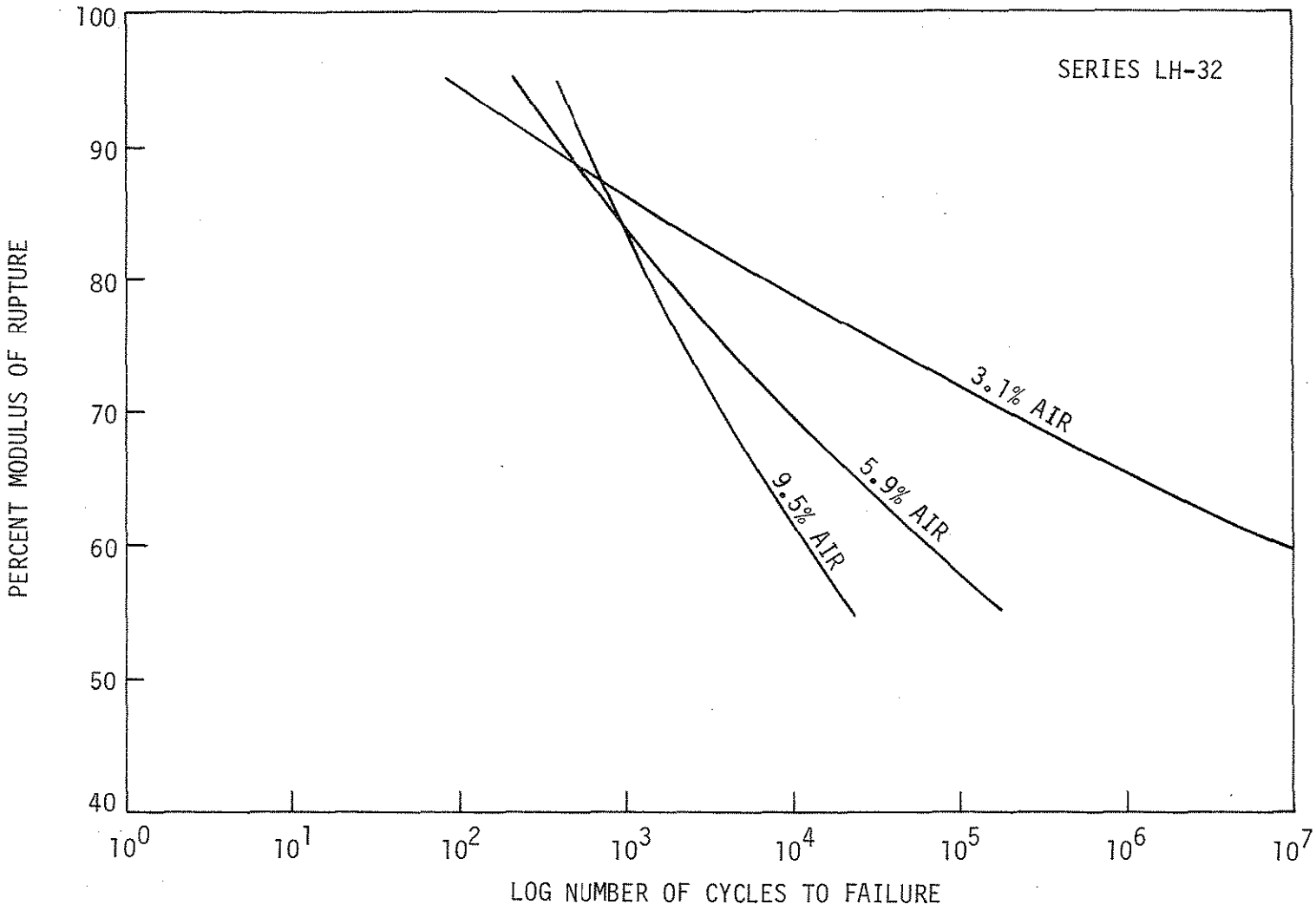

Figure 19. Composite S-N plot for Series LH-32.

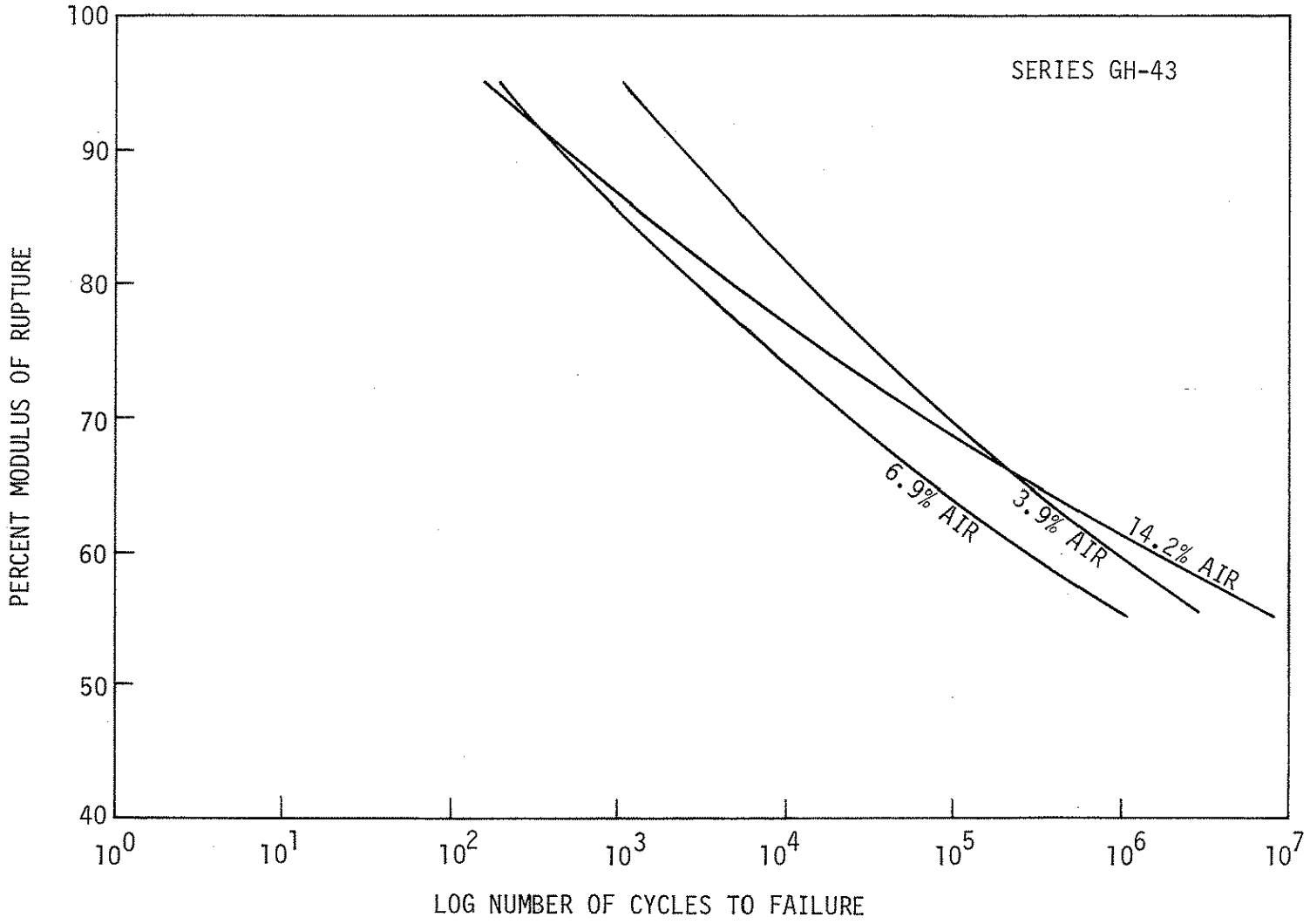

Figure 20. Composite S-N plot for Series GH-43.

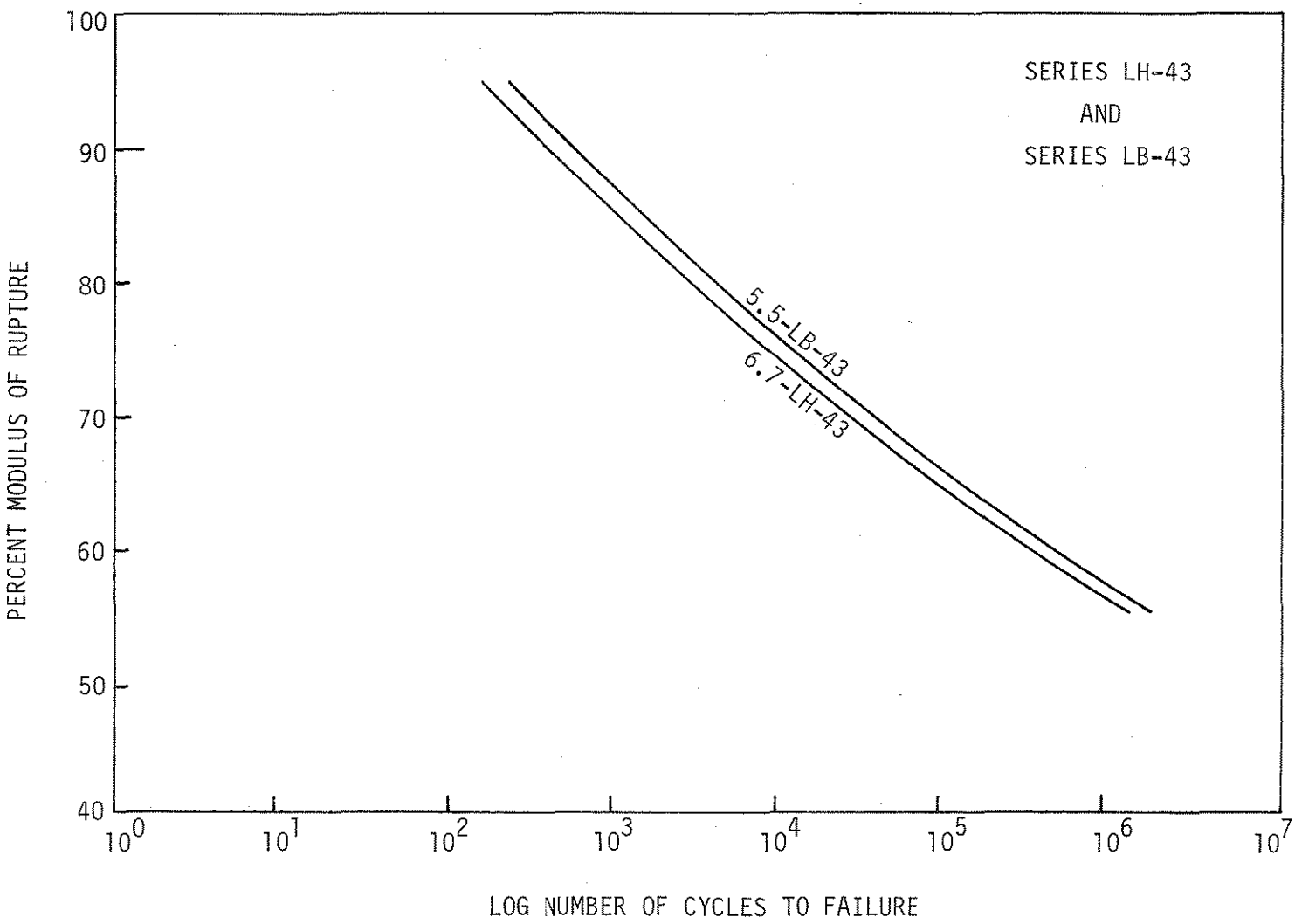

Figure 21. Composite S-N plot for Series LH-43 and Series LB-43.

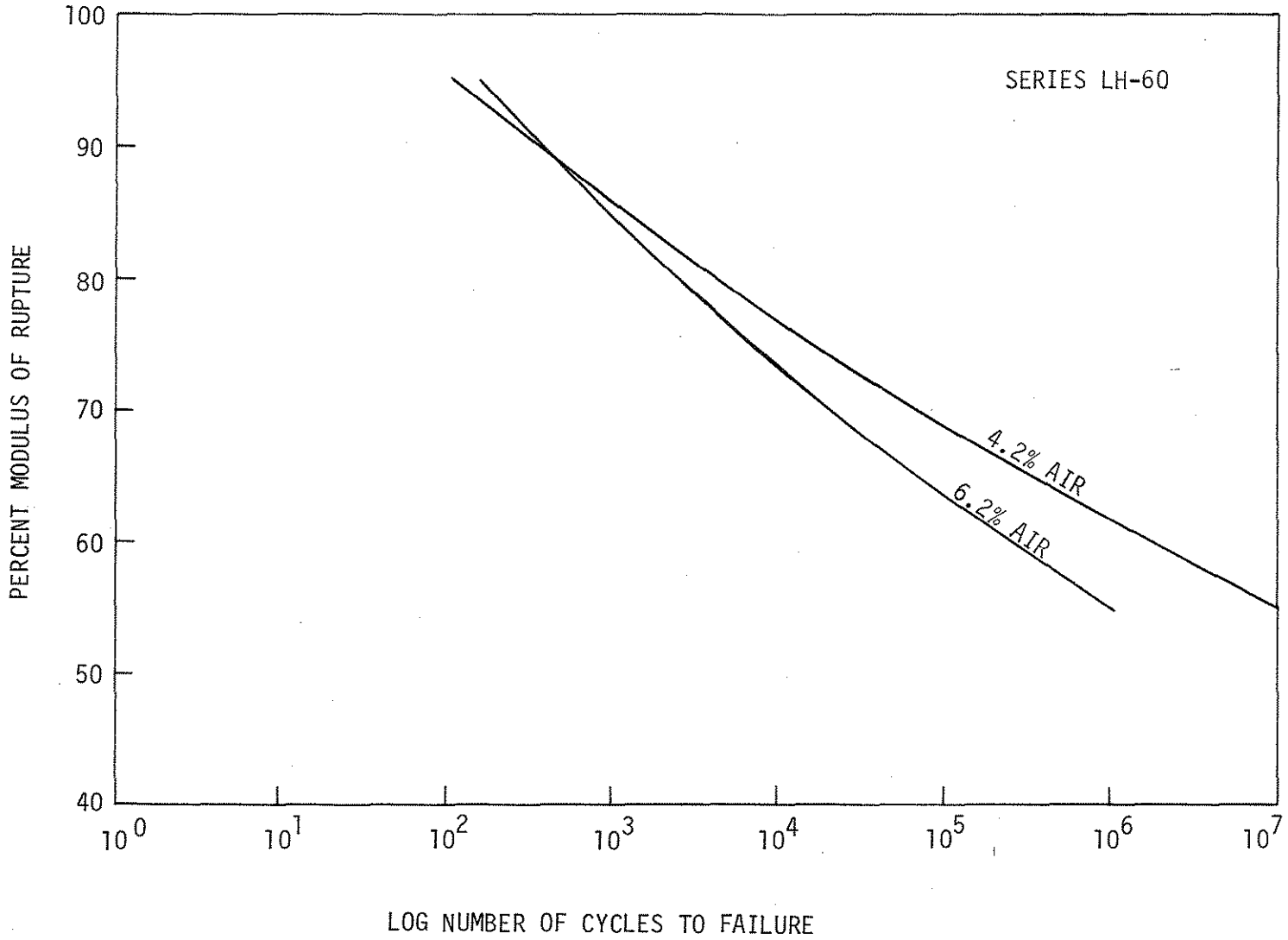

Figure 22. Composite S-N plot for Series LH-60.

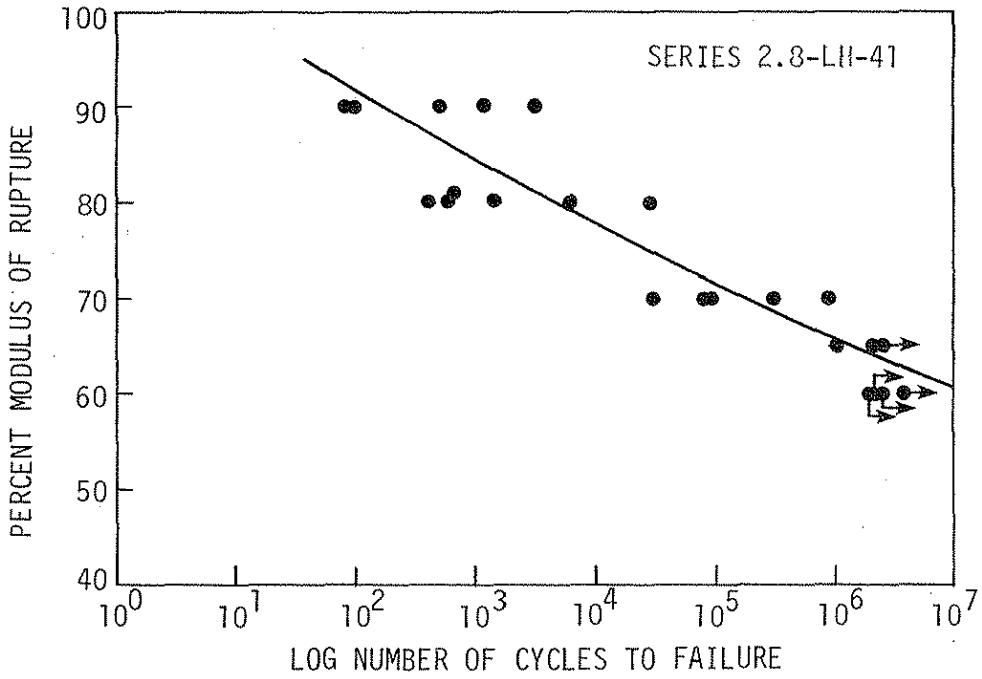

Figure 23. S-N curve for Series 2.8-LH-41.

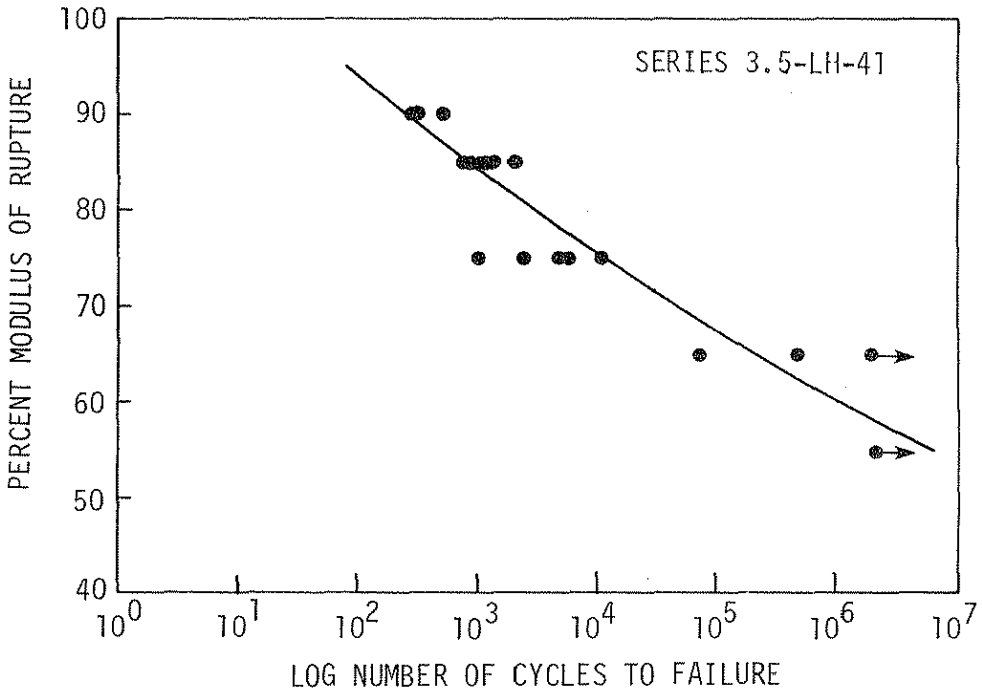

Figure 24. S-N curve for Series 3.5-LH-41.

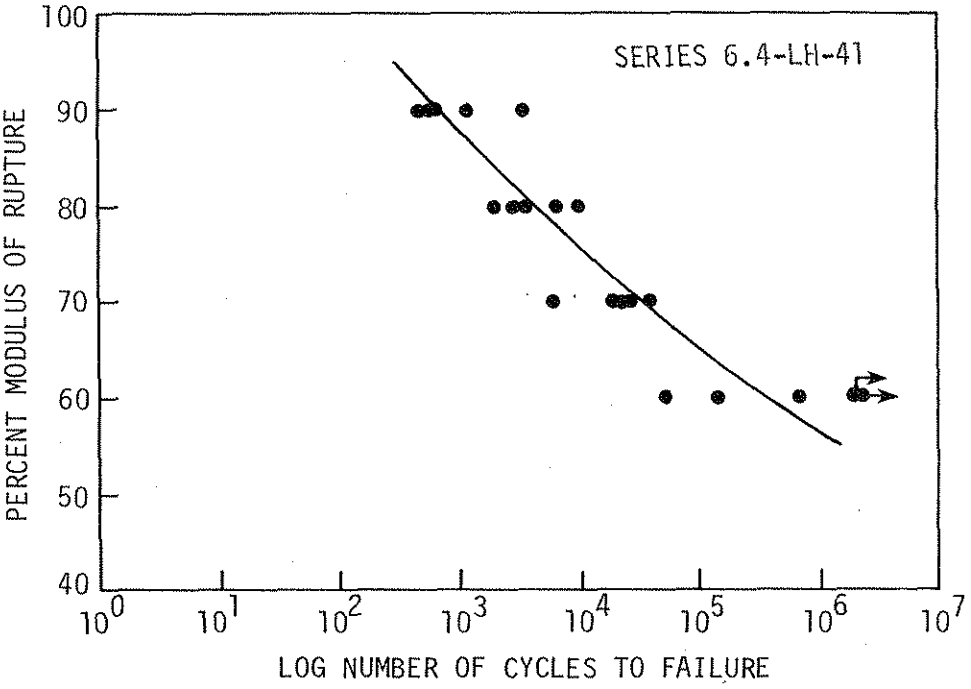

Figure 25. S-N curve for Series 6.4-LH-41.

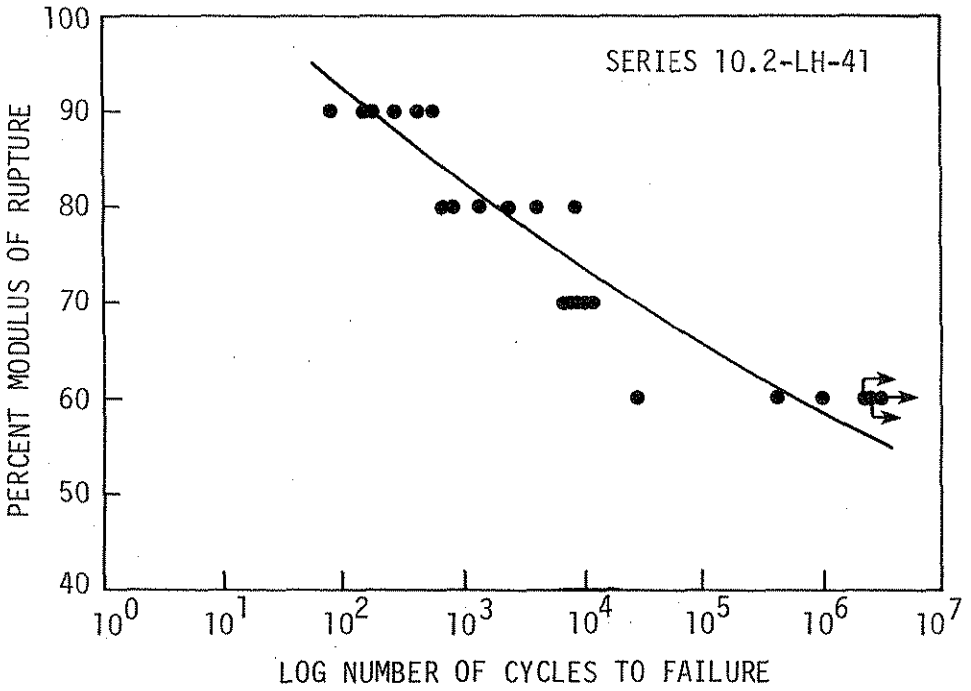

Figure 26. S-N curve for Series 10.2-LH-41.

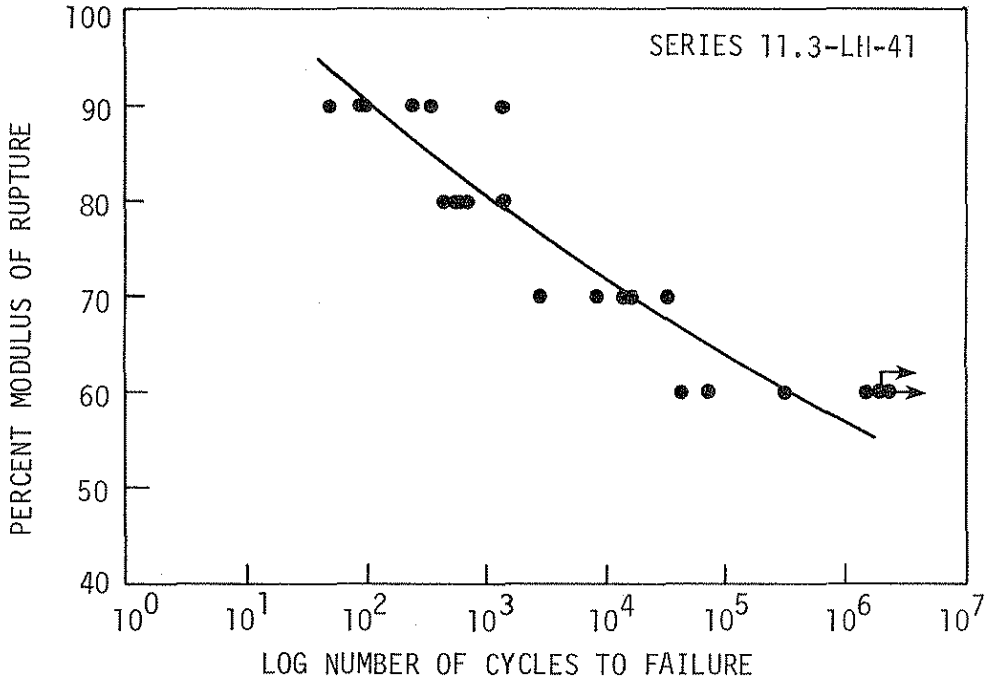

Figure 27. S-N curve for Series 11.3-LH-41.

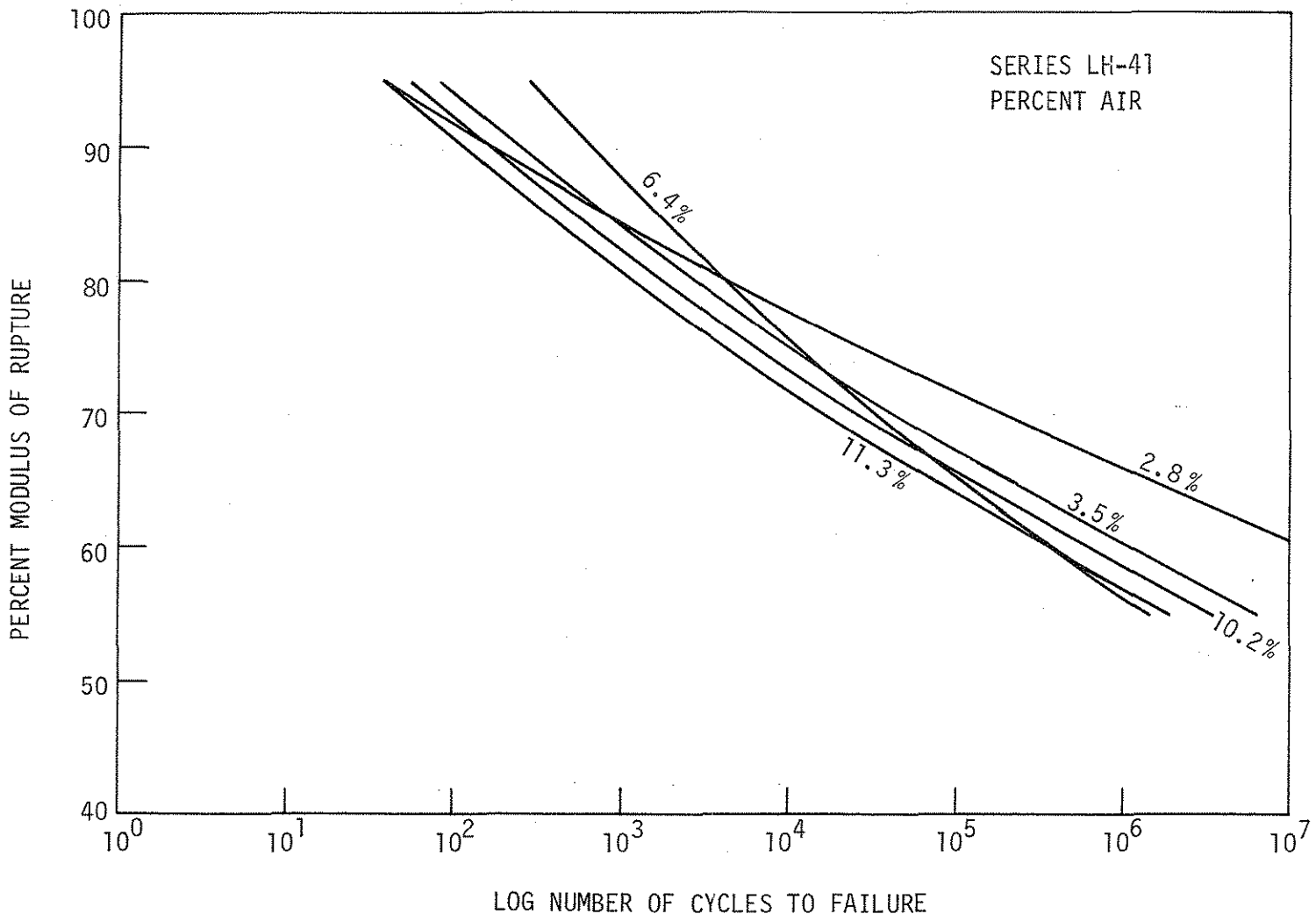

Figure 28. Composite S-N plot for Series LH-41.

Comparing the composite plots, it can be seen that the curves diverge at the lower stress levels. The divergence may not seem to be significant, because these are semi-log plots. For instance, in Series LH-32 (Figure 19), at 70% modulus of rupture, the difference between Series 9.5-LH-32 and Series 3.1-LH-32 is 171,000, while at 60% the difference is 8,260,000. This divergence is important to pavement design since traffic normally causes stresses within these lower stress ranges.

There does not seem to be a general trend when comparing concretes with varying water-cement ratios, keeping the air contents and aggregate types constant. For low air content, the low water-cement ratio (0.32, Series 3.1-LH-32, Figure 9) produces a concrete with a higher fatigue strength than the medium water-cement ratio (0.41, Series 3.5-LH-41, Figure 24) and the high water-cement ratio, (0.60, Series 4.2-LH-60, Figure 17). The concretes made with water cement ratios of 0.41 and 0.60 have similar fatigue strengths. For air contents around 6%, the low water-cement ratio (0.32, Series 5.9-LH-32, Figure 10) seems to produce a concrete with a lower fatigue strength than the medium water-cement ratio concretes (0.43, Series 6.7-LH-43, Figure 15, and 0.41, Series 6.4-LH-41, Figure 25) and the high water-cement ratio concrete (0.60, Series 6.2-LH-60, Figure 18). Again, the 0.43 and 0.60 water-cement ratio concretes produce fatigue curves that are practically incidental, indicating no difference in fatigue life. For air contents around 10%, the low water-cement ratio (0.32, Series 9.5-LH-32, Figure 11) produces a concrete with a much lower fatigue strength than a concrete made with a water-cement ratio of 0.41 (10.2-LH-41, Figure 25). No series at a water-cement ratio of 0.60 at a high air content was

tested. Thus it may be concluded that, for water-cement ratios in the range of 0.40 - 0.60, the flexural fatigue strength is independent of compressive strength.

At a water-cement ratio around 0.40 and at a low air content, the concrete made with gravel (Series 3.9-GH-43, Figure 12) exhibited a higher fatigue strength at the higher stress levels than the concrete made with limestone (Series 3.5-LH-41, Figure 24). At the lower stress levels there did not seem to be a significant difference in fatigue strength. At the water-cement ratio around 0.40 and at an air content around 6%, there was not a significant difference in the fatigue strength of the concrete made with gravel (Series 6.9-GH-43, Figure 13) versus that made with limestone (Series 6.7-LH-43, Figure 15, and Series 6.4-LH-41, Figure 25). At high air contents the concrete made with gravel (Series 14.2-GH-43, Figure 14) had a higher fatigue strength than the concretes made with limestone (Series 10.2-LH-41 and 11.3-LH-41, Figures 26 and 27).

The fatigue strength of Series 5.5-LB-43 (Figure 16), the one series made with a high quality of fine aggregate, was not significantly different from the fatigue strength of Series 6.7-LH-43 which was made at the same water-cement ratio and essentially the same air content but with Hallett concrete sand.

The reproducibility of the fatigue curves may be seen by comparing Series 6.9-LH-43 (Figure 21) and Series 6.4-LH-41 (Figure 28). Although there is a slight difference in the air content and water-cement ratio, the curves are essentially identical.

4.2. Characterization of Air Voids System

In addition to the total air content, the effect of air entrainment on the air bubbles and pore size distribution of hardened concrete was studied by scanning electron microscope (SEM) and mercury penetration porosimetry.

Samples examined were fragments of the mortar matrix of hardened concrete from each series taken from the same beam specimen that was used for high pressure air content determination.

The principles of operation and instruments used for SEM and mercury penetration porosimetry were described in a previous report [21]. The general procedures followed in this study were identical to those of Phase I except that several representative fragments of concrete pieces (6 - 10 gm) rather than drilled cores were used in mercury intrusion tests.

Because of (a) the small specimens that SEM and mercury intrusion techniques can accommodate, (b) the presence of large aggregate particles making the selection of representative samples for examination difficult, and (c) air voids mainly distributed in the paste-mortar matrix, additional mortar specimens were prepared to determine the effect of the air-entraining agent on the void characteristics as shown by SEM and mercury porosimetry. Two batches of mortar of plastic consistency were prepared using Hallett concrete sand and three batches of mortar were made using ASTM C-109 graded Ottawa sand, all at a constant water-cement ratio of 0.41 but at different levels of air-entrainment. Sand content was adjusted to give a flow of 90%. The air content of the mortar was determined in accordance with ASTM C-185. After air content determinations, the fresh

mortars were placed in molds 20 mm in diameter by 25 mm high, externally vibrated with an electric inscriber, and allowed to set in the humidity room for 24 hours. The cylindrical specimens were then removed from the molds and cured for 7 and 28 days for compressive strength and examined for pore size and size distribution by SEM and mercury penetration porosimetry. To facilitate easy fracture for SEM examination, some specimens in each batch were molded in two layers with an aluminum foil disk having a 5-mm diameter hole at the center placed between the layers, resulting in a weakened middle section of smaller diameter. Bulk specific gravity and water absorption of the 28-day mortar cylinders were determined following ASTM C-127. The composition and characteristics of the mortar specimens are given in Table 5.

4.2.1. Air-Entrained Concrete

A JEOL/JSM-U3 scanning electron microscope was used to examine visually the voids system of mortar fragments of hardened concrete from all batches. The specimens were mounted, coated with gold and viewed under SEM. Photomicrographs were made at 100X magnification. These micrographs were compared with Phase I micrographs and photographs reported by Mullen and Waggoner [30] on hardened concrete of various air contents (1 - 20%). The same conclusions as observed in Phase I can be applied to Phase II specimens as well as photographs presented by Mullen and Waggoner, that is:

- The introduction of air-entraining agent increased the number of bubbles, the bubble density, and the uniformity of air bubbles.

Table 5. Characteristics of air-entrained mortars (w/c = 0.41)

	Standard Sand (ASTM C 109)			Concrete Sand	
Sand, g	800	800	800	900	900
Cement, g	350	350	350	350	350
Water, g	143.5	143.5	143.5	143.5	143.5
Ad Aire, g	0	0.23	0.70	0	0.30
Fresh air content, %	7.46	9.68	14.55	4.19	9.30
Avg. 7 day compressive strength (psi)	992.3	1298.7	1685.8	1932.7	1225.7
Avg. 28 day compressive strength (psi)	1914.1	1943.8	2096.6	3127.9	1872.5
Bulk specific gravity	2.198	2.160	2.075	2.229	2.162
Absorption (%)	7.19	7.39	7.97	7.96	7.92
Water Permeable Porosity, %	15.80	15.96	16.53	17.74	17.12
Total porosity (mercury porosimeter), %	13.2	13.5	15.9	14.1	12.1

- Air bubbles in air-entrained concrete consist of a uniform distribution of very small air voids, mostly between 0.02 and 0.10 mm (20 and 100 μm); few are as large as 0.2 mm and some are as small as 0.005 mm (5 μm); they are usually spherical in shape. The interior of most air bubbles is usually smooth in appearance.
- The air bubbles of the non-air-entrained concrete can usually be characterized by a lack of intermediate size bubbles, presence of large bubbles (as large as 2 mm), and by bubbles of more irregular shapes and rough interior texture.

The porosimeter used in this study was a Micromeritics Model 905-1 Mercury Penetration Porosimeter. It has a pressure range from about 2.7 to 50,000 psi for a large sample cell. Using a mercury surface tension of 474 dyn/cm at 25°C and a contact angle with concrete at 130°, it is possible to measure pore diameters between 65.5 and 0.00354 μm. The maximum pressures applied during this work were between 34,000 and 37,000 psi. Several representative mortar fragments broken from the hardened concrete (6 to 10 gm) were used in the tests. The pore size distribution data are presented in two ways: (a) percent of total pore volume in various pore diameter ranges (Figures 29, 30 and 31) and (b) cumulative pore volume as percent of bulk volume of concrete vs. pore diameter (Figures 32, 33 and 34). The pore size distributions in terms of pore volume as percent of concrete volume for the concrete studied in Phase II are given in Table 6. The following can be observed:

- As the air content increases, there is an increase in total pore volume. This increase was mainly reflected in the volume of pores with diameter larger than 1 μm. The consistent increase in pore volume between 1 and 10 μm with increasing air content suggests that it was the direct result of air entrainment.

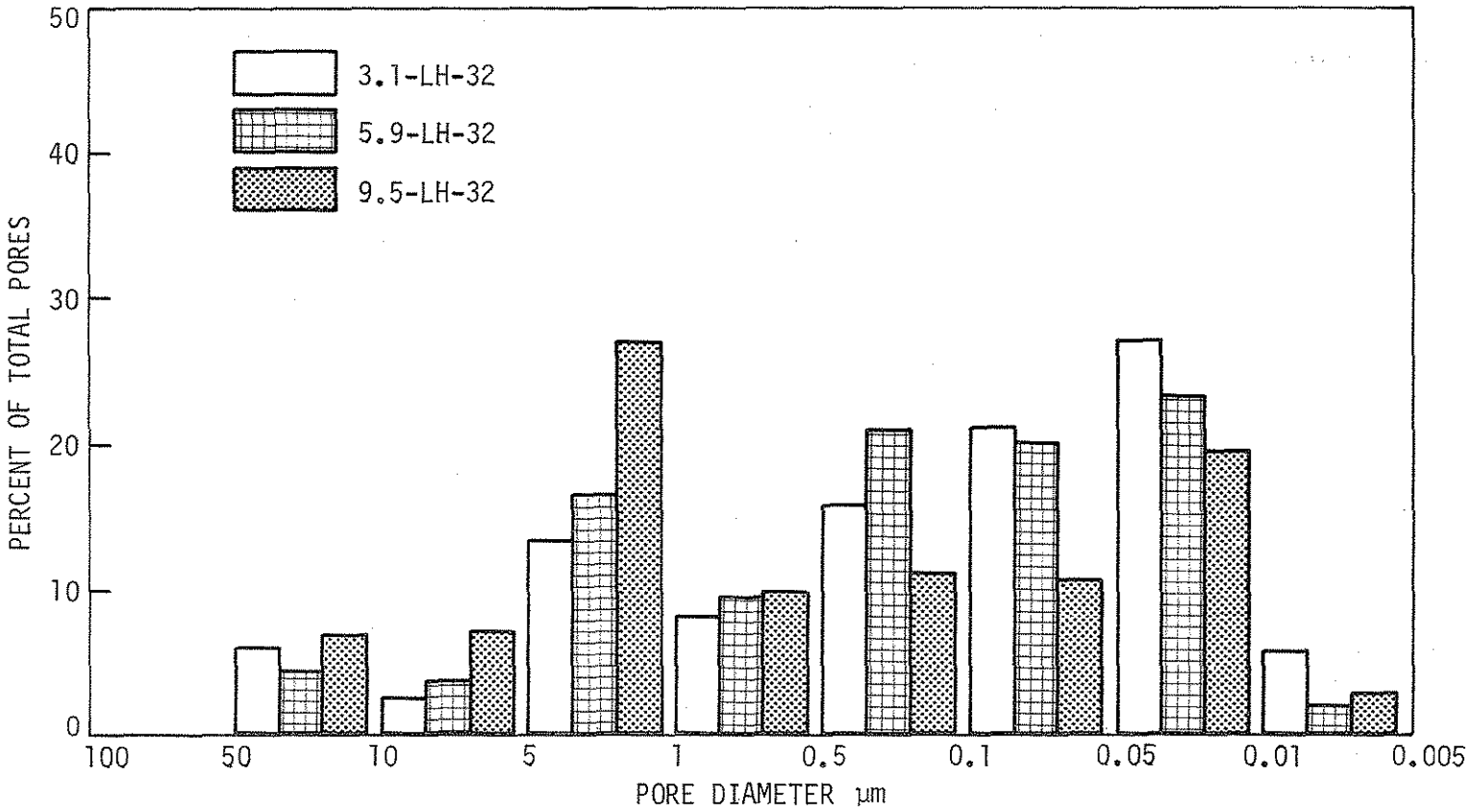

Figure 29. Pore size distribution of concrete (w/c = 0.32).

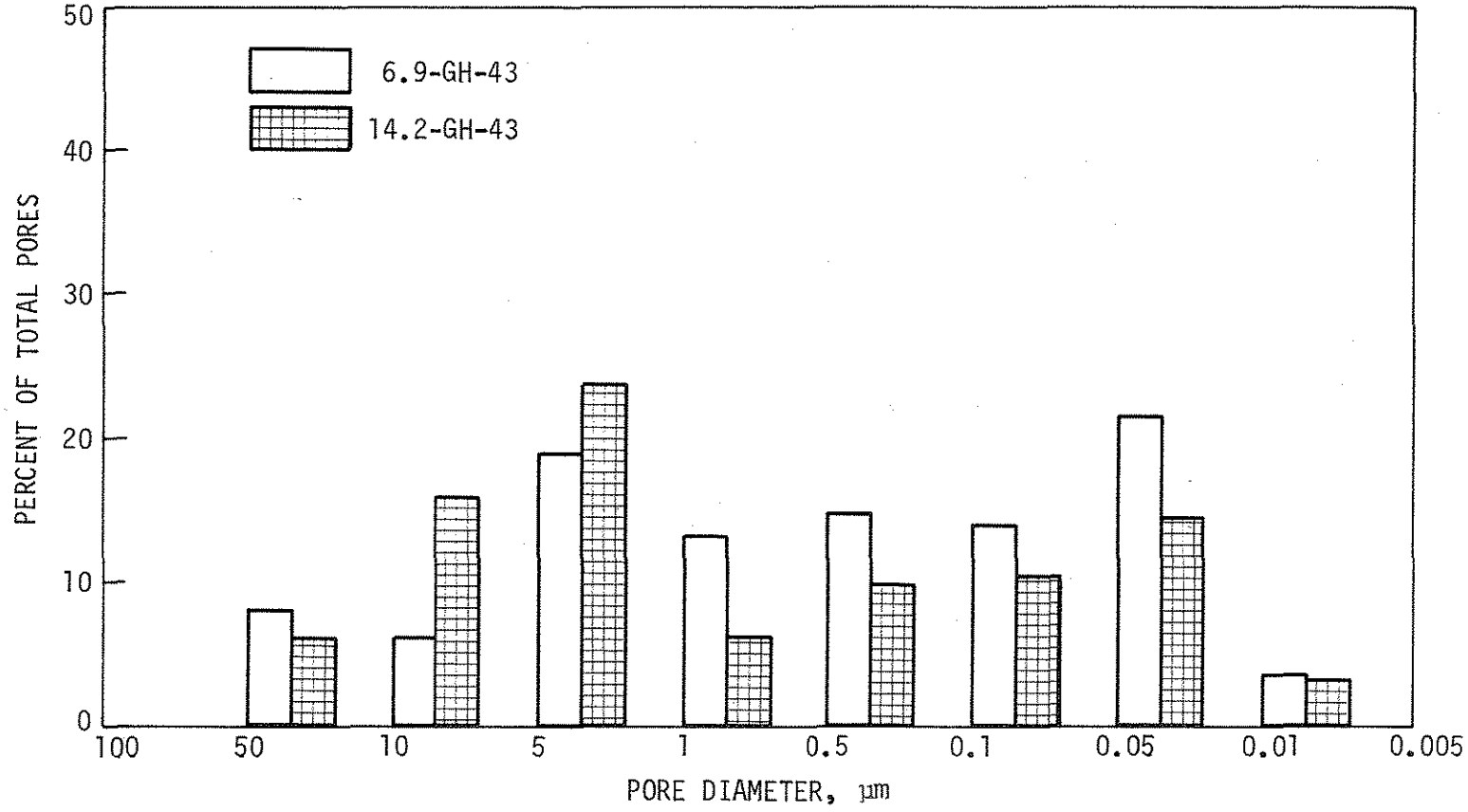

Figure 30. Pore size distribution of concrete (w/c = 0.43).

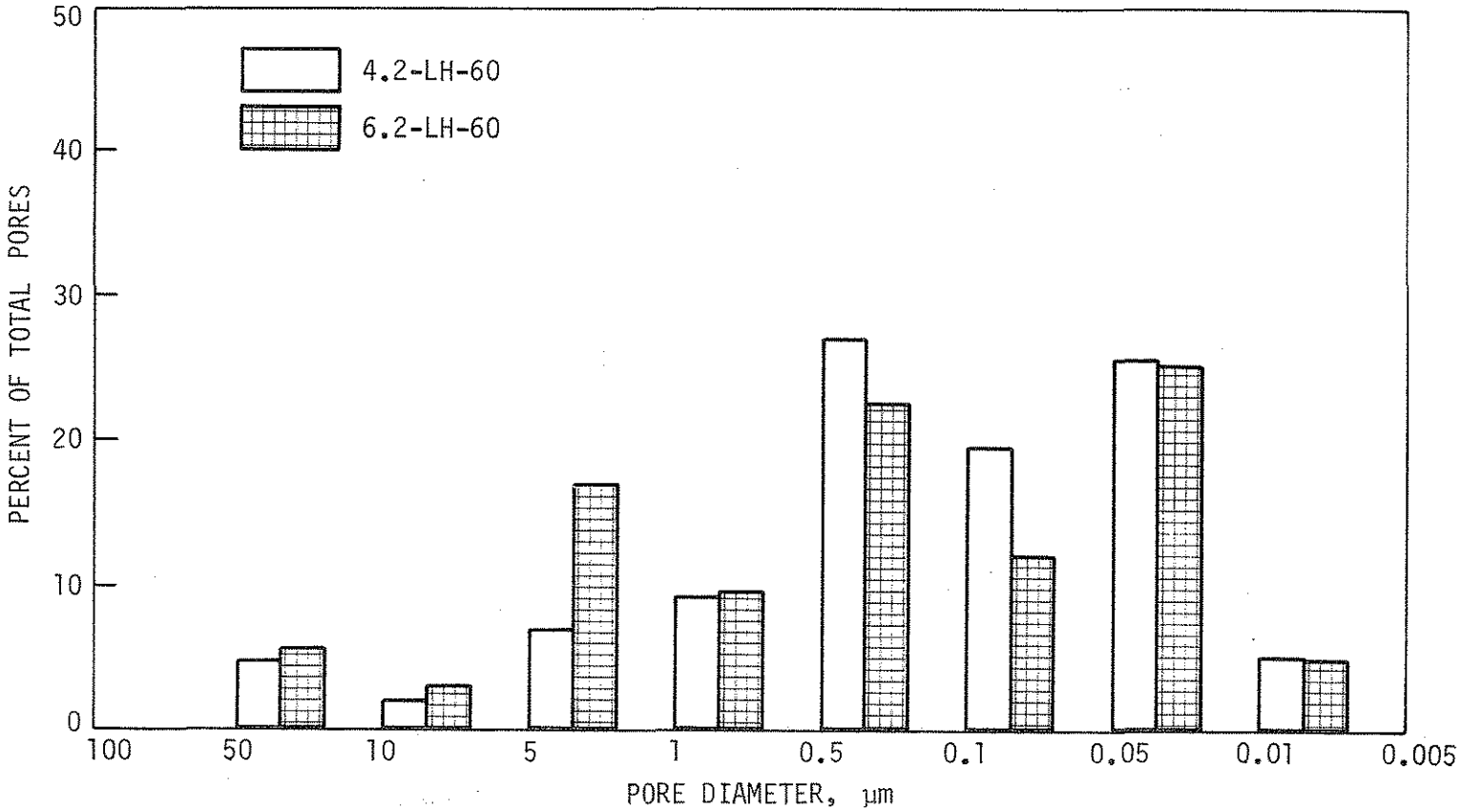

Figure 31. Pore size distribution of concrete (w/c = 0.60).

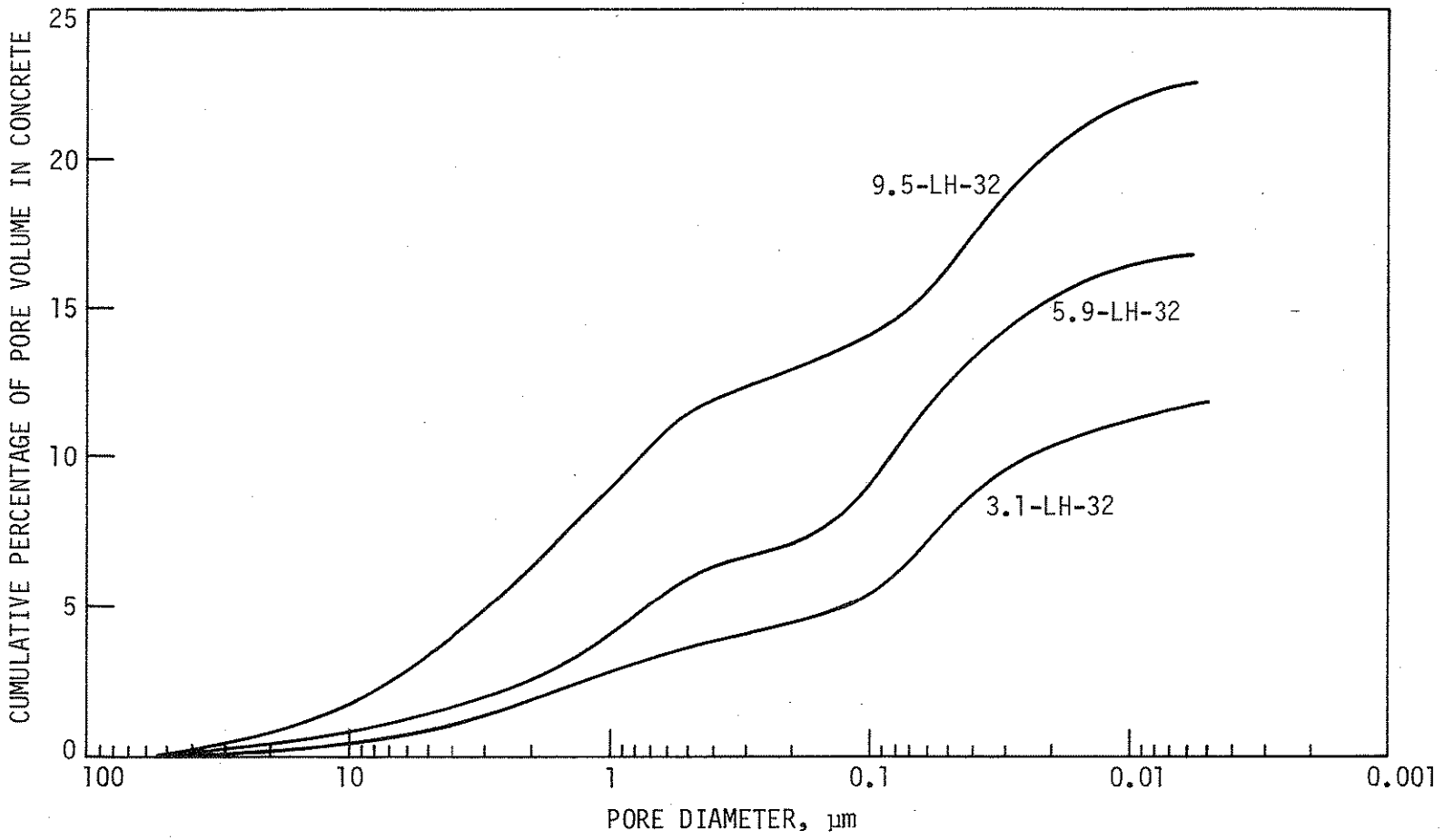

Figure 32. Cumulative pore volume as percent of bulk volume of concrete vs. pore diameter (w/c = 0.32).

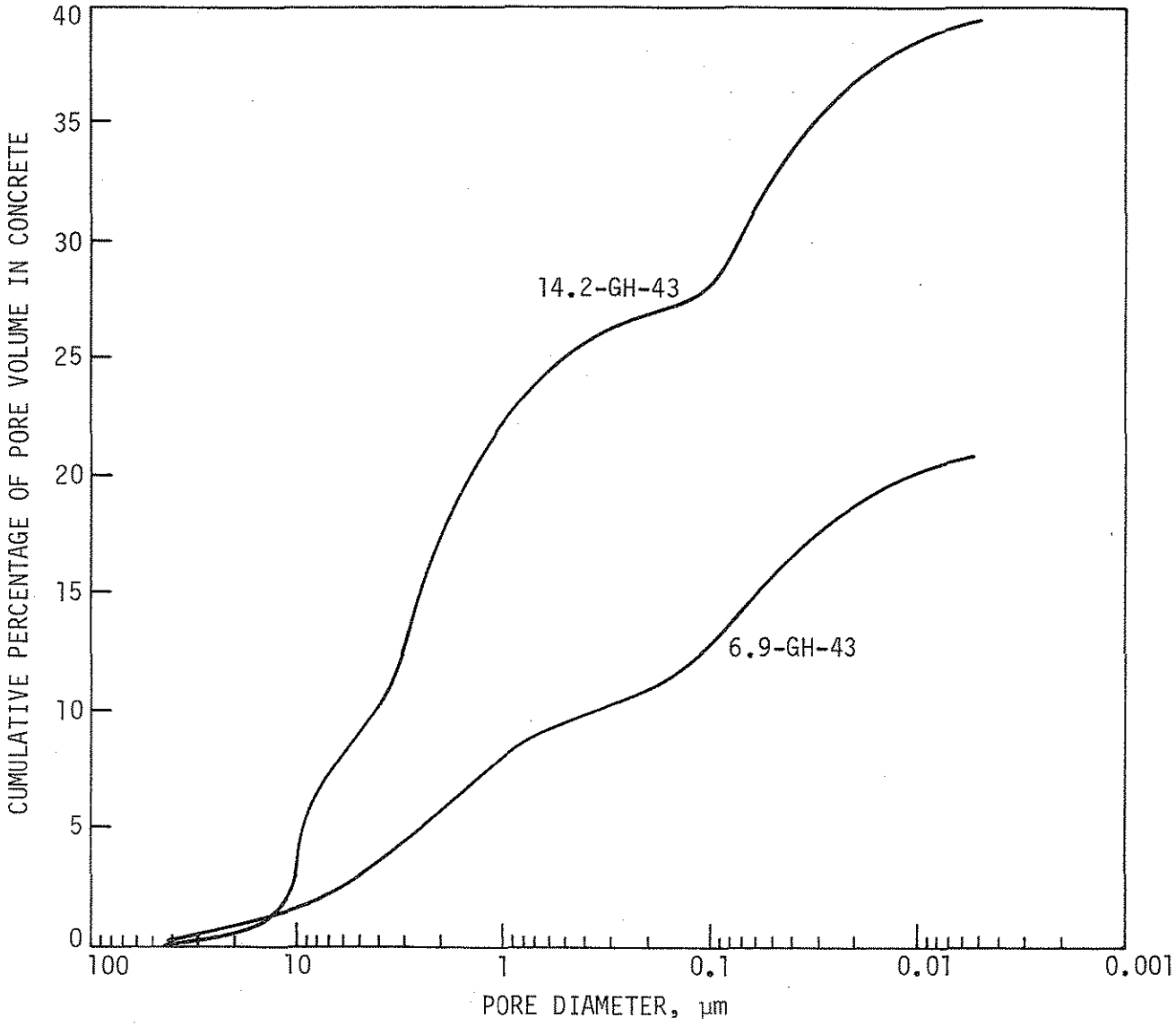

Figure 33. Cumulative pore volume as percent of bulk volume of concrete vs. pore diameter (w/c = 0.43).

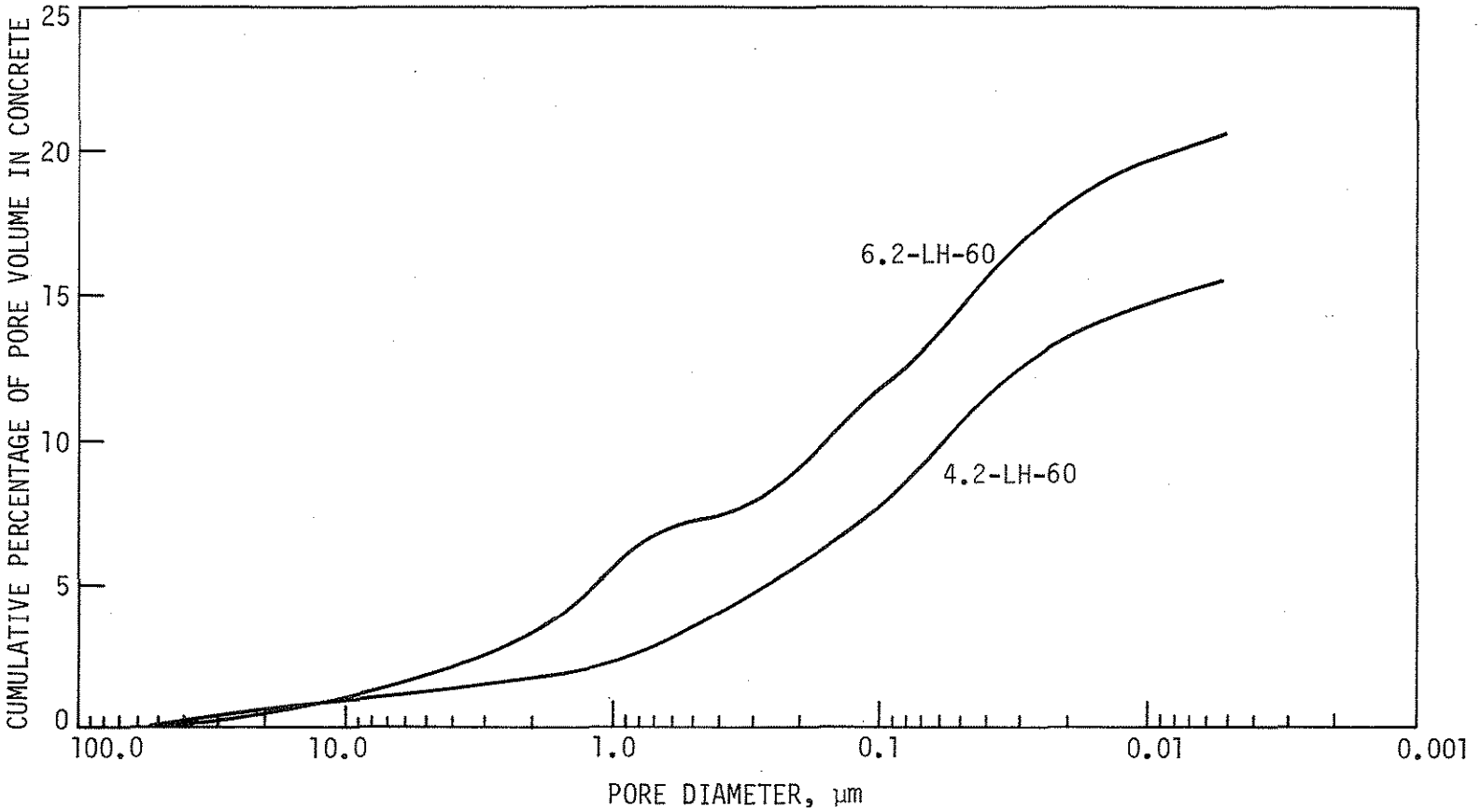

Figure 34. Cumulative pore volume as percent of bulk volume of concrete vs. pore diameter (w/c = 0.60).

Table 6. Pore size distribution, % pore volume in concrete.

			Pore Size, μm						
Aggregate	w/c	Air, %	>10	10-5	5-1	1-0.5	0.5-0.1	<0.1	Total
LH	0.32	3.1	0.7	0.3	1.6	0.9	2.2	6.1	11.8
		5.9	0.7	0.5	3.0	1.5	3.3	7.7	16.7
		9.5	1.7	1.5	5.9	2.1	2.9	8.4	22.5
GH	0.43	6.9	1.4	1.6	4.9	1.7	3.1	8.0	20.7
		14.2	2.6	6.6	13.0	2.7	3.2	11.1	39.2
LH	0.43	6.7	1.2	1.0	5.5	1.8	3.5	11.5	24.5
LB	0.43	5.5	0.8	0.7	1.4	1.6	2.7	6.4	14.6
LH	0.60	4.2	1.0	0.4	0.9	1.1	4.8	7.7	15.5
		6.2	1.1	0.7	3.6	2.3	4.3	8.6	20.6

- As water-cement ratio increases, "capillary/gel" porosity (difference between total porosity and air content) increases.
- Entrained air bubble size distribution for sizes larger than 1 μm was not affected by coarse and fine aggregate type.
- The median pore diameter increased with total air content.

4.2.2. Pore Structure of Mortars

Fragments of mortar specimens were subjected to studies by scanning electron microscope at magnifications from 100X to 3,000X. However, these efforts were not very rewarding. No significant differences could be detected by the micrographs of different mortars.

The pore size distributions of the mortar cylinders from each composition were determined by the mercury penetration porosimeter. In order to better characterize the pore shapes of the specimens, the second intrusion method [8] was used. In this method, the specimen is intruded by the mercury a second time.

The second intrusion pore-size distribution curve indicates pores with more or less uniform cross sections while the difference in pore volume between the first and the second intrusion curves indicates the pores with enlargements or constrictions (ink-bottle pores). The pore-size distribution curves of mortars made with standard ASTM C-109 sand are shown in Figures 35 and 36.

Comparison of Figure 35 and Figure 36 shows that the second intrusion pore size distribution curves of the two mortars are almost identical. The difference in air content is reflected in the higher pore volume of the first intrusion curve of the mortar containing higher air content (Figure 36) and its higher volume of ink-bottle pores. It can be concluded that air entrainment introduces only large ink-bottle pores and does not affect the pore volume and size distribution of small uniform and, presumably, capillary/gel pores.

Figure 37 shows the effect of air content on the first intrusion pore-size distributions of mortars made with standard sand. Again it appears that the air entrainment increased the percent of pores mainly in the 1 to 50 μm range.

4.3. Applications to Concrete Pavement Design

The principal design considerations for the Portland cement concrete pavement thickness by the PCA procedure [40] are:

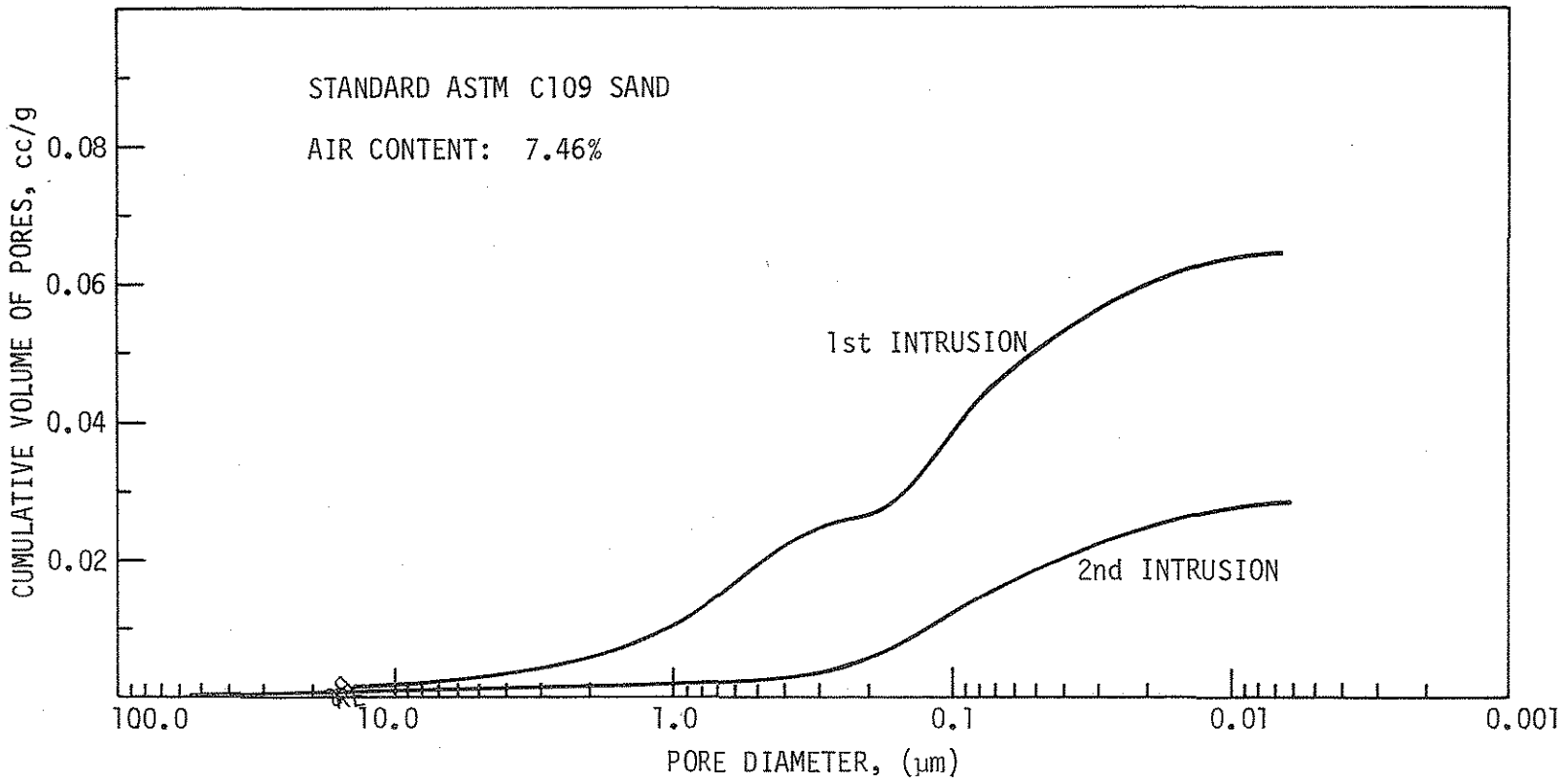

Figure 35. Pore size distribution of hardened mortar (standard sand; air content = 7.46%).

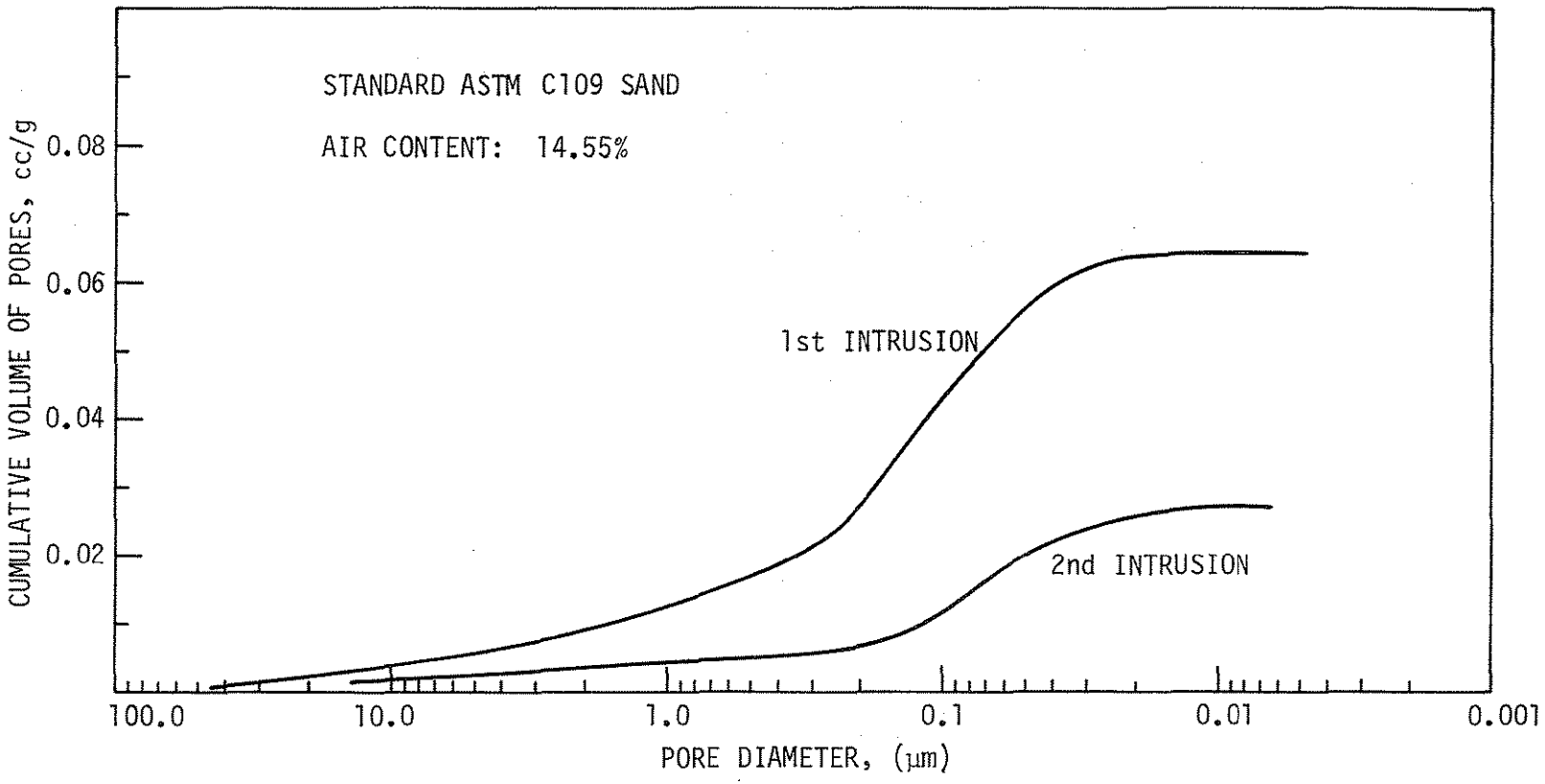

Figure 36. Pore size distribution of hardened mortar (standard sand; air content = 14.55%).

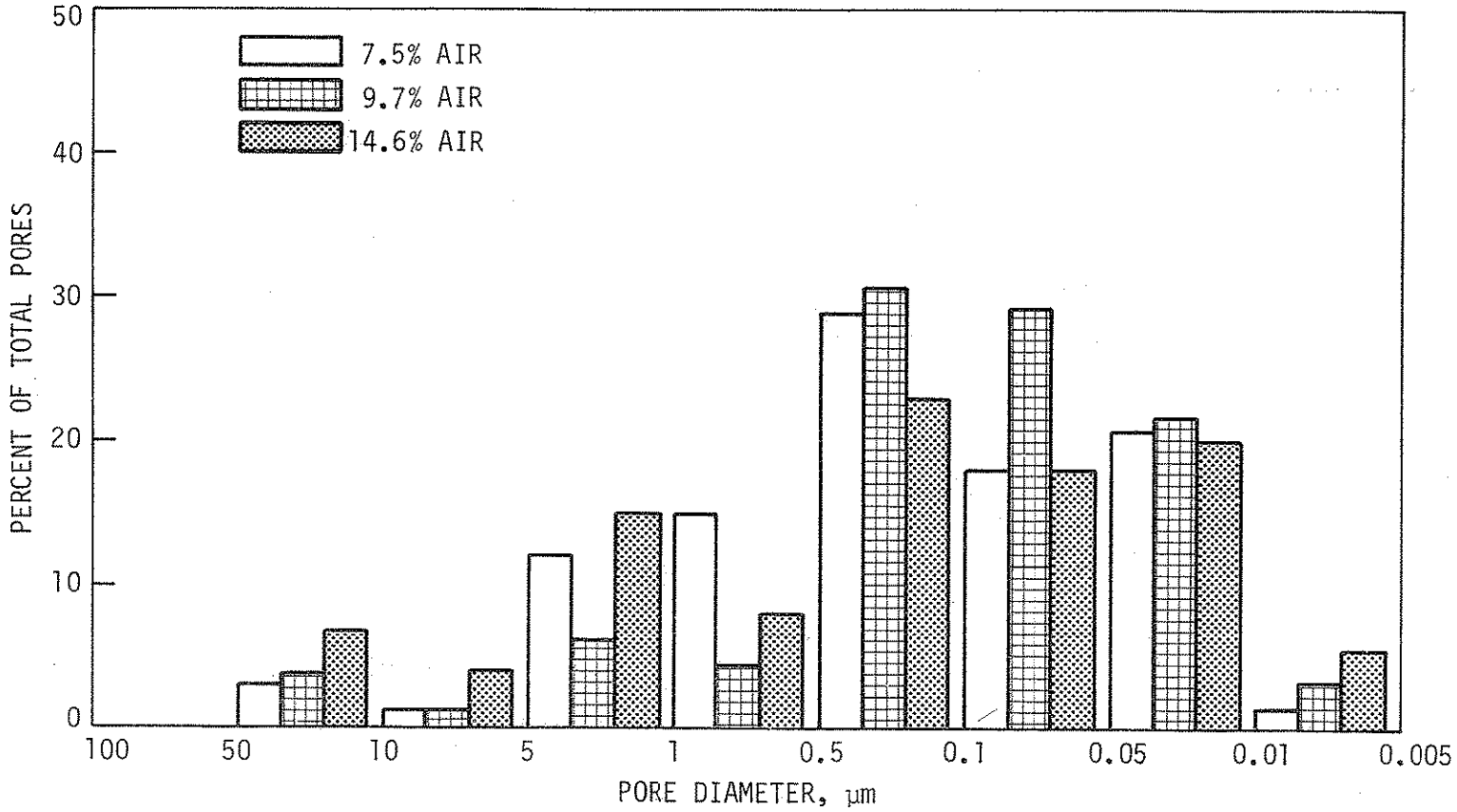

Figure 37. Pore size distribution of mortars, standard sand.

1. The pavement thickness is a function of the modulus of rupture of the concrete, the applied load, and the subgrade modulus k;
2. The fatigue failure in flexure is the key to thickness requirements and its effects are considered by the use of a linear summation of cycle ratios to account for mixed traffic loading and the cumulative fatigue damage (Minor's hypothesis); and
3. The thickness design makes use of a general fatigue curve (or table) in which the ratio of applied stress to the modulus of rupture is related to the allowable number of stress applications.

The 1933 PCA fatigue curve shown in Figures 38-41 is based on the research conducted by the Illinois Department of Highways and Purdue University in the early 1920s. This curve was used with Minor's hypothesis to estimate the accumulated fatigue damage in order to design a pavement of adequate thickness. Minor's hypothesis applies to stress repetitions above the endurance limit and postulates that fatigue strength not used by repetitions at one stress level is available for repetitions at other stress levels. The 1933 fatigue curve was replaced by the present 1966 curve, also shown in Figures 38-41, partly because of the work of Hilsdorf and Kesler [15] in the early 1960s and partly because of theoretical analysis, full scale test roads, and observations of pavements in normal service.

The fatigue curve that is the result of the work by Hilsdorf and Kesler, shown in Figures 38-41, represents a constant probability of 0.05. Use of the Hilsdorf and Kesler curve in pavement design calculations gave reasonable results, and their curve was considered for replacement of the

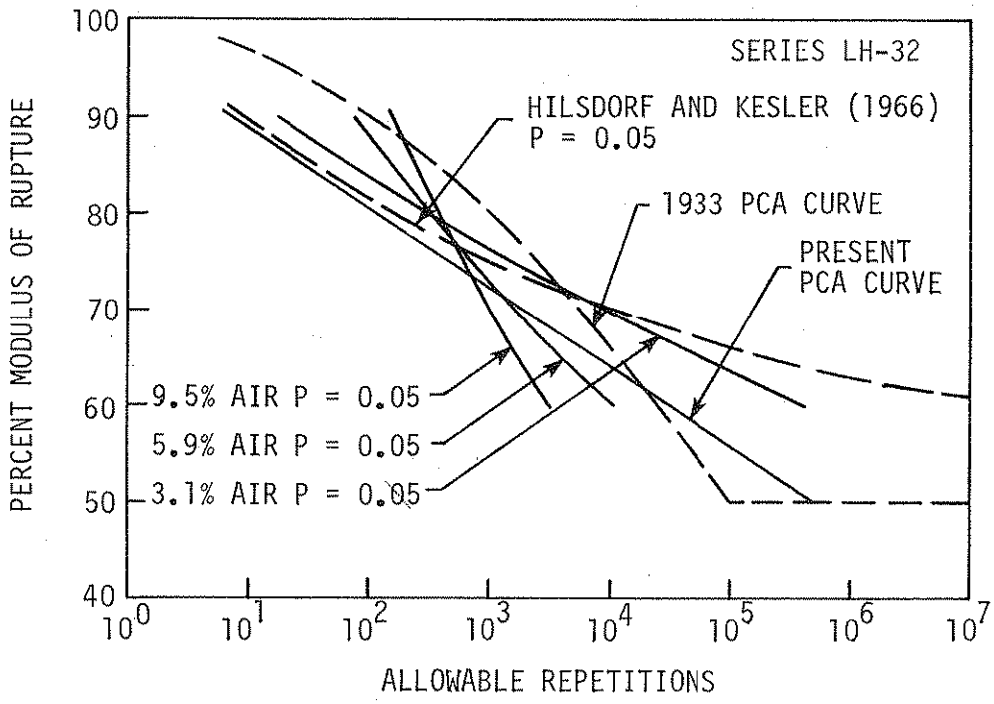

Figure 38. Comparison of pavement fatigue design curves with Series LH-32.

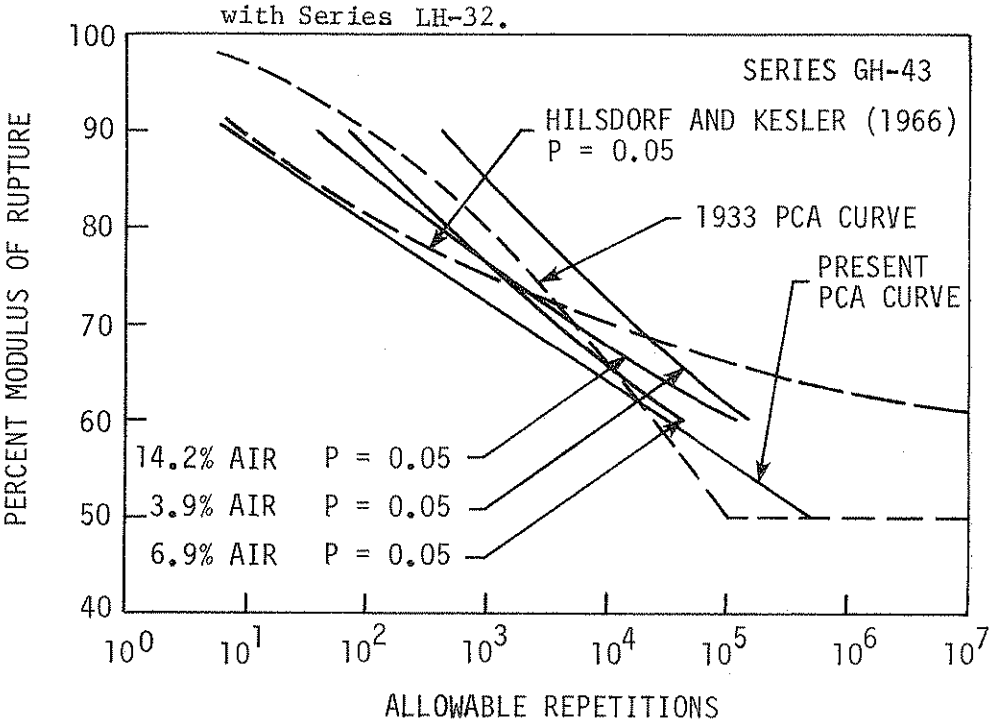

Figure 39. Comparison of pavement fatigue design curves with Series GH-43.

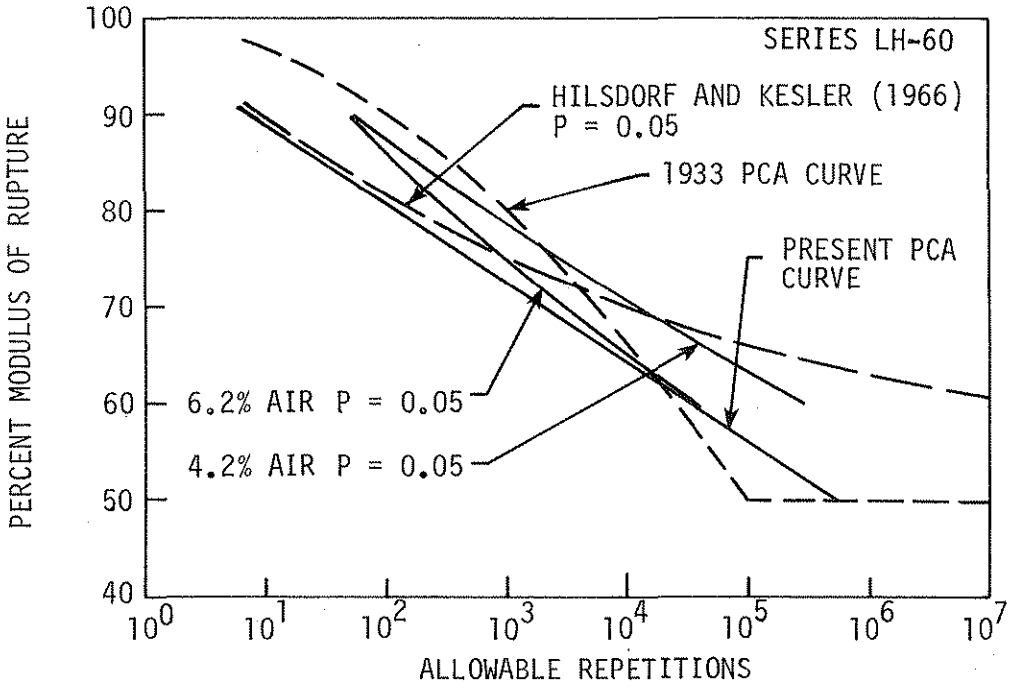

Figure 40. Comparison of pavement fatigue design curves with Series LH-60.

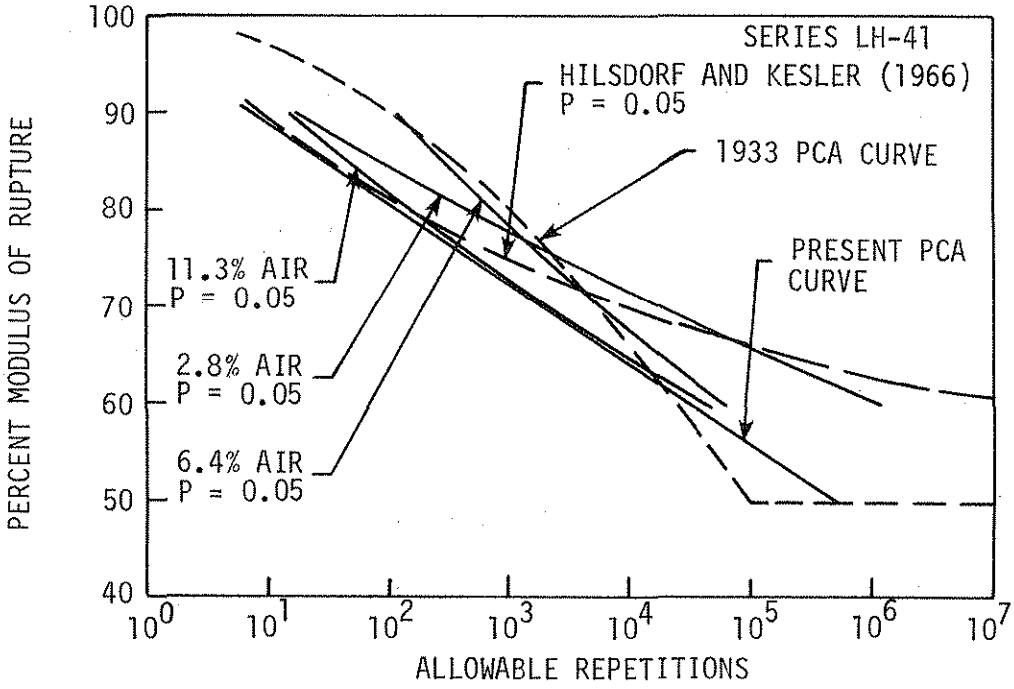

Figure 41. Comparison of pavement fatigue design curves with Series LH-41.

1933 PCA curve. However, Hilsdorf and Kesler felt their research was too limited for general use and therefore, the 1966 PCA curve was adopted. The 1966 PCA curve is based on additional research, test roads that were loaded with controlled test traffic, and performance of normally constructed pavements currently in use.

For design purposes, fatigue curves at 0.05 probability were generated for the results obtained from both Phase I and Phase II of this study by use of the computer program CENSOR (Appendix C). These curves are shown in Figures 42-46 and represent a constant probability of 0.05, which means that for 100 fatigue tests at any one stress level, not more than five would fail at load applications less than that indicated by the curve. For easy comparison with the PCA values and design usage, the information given by these curves is shown in tabulated form in Tables D-1 to D-6 of Appendix D.

Design curves resulting from this investigation are also shown in Figures 38-41 for comparison with the PCA curves and the work of Hilsdorf and Kesler. Since these curves represent a constant probability of 0.05, they can be compared directly with the work of Hilsdorf and Kesler. It should be remembered that the curve presented by Hilsdorf and Kesler is the result of varying stress fatigue, while findings of this study are the result of constant stress fatigue.

From Figures 38-41 it may be observed that the present PCA fatigue curve is conservative with respect to the Hilsdorf and Kesler curve as well as to most of the curves of this study. However, as may be seen in Figure 38, the present PCA curve overestimates the fatigue strength in terms of allowable load applications for a low water-cement ratio, 0.32,

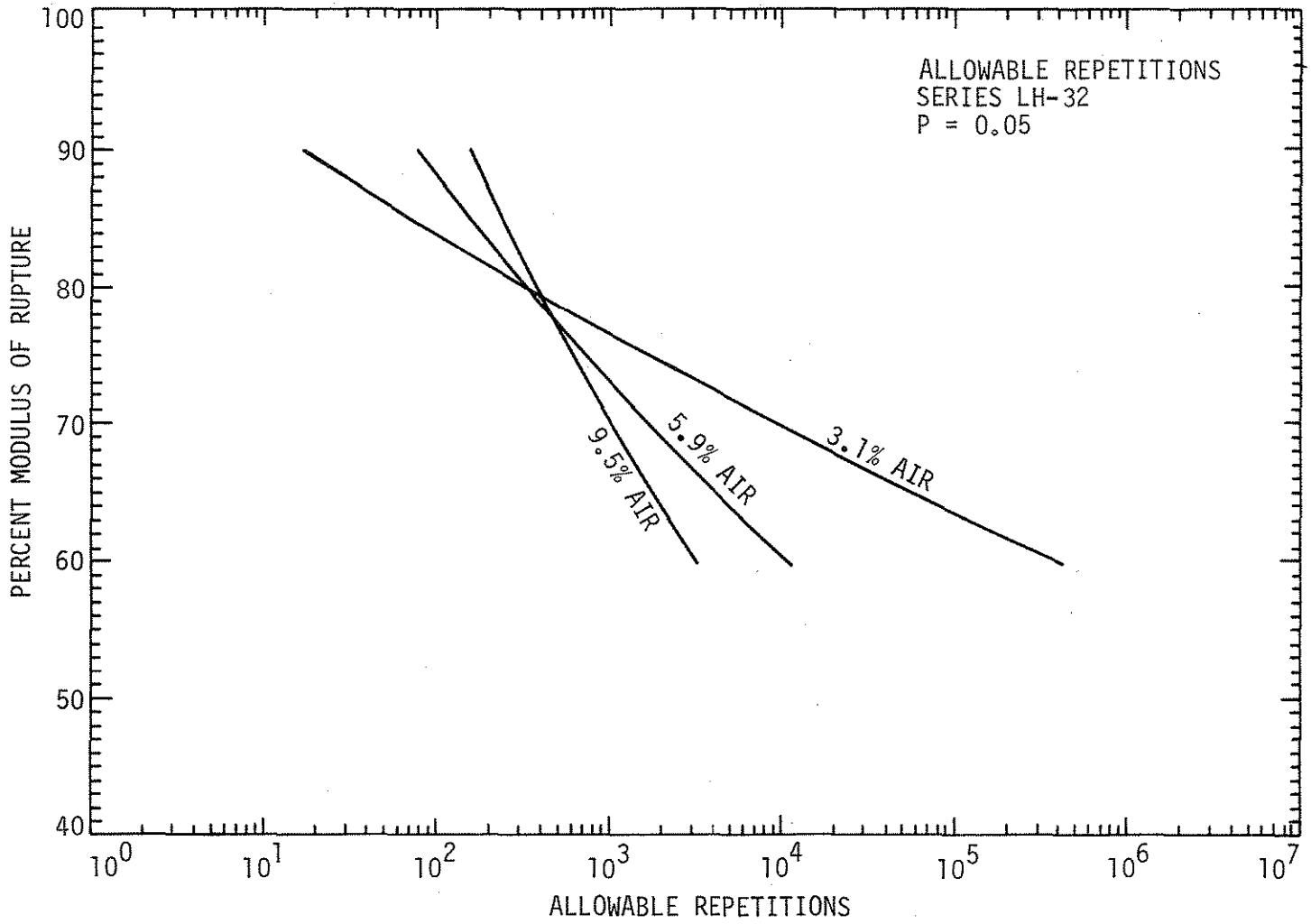

Figure 42. S-N curves showing allowable repetitions for Series LH-32.

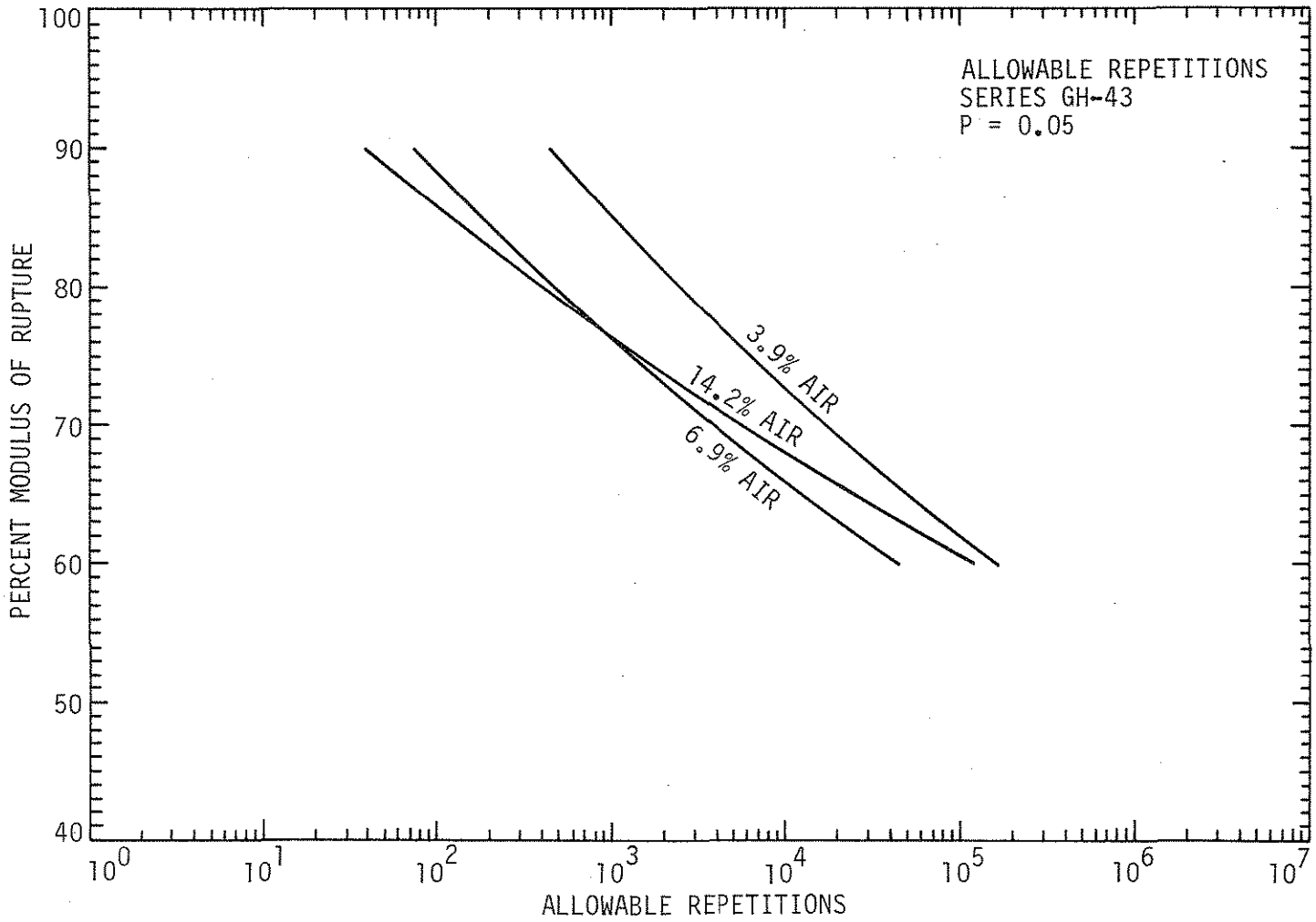

Figure 43. S-N curves showing allowable repetitions for Series GH-43.

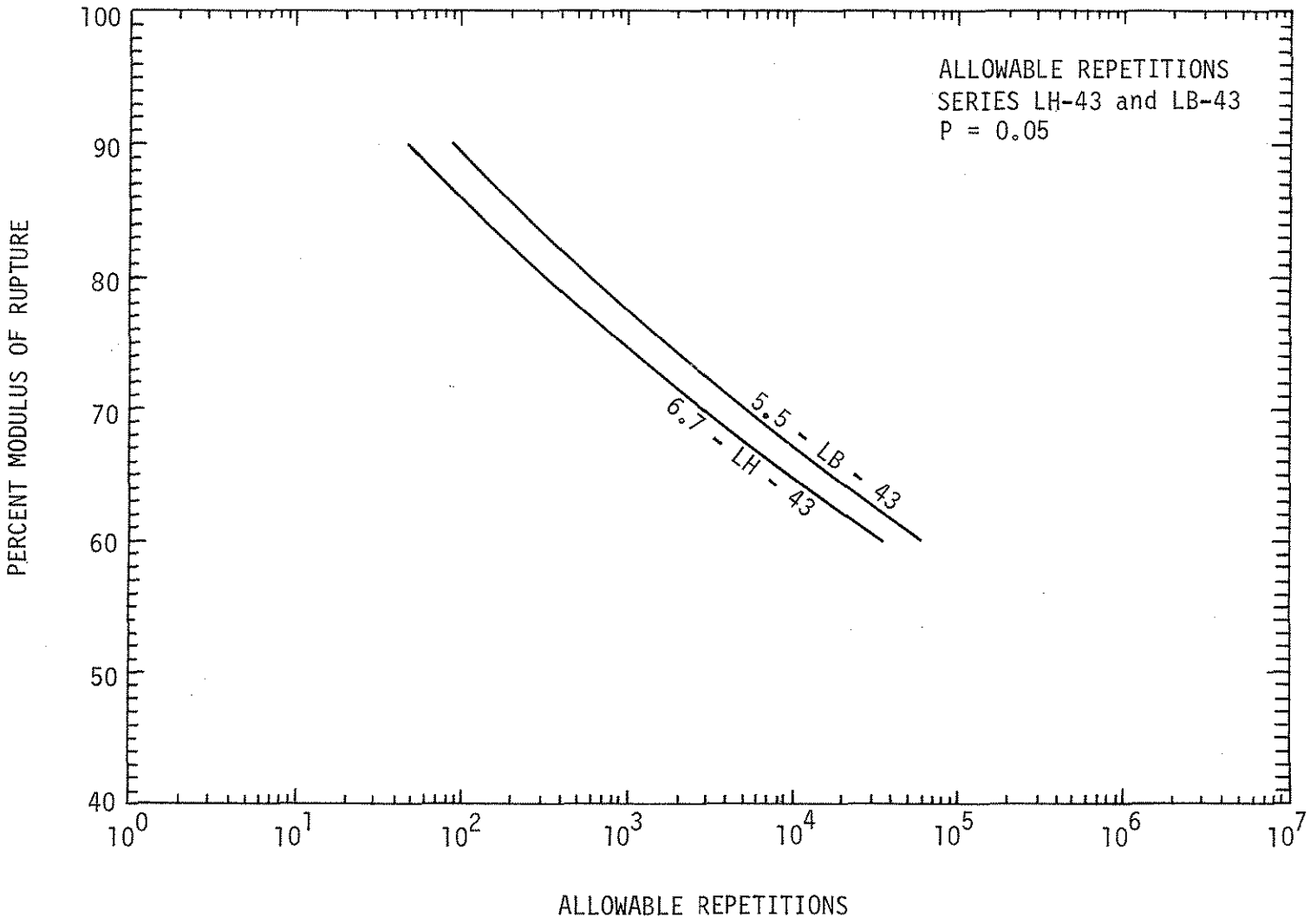

Figure 44. S-N curves showing allowable repetitions for Series LH-43 and LB-43.

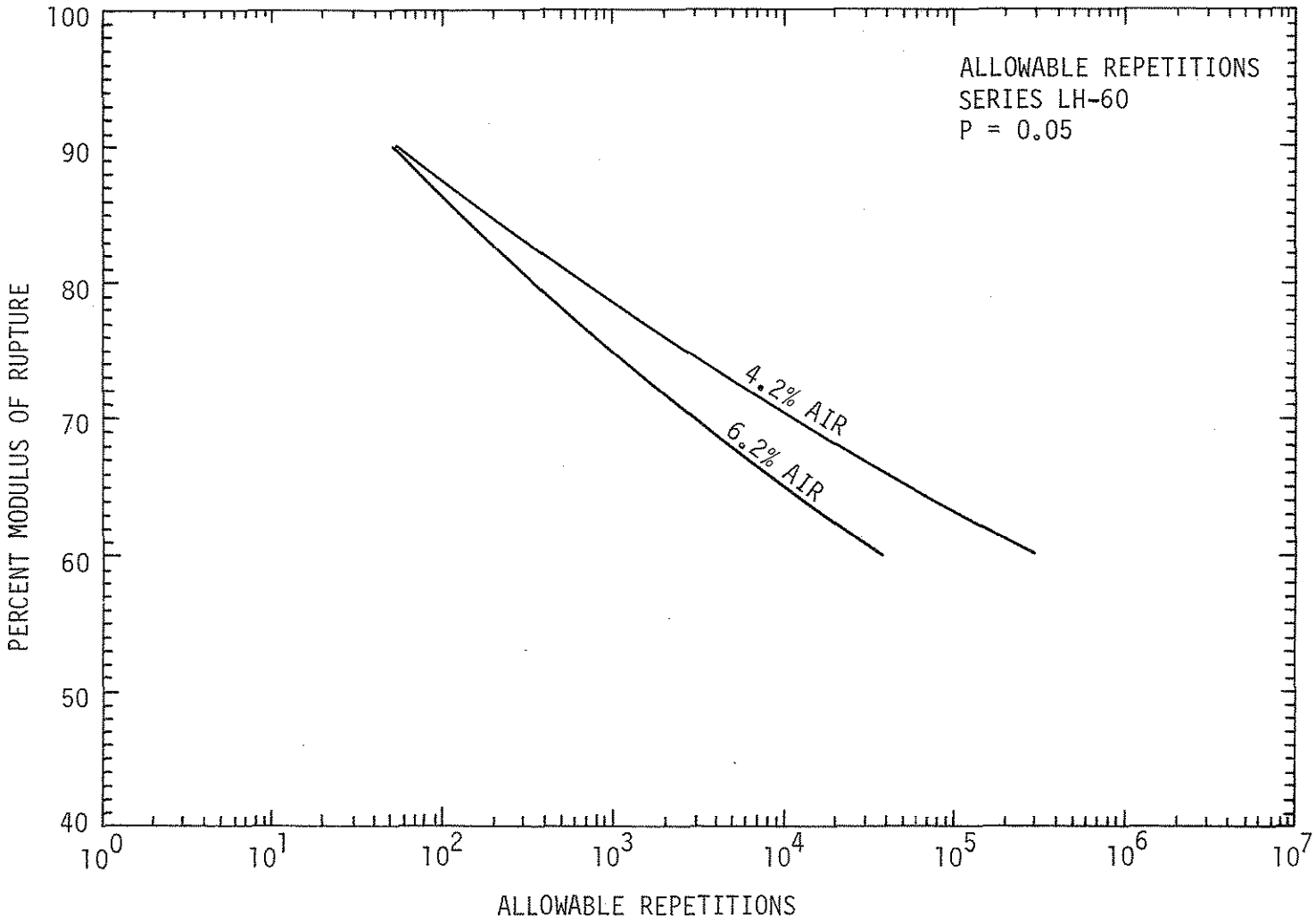

Figure 45. S-N curves showing allowable repetitions for Series LH-60.

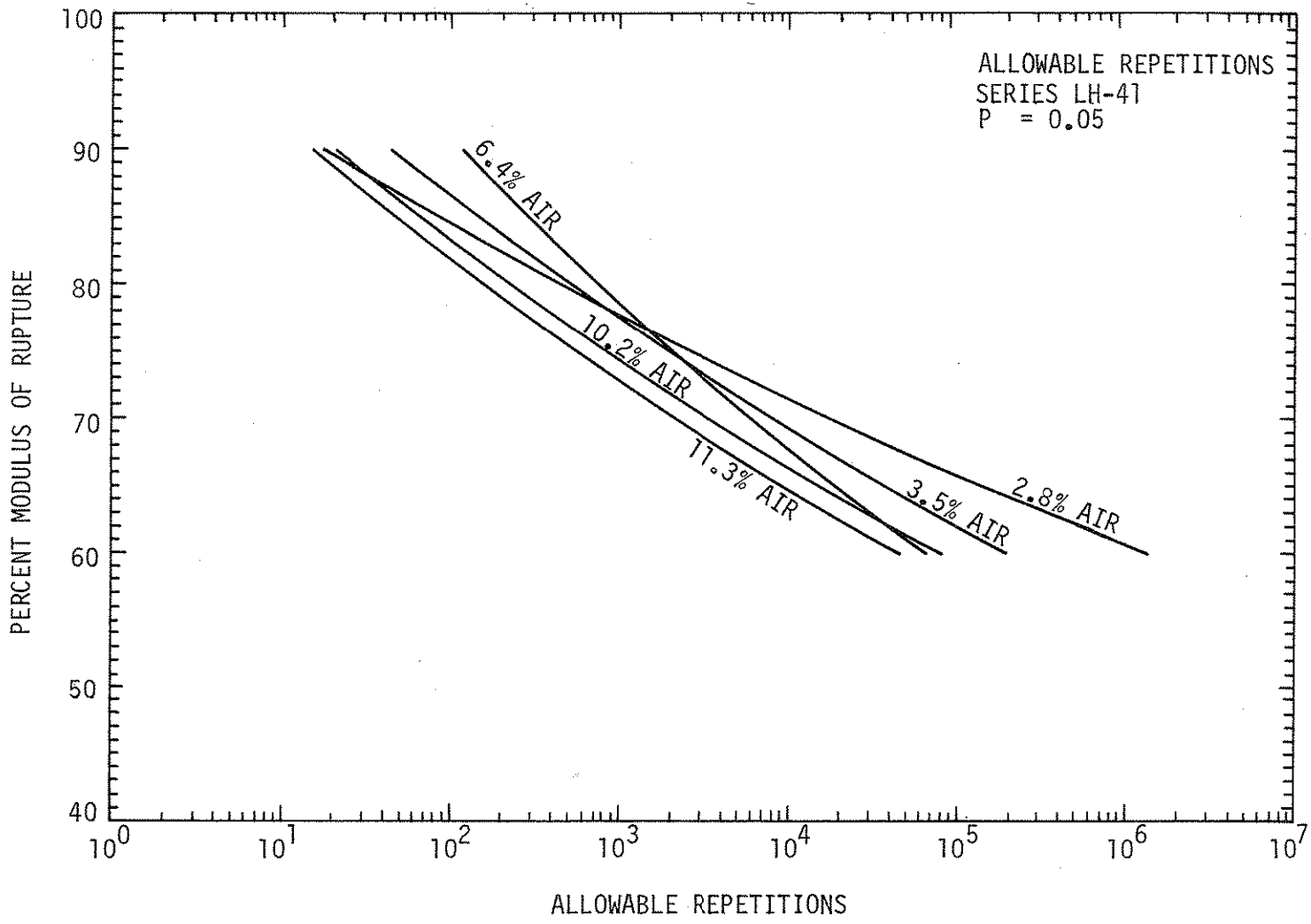

Figure 46. S-N curves showing allowable repetitions for Series LH-41.

at medium to high air contents. In other words, a concrete pavement with a water-cement ratio of 0.32 designed according to the current PCA curve, containing a range of air from 6% to 9.5%, could fail prematurely.

To illustrate the effects of air content, water-cement ratio, and aggregate type on thickness requirements, pavement designs were performed using the Iowa DOT Pavement Design Procedure [12] with fatigue curves from this study (Phase I and II) as well as the standard PCA 1933 and 1966 fatigue curves. The results are compared in terms of the required slab thickness. The same design traffic data and subgrade k values were used in all cases. The fatigue curves that were used are shown in Figures 42-46. The distribution of axle loads during the design life correspond to Design Example Number 2 of reference 40 (see Figure D-7 of Appendix D). Representative samples of the design calculations are presented in Figures D-8 - D-11 of Appendix D. The effects of air content, water-cement ratio, and aggregate type on the modulus of rupture were taken into account by using modulus of rupture values which could be expected from a given concrete mix based on the results of this study. The results of the thickness design calculations are presented in Table 7.

As may be seen in Table 7, designs utilizing the curves developed in this study, for the selected subgrade and traffic data, give results identical to those obtained by using the 1966 PCA curve in five of the 15 cases. In eight of the 15 cases, the PCA curve requires thicker pavement than designs based on the curves developed in this study, and in two cases the PCA curve underdesigns by 1/2 to 1 in.

It should be remembered that these comparisons are based on designs for one set of subgrade and traffic data. The differences could be more or less for different subgrade and traffic conditions.

Table 7. Comparison of pavement thickness design curves.

Design No.	Pavement Thickness Design Curve	Assumed Modulus of Rupture, psi	Pavement Thickness Required For Less Thank 125% Fatigue Life Consumption, in.	
			Proposed Curve	1966 PCA Curve
1	1933 PCA	600	10.0	9.5
2	Series 3.1-LH-32	750	7.5	8.0
3	Series 5.9-LH-32	650	9.5	9.0
4	Series 9.5-LH-32	550	11.5	10.5
5	Series 3.9-GH-43	800	7.5	8.0
6	Series 6.9-GH-43	700	8.5	8.5
7	Series 14.2-GH-43	500	10.5	11.0
8	Series 6.7-LH-43	500	11.0	11.0
9	Series 5.5-LB-43	650	9.0	9.0
10	Series 4.2-LH-60	600	9.0	9.5
11	Series 6.2-LH-60	550	10.5	10.5
12	Series 2.8-LH-41	850	6.5	7.5
13	Series 3.5-LH-41	800	7.5	8.0
14	Series 6.4-LH-41	550	10.0	10.5
15	Series 10.2-LH-41	500	10.5	11.0
16	Series 11.3-LH-41	500	11.0	11.0

Other general observations that can be made from this comparison are:

- For a given water-cement ratio, the pavement thickness required increases with increasing air content.
- For concretes of different water-cement ratios, the same coarse aggregate, and similar air contents, as the water-cement ratio increases, the required pavement thickness increases.
- Concretes made with gravel require less thickness of pavement than the concretes made with limestone at similar air contents and water-cement ratios.

It may be argued that some of the air contents and water-cement ratios used in this comparison are out of the range of normal design for concrete mixes. But this investigation shows that the air content and the water-cement ratio do affect the flexural fatigue strength of plain concrete, and these variables should be considered for optimum design of concrete pavements.

5. SUMMARY AND CONCLUSIONS

5.1. Summary

The rigid pavement design procedures currently in use consider only the modulus of rupture strength of concrete in determining the fatigue life of concrete highway pavements. The effects of entrained air, water-cement ratio, and aggregate type are not considered. The purpose of this study was to determine the effects of various air contents, various water-cement ratios, and different aggregate types on the flexural fatigue strength of plain concrete and to develop fatigue curves that incorporate these effects and could be used for design.

Fifteen series of concrete were investigated in this study. The variables consisted of air content, water-cement ratios, coarse aggregate types, and fine aggregate types. The fatigue specimens consisted of 6 in. × 6 in. × 36 in. beams and were subjected to flexural one-third point loading. The bottom fiber stress varied from essentially zero to a maximum stress corresponding to 60, 70, 80, or 90% of the modulus of rupture. As the bottom fibers were in constant tension, there was no reversal of stress. All concrete was mixed and placed in the laboratory to assure proper control of the mix. The fatigue specimens were cured in water until testing which took place at a specimen age of 28 to 56 days.

Thirteen series were tested using an Instron Model 1211 dynamic cycler, and two series were tested utilizing a MTS fatigue test machine. Both fatigue test machines were fitted with load fixtures which enabled loads to be applied at the same geometry as the modulus of rupture machine. Three hundred fifty-one fatigue tests were conducted. Results

of these tests (Phase II) are presented in graphic form in the text (Figure 9 through 18) and in tabular form in Appendix B.

The S-N diagrams show a reduction in fatigue life as the air content increases and as the water-cement ratio is decreased to 0.32. However, these curves may not be used for design, as they allow no factor of safety against failure. Curves that are suitable for design are presented in Figures 42 through 46. These figures present repetitions of stress with a constant probability of 0.05. The constant probability of 0.05 means that for 100 specimens tested at given stress level, only five would exhibit a fatigue life less than that indicated by the curve.

The fatigue curves developed in this study were used in pavement designs following the Iowa DOT Pavement Design Procedure and compared to designs using the PCA fatigue curve for a given subgrade and traffic. The PCA curve generally yields a more conservative design. However, in some instances the PCA curve produced inadequate thicknesses.

The main fatigue test program was supplemented by additional investigations. The compressive strength, modulus of rupture, modulus of elasticity, and unit weight were determined for each series. Plastic air content determinations were compared with hardened air contents determined by high pressure air meter methods. Scanning electron microscope photographs were taken at various magnifications and various air contents, water-cement ratios, and aggregate combinations to determine characteristics of the air void system. A mercury penetration porosimeter was used to characterize the void properties of the various concretes at the various air contents.

5.2. Conclusions

The following conclusions can be made as a result of the tests performed in this investigation:

1. The fatigue behavior of plain concrete in flexure is affected by the air content of the concrete. The fatigue strength decreases as the air content increases. Fatigue curves obtained from this study (Figures 42-46) provide a basis for improved rigid pavement design.
2. The fatigue behavior of plain concrete in flexure is affected by the water-cement ratio of the concrete. The fatigue strength is decreased for a low water-cement ratio (0.32). There did not seem to be a discernible difference in fatigue strength for concretes with a water-cement ratio in the range 0.40 to 0.60
3. The fatigue behavior of plain concrete in flexure is affected by the coarse aggregate type used in the concrete. At high stress levels, the concrete made with gravel exhibits a higher fatigue strength than that exhibited by the concrete made with limestone. At lower stress levels there does not seem to be a significant difference in fatigue strength.
4. The fatigue behavior of plain concrete in flexure may be affected by the fine aggregate type used in the concrete. There is a slight increase in fatigue strength when the higher quality fine aggregate is used, although it is difficult to determine whether this trend is significant with the limited data available from this study.

5. As the air content increases, the failure of concrete occurs increasingly at the aggregate-cement paste boundary. In other words, as air content rises, failure around the aggregate, as opposed to through the aggregate, predominates.
6. For similar air contents, the failure surface for gravel tends to be at the aggregate-cement paste interface. For limestone, the failure surface seems to pass through the coarse aggregate.
7. The modulus of elasticity, compressive strength, modulus of rupture, and unit weight generally decrease as the air content of the concrete increases.
8. The modulus of elasticity, compressive strength, modulus of rupture, and unit weight of concrete decrease as the water-cement ratio increases.
9. For similar air contents, concrete made with gravel has a higher modulus of elasticity, modulus of rupture, and unit weight than concrete made with limestone.
10. Studies of hardened concrete by SEM show that the introduction of an air-entraining agent increased the number of bubbles, the bubble density, and the uniformity of air bubbles. Air bubbles in air-entrained concrete consist of a uniform distribution of very small air voids, mostly between 0.02 and 0.10 mm (20 and 100 μm); and are usually spherical in shape.
11. Pore size distribution curves obtained by mercury porosimeter indicate that as the air content increases, there is an increase in total pore volume. This increase was mainly reflected in the volume of pores with diameter larger than 1 μm. The consistent

increase in pore volume between 1 and 10 μm with increasing air content suggests that it was the direct result of air entrainment.

12. The second intrusion method was used to characterize the effect of air-entrainment on the pore shapes of hardened mortars. There is evidence that air entrainment introduces only large ink-bottle pores and does not affect the pore volume and size distribution of small uniform and, presumably, capillary/gel pores.

6. RECOMMENDED FUTURE STUDIES

The present study has shown that air content, water-cement ratio, and aggregate type do affect the flexural fatigue strength of plain concrete. In view of these findings the following areas of flexural fatigue of concrete should be pursued:

- the effects of low and high water-cement ratio on concrete made with gravel
- the effects of varied water-cement ratio and air contents on concrete made with a high quality sand
- the effects of air content, water-cement ratio, and aggregate type on reinforced concrete
- the effects of axial loads on fatigue life
- the effects of surface treatments (high density surface, polymer, sulfur penetration, etc.) on concrete fatigue life

7. ACKNOWLEDGMENT

The study presented in this report was sponsored by the Highway Division of the Iowa Department of Transportation under Research Project HR-197. This study, under the same title, was also supported by and designated as Project 1324 of the Engineering Research Institute, Iowa State University.

The authors wish to extend sincere appreciation to the engineers of Iowa DOT for their support, cooperation, and counseling. A special thanks is extended to Messrs. Bernard Brown, Sam Moussali and LaVern Huckstadt for their assistance in running the high pressure air tests.

Appreciation is also extended to Dr. Herb T. David, Dr. Craig Van Nostrand, and Neil Werner, Statistics, for their assistance in the statistical analysis of the fatigue data.

Special thanks are accorded Cheryl R. Heyveld and James Julstrom, for their assistance in various phases of the project.

The following individuals also contributed, in various capacities, to this investigation: Tony Zelinskas, P. H. Chung and Fran Caulthard.

8. REFERENCES

1. AASHTO Interim Guide for Design of Pavement Structures, Washington, D.C.: American Association of State Highway and Transportation Officials, 1974.

2. Al-Rawi, R. S., and K. Al-Murshidi. "Effects of Maximum Size and Surface Texture of Aggregate in Accelerated Testing of Concrete." Cement and Concrete Research, 8 (1978) 201-210.

3. A Guide to the Structural Design of Pavements for New Roads, Road Research Laboratory, Road Note 29, 1970.

4. Antrim, J. C. and J. F. McLaughlin. "Fatigue Study of Air Entrained Concrete," American Concrete Institue Journal, Proceedings, Vol. 55, May 1959, pp. 1173-1182.

5. Ballinger, C. A. Effect of Load Variations on the Flexural Fatigue Strength of Plain Concrete. Washington, D.C.: Federal Highway Administration, September, 1972.

6. Bennett, E. W. "Fatigue in Concrete." Concrete (Chicago), May 1974, pp. 43-45.

7. Causes, Mechanism, and Control of Cracking in Concrete. Detroit, Michigan, American Concrete Institute, Publication SP-20, 1968.

8. Cebeci, O. Z. "Mercury Intrusion Porosimetry Theory and its Application to Air-entrained Cement Paste and Mortars." Ph.D. dissertation, Iowa State University, Ames, 1977.

9. Clemmer, H. F. "Fatigue of Concrete." Proceedings, American Society of Testing and Materials, Vol. 22, Part II, 1922, pp. 409-419.

10. Fordyce, P. and W. A. Yrjanson. "Modern Techniques for Thickness Design of Concrete Pavements." American Society of Civil Engineers Annual Meeting and National Meeting on Structural Engineering, 1968 (also available from Portland Cement Association).

11. Gregg, L. E. Experiments with Air Entrainment in Cement Concrete. Lexington, Kentucky, Kentucky Department of Highways, Bulletin No. 5, September 1947.

12. Guide for Primary and Interstate Road Pavement Design, Iowa Department of Transportation, 1976.

13. Hatt, W. K. "Fatigue of Concrete." Highway Research Board, Proceedings, Vol. 4, 1924, pp. 47-60.

14. Hawkings, N. M., A. N. Wyss and A. H. Mattock. "Fracture Analysis of Cracking in Concrete Beams." ASCE Journal of the Structural Division, May 1977, pp. 1015-1030.

15. Hilsdorf, H. K. and C. E. Kesler. "Fatigue Strength of Concrete Under Varying Flexural Stresses." American Concrete Institute Journal, Proceedings, Vol. 63, October 1966, pp. 1059-1075.

16. Hollen, G. W. and M. E. Prior. "Factors Influencing Proportioning of Air Entrained Concrete." American Concrete Institute, Publication SP-46, 1974.

17. Kaplan, M. F. "Flexural and Compressive Strength of Concrete as Affected by the Properties of Coarse Aggregates." American Concrete Institute Journal, Proceedings, Vol. 55, May 1959, pp. 1193-1208.

18. Kesler, C. E. "Effect of Speed of Testing on Flexural Fatigue Strength of Plain Concrete." Highway Research Board, Proceedings, Vol. 32, 1953, pp. 251-258.

19. Kesler, C. E. Significance of Tests and Properties of Concrete-Making Materials. American Society of Testing and Materials: Special Technical Publication 169A, 1966, pp. 144-159.

20. Kosteas, D. "Effect of the Number of Samples on the Statistical and Regression Analysis of Fatigue Tests." Aluminum, 50 (1974) 165-170.

21. Lee, D. Y., F. W. Klaiber, and J. W. Coleman. Fatigue Behavior of Air-entrained Concrete. Ames, Iowa: Engineering Research Institute, Iowa State University, July 1977.

22. Lerch, W. Basic Principals of Air Entrained Concrete. Portland Cement Association, 1953.

23. McCall, J. T. "Probability of Fatigue Failure of Plain Concrete." American Concrete Institute Journal, Proceedings, Vol. 55, August 1958, pp. 233-244.

24. Mielenz, R. C., V. E. Wolkodoff, J. E. Backstrom and H. L. Flack. "Origin, Evolution, and Effects of the Air Void System in Concrete. Part 1--Entrained Air in Unhardened Concrete." American Concrete Institute Journal, Proceedings, Vol. 55, July 1958, pp. 95-122.

25. Mielenz, R. C., V. E. Wolkodoff, J. E. Backstrom and H. L. Flack. "Origin, Evolution, and Effects of the Air Void System in Concrete. Part 2--Influence of Type and Amount of Air-Entraining Agent." American Concrete Institute Journal, Proceedings, Vol. 55, August 1958, pp. 261-283.

26. Mielenz, R. C., V. E. Wolkodoff, J. E. Backstrom and H. L. Flack. "Origin, Evolution, and Effects of the Air Void System in Concrete. Part 3--Influence of Water-Cement Ratio and Compaction." American Concrete Institute Journal, Proceedings, Vol. 55, September 1958, pp. 359-376.

27. Mielenz, R. C., V. E. Wolkodoff, J. E. Backstrom and H. L. Flack. "Origin, Evolution, and Effects of the Air Void System in Concrete. Part 4--The Air Void System in Job Concrete." American Concrete Institute Journal, Proceedings, Vol. 55. October 1958, pp. 507-518.

28. Mills, R. E., and R. F. Dawson. "Fatigue of Concrete." Highway Research Board, Proceedings, Vol. 7, 1927, pp. 160-172.

29. Miner, M. A. "Cumulative Damage in Fatigue." Transactions of the ASME, 67 (1945) A159-A164.

30. Mullen, W. G. and Waggoner, C. K., Determination of Air Void Content and Mixing Water Void Content of Hardened Concrete Using Electron Microscope Techniques. Final Report, Engineering Research Services Division, North Carolina State University, Raleigh, North Carolina, 1978.

31. Murdock, J. W., and C. E. Kesler. "Effect of Range of Stress on Fatigue Strength of Plain Concrete Beams." American Concrete Institute Journal, Proceedings, Vol. 55, August 1958, pp. 221-232.

32. Neville, A. M. Properties of Concrete. New York: John Wiley and Sons, Inc., 1973.

33. Nordby, G. M. "Fatigue of Concrete--A Review of Research." American Concrete Institute Journal, Proceedings, Vol. 55, August 1958, pp. 191-220.

34. Older, C. "Bates Experimental Road." State of Illinois, Department of Public Works and Buildings, Division of Highways, Bulletin No. 18, January 1922.

35. Older, C. "Highway Research in Illinois." American Society of Civil Engineers, Transactions, 87 (1924) 1180-1222.

36. Raithby, K. D. and J. W. Galloway, "Effects of Moisture Condition, Age, and Rate of Loading on Fatigue of Plain Concrete." American Concrete Institute, Publication SP-41, 1974, pp. 15-34.

37. Ray, G. K. "History and Development of Concrete Pavement Design." American Society of Civil Engineers, Journal of the Highway Division, 90 (1964) 79-98.

38. Shah, S. P. and S. Chandra. "Fracture of Concrete Subjected to Cyclic and Sustained Loading." American Concrete Institute Journal, Proceedings, Vol. 67, October 1970, pp. 816-825.

39. Standard Specifications for Highway and Bridge Construction. Ames, Iowa: Iowa Department of Transportation, 1977.

40. Thickness Design for Concrete Pavements. Portland Cement Association, 1966.

41. Troxell, G. E., H. F. Davis and J. W. Kelly. Composition and Properties of Concrete. New York: McGraw Hill Book Co., 1968.

42. Westergaard, H. M. "Computation of Stresses in Concrete Roads." Highway Research Board, Proceedings, Vol. 5, 1925, Pt. I, pp. 90-112.

43. Westergaard, H. M. "Stresses in Concrete Pavements Computed by Theoretical Analysis." Public Roads, 7 (April 1926) 25-35.

44. Wuerpel, C. E. Purposeful Entrainment of Air in Concrete. Wilmington, Delaware: Hercules Powder Company, 1970.

45. Yoshimoto, A., S. Ogino and M. Kawakami. "Microcracking Effect on Flexural Strength of Concrete after Repeated Loading." American Concrete Institute Journal, Proceedings, April 1972, pp. 233-240.

APPENDIX A

MATERIAL PROPERTIES AND PROPORTIONS

Table A-1. Gradation of fine aggregate.

Seive Size	% Passing Bellevue Sand	% Passing Hallett Sand	Iowa D.O.T. Specifications
3/8 in.	100	100	100
No. 4	97.0	99.0	90-100
No. 8	74.5	85.2	70-100
No. 16		65.0	
No. 30	42.5	40.2	
No. 50	6.5	8.2	
No. 100	0.5	0.4	
No. 200	0.1	0.1	0-1.5

Table A-2. Gradation of coarse aggregate.

Sieve Size	% Passing Limestone	% Passing Gravel	Iowa D.O.T. Specifications
1 1/2 in.	100	100	100
1 in.	98.0	91.0	95-100
3/4 in.	70.4	60.2	
1/2 in.	41.0	39.0	25-60
3/8 in.	15.1	19.1	
No. 4	5.0	1.0	0-10
No. 8	2.0	0.5	0-5
No. 200	1.0	0.2	0-1.5

Table A-3. Cement properties.

Property	Test Value	Specification*
Chemical data		
SiO_2	22.0	-
AlO_3	5.4	7.5 max
FeO_3	2.3	6.0 max
CaO	64.5	-
MgO	2.3	5.0 max
SO_3	3.0	3.5 max
Loss on ignition	1.0	3.0 max
Insoluable residue	0.4	0.75 max
Physical data		
Fineness		
Blaine - cm^2/gm	3700	2800 min
Soundness		
Autoclave, %	0.04	0.80 max
Time of set		
Vicat, Minutes: Initial	80	45 min
Final	190	480 max
Air content, %	10	12.0 max/min
Compressive strength, psi		
3-day	2900	1800 min
7-day	3990	2800 min

* ASTM C150 and Fed. SS-C-1960/3.

Table A-4. Laboratory batch quantities.

Series	W/C	Cement lb	Water[a] lb	Sand lb	Coarse Aggregate lb	Ad Aire ml	Water Reducer ml
3.1-LH-32	0.32	852	318	1507	1731	0	1260
5.9-LH-32	0.32	825	320	1427	1651	186	1220
9.5-LH-32	0.32	971	334	1382	1539	3800	1260
3.9-GH-43	0.43	640	309	1500	1870	0	0
6.2-GH-43	0.43	647	307	1479	1841	160	0
14.2-GH-43	0.43	578	270	1465	1805	3113	0
6.7-LH-43	0.43	638	314	1540	1773	200	0
5.5-LB-43	0.43	638	324	1485	1720	185	0
4.2-LH-60	0.60	440	305	1464	1694	0	0
6.2-LH-60	0.60	451	317	1575	1805	120	0

[a] Includes water required to bring aggregate to saturated surface dry condition.

APPENDIX B

FATIGUE TEST DATA

Table B-1. Fatigue test data for Series 3.1-LH-32.

Specimen	Modulus of rupture	Percent modulus of rupture	Fatigue life, number of load applications for failure
3.1-LH-32.5	745	90	639
3.1-LH-32.11	780	90	233
3.1-LH-32.29	795	90	1,040
3.1-LH-32.22	876	90	42
3.1-LH-32.25	780	90	953
3.1-LH-32.16	756	90	434
3.1-LH-32.4	766	80	11,045
3.1-LH-32.26	762	80	80,091
3.1-LH-32.12	835	80	401
3.1-LH-32.1	738	80	9,440
3.1-LH-32.23	823	80	3,740
3.1-LH-32.15	833	80	4,300
3.1-LH-32.2	728	70	1,208,300[a]
3.1-LH-32.10	784	70	34,520
3.1-LH-32.27	779	70	95,190
3.1-LH-32.21	790	70	830,880
3.1-LH-32.6	746	70	47,970
3.1-LH-32.14	788	70	48,440
3.1-LH-32.19	769	65	2,106,900[a]
3.1-LH-32.7	740	65	114,440
3.1-LH-32.24	798	65	2,102,920[a]
3.1-LH-32.17	838	65	11,920
3.1-LH-32.3	736	60	2,050,000[a]
3.1-LH-32.28	799	60	2,098,690[a]
3.1-LH-32.8	735	60	2,138,440[a]
3.1-LH-32.13	848	60	2,187,540[a]

[a]Specimen did not fail

Table B-2. Fatigue test data for Series 5.9-LH-32.

Specimen	Modulus of rupture	Percent modulus of rupture	Fatigue life, number of load applications for failure
5.9-LH-32.15	665	90	170
5.9-LH-32.7	620	90	640
5.9-LH-32.28	640	90	950
5.9-LH-32.10	690	90	540
5.9-LH-32.6	650	90	290
5.9-LH-32.20	680	90	610
5.9-LH-32.17	650	80	1,960
5.9-LH-32.12	610	80	1,640
5.9-LH-32.29	660	80	850
5.9-LH-32.4	620	80	2,060
5.9-LH-32.22	680	80	1,770
5.9-LH-32.26	715	80	2,150
5.9-LH-32.13	660	70	8,400
5.9-LH-32.8	640	70	2,890
5.9-LH-32.30	700	70	8,790
5.9-LH-32.11	700	70	6,800
5.9-LH-32.5	590	70	13,430
5.9-LH-32.23	690	70	15,690
5.9-LH-32.16	645	60	24,280
5.9-LH-32.14	655	60	19,500
5.9-LH-32.27	690	60	18,670
5.9-LH-32.24	680	60	79,880
5.9-LH-32.9	610	60	3,032,130[a]
5.9-LH-32.3	640	60	32,280

[a]Specimen did not fail

Table B-3. Fatigue test data for Series 9.5-LH-32.

Specimen	Modulus of rupture psi	Percent modulus of rupture	Fatigue life, number of load applications for failure
9.5-LH-32.21	542	90	540
9.5-LH-32.29	585	90	430
9.5-LH-32.6	470	90	1,530
9.5-LH-32.16	514	90	510
9.5-LH-32.7	542	90	230
9.5-LH-32.11	640	90	180
9.5-LH-32.24	529	80	1,250
9.5-LH-32.26	569	80	790
9.5-LH-32.2	578	80	660
9.5-LH-32.15	545	80	620
9.5-LH-32.18	540	80	950
9.5-LH-32.20	578	80	1,320
9.5-LH-32.23	539	70	3,440
9.5-LH-32.28	575	70	5,960
9.5-LH-32.19	555	70	4,330
9.5-LH-32.5	540	70	3,040
9.5-LH-32.25	585	70	3,990
9.5-LH-32.10	585	70	3,260
9.5-LH-32.22	554	60	15,450
9.5-LH-32.27	554	60	12,100
9.5-LH-32.4	553	60	10,170
9.5-LH-32.9	544	60	7,410
9.5-LH-32.13	600	60	8,510
9.5-LH-32.12	575	60	8,370

Table B-4. Fatigue test data for Series 3.9-GH-43.

Specimen	Modulus of rupture psi	Percent modulus of rupture	Fatigue life, number of load applications for failure
3.9-GH-43.25	845	90	4,210
3.9-GH-43.10	825	90	3,570
3.9-GH-43.15	825	90	1,870
3.9-GH-43.6	860	90	1,340
3.9-GH-43.24	860	90	3,240
3.9-GH-43.23	800	80	22,660
3.9-GH-43.16	885	80	12,710
3.9-GH-43.18	860	80	8,400
3.9-GH-43.5	790	80	7,240
3.9-GH-43.12	840	80	12,130
3.9-GH-43.14	860	70	51,180
3.9-GH-43.27	835	70	33,190
3.9-GH-43.22	853	70	65,170
3.9-GH-43.11	800	70	62,050
3.9-GH-43.8	810	70	127,490
3.9-GH-43.20	840	60	1,287,300
3.9-GH-43.26	890	60	257,570
3.9-GH-43.13	850	60	2,316,280[a]
3.9-GH-43.4	800	60	2,138,260[a]
3.9-GH-43.29	940	60	2,112,750[a]

[a]Specimen did not fail

Table B-5. Fatigue test data for Series 6.9-GH-43.

Specimen	Modulus of rupture psi	Percent modulus of rupture	Fatigue life, number of load applications for failure
6.9-GH-43.23	755	90	200
6.9-GH-43.25	715	90	940
6.9-GH-43.18	775	90	1,620
6.9-GH-43.29	760	90	280
6.9-GH-43.13	700	90	1,760
6.9-GH-43.4	759	90	300
6.9-GH-43.20	700	80	1,980
6.9-GH-43.22	730	80	2,490
6.9-GH-43.16	765	80	880
6.9-GH-43.28	702	80	5,190
6.9-GH-43.9	745	80	1,340
6.9-GH-43.3	720	80	1,250
6.9-GH-43.21	730	70	59,090
6.9-GH-43.17	728	70	23,100
6.9-GH-43.30	745	70	17,290
6.9-GH-43.26	728	70	55,000
6.9-GH-43.2	690	70	30,640
6.9-GH-43.7	745	70	4,880
6.9-GH-43.19	710	60	1,614,640[a]
6.9-GH-43.27	748	60	30,060
6.9-GH-43.1	700	60	144,830
6.9-GH-43.11	787	60	137,180
6.9-GH-43.15	710	60	1,123,220[a]

[a]Specimen did not fail

Table B-6. Fatigue test data for Series 14.2-GH-43.

Specimen	Modulus of rupture psi	Percent modulus of rupture	Fatigue life, number of load applications for failure
14.2-GH-43.21	415	90	910
14.2-GH-43.18	430	90	740
14.2-GH-43.14	436	90	350
14.2-GH-43.9	395	90	520
14.2-GH-43.28	400	90	2,170
14.2-GH-43.25	372	90	2,370
14.2-GH-43.23	440	80	1,950
14.2-GH-43.19	440	80	4,020
14.2-GH-43.13	440	80	22,030
14.2-GH-43.2	436	80	5,200
14.2-GH-43.16	446	80	16,370
14.2-GH-43.10	445	80	400
14.2-GH-43.24	430	70	6,670
14.2-GH-43.17	451	70	25,310
14.2-GH-43.29	400	70	19,280
14.2-GH-43.12	450	70	77,160
14.2-GH-43.7	460	70	16,920
14.2-GH-43.6	455	70	2,580
14.2-GH-43.1	450	65	946,530
14.2-GH-43.26	411	65	46,970
14.2-GH-43.20	450	60	2,507,790[a]
14.2-GH-43.30	427	60	3,065,610[a]
14.2-GH-43.15	445	60	2,039,420[a]
14.2-GH-43.11	426	60	2,702,980[a]

[a]Specimen did not fail

Table B-7. Fatigue test data for Series 6.7-LH-43.

Specimen	Modulus of rupture psi	Percent modulus of rupture	Fatigue life, number of load applications for failure
6.7-LH-43.1	520	90	440
6.7-LH-43.21	544	90	210
6.7-LH-43.27	505	90	680
6.7-LH-43.17	535	90	270
6.7-LH-43.23	490	90	1,350
6.7-LH-43.8	520	90	810
6.7-LH-43.2	529	80	2,830
6.7-LH-43.20	495	80	3,250
6.7-LH-43.28	534	80	1,810
6.7-LH-43.16	525	80	5,230
6.7-LH-43.9	543	80	4,000
6.7-LH-43.13	530	80	2,120
6.7-LH-43.24	515	70	7,640
6.7-LH-43.18	550	70	7,170
6.7-LH-43.22	529	70	5,700
6.7-LH-43.10	537	70	32,770
6.7-LH-43.14	490	70	24,830
6.7-LH-43.3	565	70	8,450
6.7-LH-43.11	505	60	2,122,260[a]
6.7-LH-43.25	530	60	105,160
6.7-LH-43.15	530	60	70,970
6.7-LH-43.4	518	60	2,031,950[a]
6.7-LH-43.7	570	60	23,810
6.7-LH-43.19	530	60	2,996,910[a]

[a]Specimen did not fail

Table B-8. Fatigue test data for Series 5.5-LB-43.

Specimen	Modulus of rupture psi	Percent modulus of rupture	Fatigue life, number of load applications for failure
5.5-LB-43.25	608	90	2,260
5.5-LB-43.29	680	90	480
5.5-LB-43.21	642	90	580
5.5-LB-43.18	657	90	2,620
5.5-LB-43.1	645	90	630
5.5-LB-43.9	707	90	300
5.5-LB-43.19	666	80	4,820
5.5-LB-43.26	654	80	1,190
5.5-LB-43.13	608	80	2,470
5.5-LB-43.10	671	80	1,640
5.5-LB-43.6	657	80	2,210
5.5-LB-43.16	688	80	5,900
5.5-LB-43.20	653	70	18,290
5.5-LB-43.30	633	70	40,820
5.5-LB-43.27	662	70	43,330
5.5-LB-43.8	655	70	28,400
5.5-LB-43.17	678	70	11,770
5.5-LB-43.2	668	70	76,500
5.5-LB-43.28	652	60	2,195,190[a]
5.5-LB-43.22	720	60	157,800
5.5-LB-43.14	673	60	107,530
5.5-LB-43.9	660	60	2,199,280[a]
5.5-LB-43.3	668	60	2,148,830[a]
5.5-LB-43.11	679	60	51,920
5.5-LB-43.5	710	60	107,930

[a]Specimen did not fail

Table B-9. Fatigue test data for Series 4.2-LH-60.

Specimen	Modulus of rupture psi	Percent modulus of rupture	Fatigue life, number of load applications for failure
4.2-LH-60.17	580	90	1,060
4.2-LH-60.21	635	90	210
4.2-LH-60.24	617	90	740
4.2-LH-60.27	595	90	1,010
4.2-LH-60.2	610	90	420
4.2-LH-60.9	675	90	420
4.2-LH-60.18	610	80	960
4.2-LH-60.22	600	80	1,960
4.2-LH-60.25	660	80	1,080
4.2-LH-60.29	635	80	1,940
4.2-LH-60.3	625	80	1,150
4.2-LH-60.8	630	80	4,320
4.2-LH-60.19	632	70	21,740
4.2-LH-60.23	578	70	366,830
4.2-LH-60.26	590	70	1,075,160
4.2-LH-60.1	683	70	26,380
4.2-LH-60.10	653	70	53,190
4.2-LH-60.15	625	70	117,120
4.2-LH-60.16	595	60	1,233,530[a]
4.2-LH-60.20	660	60	385,160
4.2-LH-60.28	614	60	2,034,460[a]
4.2-LH-60.4	652	60	935,460
4.2-LH-60.7	645	60	2,035,170[a]
4.2-LH-60.11	620	60	1,595,560

[a]Specimen did not fail

Table B-10. Fatigue test data for Series 6.2-LH-60.

Specimen	Modulus of rupture psi	Percent modulus of rupture	Fatigue life, number of load applications for failure
6.2-LH-60.23	605	90	212
6.2-LH-60.16	545	90	426
6.2-LH-60.26	590	90	128
6.2-LH-60.5	588	90	456
6.2-LH-60.7	547	90	1,975
6.2-LH-60.19	573	90	502
6.2-LH-60.20	547	80	13,300
6.2-LH-60.17	573	80	1,510
6.2-LH-60.25	579	80	1,261
6.2-LH-60.2	538	80	1,310
6.2-LH-60.14	520	80	3,930
6.2-LH-60.6	555	80	5,054
6.2-LH-60.22	550	70	12,430
6.2-LH-60.18	553	70	16,360
6.2-LH-60.24	580	70	18,250
6.2-LH-60.28	580	70	12,260
6.2-LH-60.1	580	70	2,930
6.2-LH-60.8	574	70	14,340
6.2-LH-60.21	585	60	2,013,440[a]
6.2-LH-60.27	560	60	2,103,800[a]
6.2-LH-60.15	540	60	1,565,880
6.2-LH-60.3	608	60	98,860
6.2-LH-60.12	580	60	100,080
6.2-LH-60.10	544	60	60,130
6.2-LH-60.13	591	60	78,330

[a]Specimen did not fail

APPENDIX C

REGRESSION ANALYSIS

APPENDIX C

One area of statistics deals with fitting a regression equation to a set of observations in which the experiment was stopped, or "censored," before all of the observations were made; all that is known is that the observations occur at a later time. For example, situations where the test is stopped before the observation is made occur in medical research where some small percentage of the test animals live beyond the end of the test; another example is fatigue research in which some specimens loaded at a low stress level do not fail.

When observations are made at one level and some of them are censored, a weighted average can be made and a value can be assigned to the set of data considering all observations. The theory has been available for some time, but implementing it into a computer program (CENSOR) is a recent development. The CENSOR program was developed by Dr. William Q. Meeker, Jr., Associate Professor of Statistics at Iowa State University.

This computer program generates a best-fit regression equation with given experimental data as input. To construct regression curves for fatigue data, selected S values are fed in as inputs, the corresponding N values are computed at probability values from 0.0001 to 0.9990.

The equations of the curves shown in Figures 9 to 28 in the text of this report are of the form:

$$\text{Log } (N) = b_o + b_1 \text{ Log } (S)$$

where:

N = number of cycles to failure

b_o = y-intercept of the curve

b_1 = slope of the curve

S = percent modulus of rupture (i.e., 90, 80, ...)

The slopes, (b_1), and y-intercepts, (b_o), of the curves are given in Table C-1. Series 9.5-LH-32 was the only series in which all of the specimens failed; thus a standard log-log regression program was utilized for this series. As is noted in the text, a change in the air content has the greatest effect on the fatigue life. Thus an equation was desired that would relate how the fatigue curves change for a change in air content. Studying the slope and intercept associated with each series (Table C-1) reveals that in each case the intercept is essentially twice the value of the slope. Plotting intercept versus slope illustrated a linear relationship with a high correlation coefficient (0.99). This means that it is sufficient to determine how the slopes vary with change in air content to establish the relationship between cycles to failure and percent modulus of rupture for various air contents.

The procedure for determining cycles to failure for various air content is as follows:

1) Determine slope at desired air content

Series: LH-32

$$b_1 = -31.390 + 2.670 \text{ (PA)}$$

Series: GH-43

$$b_1 = -12.386 - 0.520 \text{ (PA)}$$

Series: LH-41, LB-43 and LH-60

$$b_1 = -41.2865 + 6.7097 \text{ (PA)} - 0.4369 \text{ (PA)}^2$$

where

b_1 = slope

PA = percent air

2) Determine intercept

$$b_o = 3.1958 - 1.9207\ (b_1)$$

where:

b_o = intercept

3) Determine cycles to failure for desired percent modulus of rupture

$$\text{Log}\ (N) = b_o + b_1\ \text{Log}\ (S)$$

where

N = cycles to failure

S = percent modulus of rupture

It should be noted that the above procedure has some error involved. When working with a log scale, a small error in the log value could result in a large error in the arithmetic value. The above procedure should thus be used with caution. If the cycles to failure are desired for an air content corresponding to an air content and other variables in this study, the equations for those curves should thus be used.

Table C-1. Constants for fatigue equations.

Series	Y-Intercept b_o	Slope b_1	Figure in which Curve is Found
3.1-LH-32	51.3979	-25.0149	9
5.9-LH-32	26.6026	-12.2697	10
9.5-LH-32	17.41	- 7.50	11
3.9-GH-43	31.7264	-14.5085	12
6.9-GH-43	33.5961	-15.8388	13
14.2-GH-43	41.3908	-19.8146	14
6.7-LH-43	34.5333	-16.3365	15
5.5-LB-43	34.1682	-16.0656	16
4.2-LH-60	44.0902	-21.2681	17
6.2-LH--60	34.3319	-16.2566	18
2.8-LH-41	56.5602	-27.7888	23
3.5-LH-41	42.9253	-20.7286	24
6.4-LH-41	33.3699	-15.6204	25
10.2-LH-41	42.0183	-20.3599	26
11.3-LH-41	40.7450	-19.7827	27

APPENDIX D

PAVEMENT DESIGN

Table D-1. Percent modulus of rupture and allowable load repetitions for Series LH-32.

Percent Modulus of Rupture	Allowable Repetitions		
	Percent Air		
	3.1	5.9	9.5
60	434410	11074	3180
61	287740	9049	2828
62	191161	7405	2520
63	128469	6093	2248
64	86338	5014	2008
65	58668	4148	1796
66	40133	3443	1609
67	27441	2858	1442
68	18980	2385	1295
69	13204	1996	1164
70	9185	1671	1047
71	6427	1402	944
72	4549	1184	851
73	3220	999	768
74	2292	846	694
75	1636	717	628
76	1175	609	569
77	846	519	516
78	613	443	468
79	446	379	425
80	325	325	386
81	238	279	351
82	176	240	320
83	129	206	292
84	96	178	266
85	71	154	243
86	53	134	222
87	40	116	203
88	30	101	186
89	23	88	170
90	17	77	156

Table D-2. Percent modulus of rupture and allowable load repetitions for Series GH-43.

Percent Modulus of Rupture	Allowable Repetitions		
	Percent Air		
	3.9	6.9	14.2
60	160509	45061	119784
61	126386	34714	86437
62	99701	26798	62517
63	79177	20835	45635
64	62878	16199	33312
65	50246	12682	24524
66	40318	9972	18155
67	32344	7840	13434
68	26116	6207	10032
69	21159	4934	7527
70	17144	3921	5647
71	13938	3128	4255
72	11405	2512	3236
73	9335	2019	2461
74	7663	1628	1880
75	6301	1315	1439
76	5202	1066	1108
77	4300	866	854
78	3566	706	661
79	2968	578	515
80	2471	473	401
81	2062	388	313
82	1727	320	246
83	1447	264	193
84	1216	218	152
85	1025	181	121
86	865	150	96
87	732	125	76
88	619	104	61
89	526	87	48
90	447	73	39

Table D-3. Percent modulus of rupture and allowable load repetitions for Series 6.7-LH-43.

Percent Modulus of Rupture	Allowable Repetitions		
	Percent Air		
	6.7		
60	35818		
61	27365		
62	20956		
63	16162		
64	12468		
65	9687		
66	7560		
67	5898		
68	4637		
69	3658		
70	2886		
71	2286		
72	1824		
73	1455		
74	1166		
75	935		
76	754		
77	608		
78	493		
79	401		
80	326		
81	266		
82	218		
83	178		
84	147		
85	121		
86	100		
87	83		
88	69		
89	57		
90	48		

Table D-4. Percent modulus of rupture and allowable load repetitions for Series 5.5-LB-43.

Percent Modulus of Rupture	Allowable Repetitions		
	Percent Air		
	5.5		
60	59498		
61	45667		
62	35124		
63	27208		
64	21081		
65	16448		
66	12888		
67	10097		
68	7969		
69	6311		
70	4999		
71	3975		
72	3183		
73	2550		
74	2050		
75	1650		
76	1335		
77	1081		
78	879		
79	717		
80	585		
81	479		
82	394		
83	324		
84	267		
85	221		
86	183		
87	152		
88	126		
89	106		
90	88		

Table D-5. Percent modulus of rupture and allowable load repetitions for Series LH-60.

Percent Modulus of Rupture	Allowable Repetitions		
	Percent Air		
	4.2	6.2	
60	301856	36906	
61	212716	28242	
62	150245	21647	
63	107152	16722	
64	76436	12915	
65	55030	10046	
66	39847	7851	
67	28840	6132	
68	21081	4826	
69	15485	3812	
70	11374	3011	
71	8397	2387	
72	6259	1907	
73	4666	1524	
74	3495	1222	
75	2622	981	
76	1980	791	
77	1498	639	
78	1138	518	
79	870	422	
80	665	344	
81	510	281	
82	393	230	
83	303	189	
84	235	155	
85	183	128	
86	143	106	
87	112	88	
88	87	73	
89	69	61	
90	54	51	

Table D-6. Percent modulus of rupture and allowable load repetitions for Series LH-41.

Percent Modulus of Rupture	Allowable Repetitions				
	Percent Air				
	2.8	3.5	6.4	10.2	11.3
60	1330148	197742	65872	78145	45206
61	841783	140572	50933	55886	32644
62	534564	100161	39455	40059	23621
63	343795	72061	30782	28987	17250
64	221055	51832	24016	20980	12598
65	143913	37627	18867	15314	9281
66	94406	27473	14887	11246	6874
67	61901	20049	11741	8253	5089
68	41106	14774	9326	6114	3802
69	27466	10937	7435	4550	2854
70	18357	8097	5928	3387	2141
71	12345	6023	4744	2532	1615
72	8410	4523	3822	1912	1229
73	5731	3396	3080	1443	935
74	3928	2563	2491	1094	714
75	2700	1938	2018	831	547
76	1871	1473	1642	635	421
77	1299	1122	1337	486	325
78	908	859	1093	374	252
79	639	661	897	289	196
80	449	508	736	223	153
81	318	393	606	173	119
82	227	305	501	135	94
83	161	237	414	105	74
84	116	185	343	83	58
85	83	145	286	65	46
86	60	114	238	51	36
87	44	89	199	41	29
88	32	70	166	32	23
89	23	56	139	25	19
90	17	44	117	20	15

Table D-7. Axles during design life - standard PCA design method [40]

Axle Load Groups, Kips		Axle Loads in Design Life
SINGLE		
28-30		3,700
26-28		3,700
24-26		7,410
22-24		195,000
20-22		764,400
18-20		2,139,150
16-18		2,870,400
TANDEM		
52-54		3,700
50-52		3,700
48-50		36,270
46-48		36,270
44-46		57,530
42-44		179,790
40-42		204,750
38-40		296,400
36-38		319,800
34-36		487,500
32-34		610,350
30-32		1,078,350
	Total Trucks	19,500,000

Table D-8. Design example - Series LH-32.

CALCULATION OF CONCRETE PAVEMENT THICKNESS
(Use with Case I Single & Tandem Axle Design Charts)

Project Design Example - Series LH-32
Type _____ **No. of Lanes** _____
Subgrade k 100 **pci., Subbase** _____
Combined k 130 **pci., Load Safety Factor** 1.2 **(L.S.F.)**

PROCEDURE

1. Fill in Col. 1, 2 and 6, listing axle loads in decreasing order.
2. Assume 1st trial depth. Use 1/2-in. increments.
3. Analyze 1st trial depth by completing columns 3, 4, 5 and 7.
4. Analyze other trial depths, varying M.R.*, slab depth and subbase type.**

1	2	3	4	5	6	7
Axle Loads kips	Axle Loads X L.S.F. kips	Stress psi	Stress Ratios	Allowable Repetitions No.	Expected Repetitions No.	Fatigue Resistance Used*** percent

Trial depth 7.0 **in.** **M.R.*** 750 **psi** **k** 130 **pci**

SINGLE AXLES

30	36.0	480	0.64	86,000	3,700	4.3
28	33.6	460	0.61	290,000	3,700	1.3
26	31.2	435	0.58	1,000,000[a]	7,410	0.7
24	28.8	410	0.55	3,800,000[a]	195,000	5.1
22	26.4	380	0.51	28,000,000[a]	764,400	2.7
20	24.0	350	0.47	Unlimited		

TANDEM AXLES

54	64.8	530	0.71	6,400	3,700	57.8
52	62.4	515	0.69	13,000	3,700	28.5
50	60.0	500	0.67	27,000	36,270	134.3
48	57.6	480	0.64	86,000	36,270	42.2
46	55.2	465	0.62	190,000	57,530	30.3
44	52.8	450	0.60	430,000	179,790	41.8
42	50.4	430	0.57	1,600,000[a]	204,750	12.8
40	48.0	410	0.55	3,800,000[a]	296,400	7.8
38	45.6	395	0.53	11,000,000[a]	319,800	2.9
36	43.2	375	0.50	Unlimited		

Total = 372.5%

* M.R. Modulus of Rupture for 3rd pt. loading.

** Cement-treated subbases result in greatly increased combined k values.

*** Total fatigue resistance used should not exceed about 125 percent.

[a] Extrapolated value.

Table D-9. Design example - Series LH-32.

CALCULATION OF CONCRETE PAVEMENT THICKNESS
(Use with Case I Single & Tandem Axle Design Charts)

Project Design Example - Series LH-32
Type _____ **No. of Lanes** _____
Subgrade k 100 **pci., Subbase** _____
Combined k 130 **pci., Load Safety Factor** 1.2 **(L.S.F.)**

PROCEDURE

1. *Fill in Col. 1, 2 and 6, listing axle loads in decreasing order.*
2. Assume 1st trial depth. Use 1/2-in. increments.
3. Analyze 1st trial depth by completing columns 3, 4, 5 and 7.
4. Analyze other trial depths, varying M.R.*, slab depth and subbase type.**

1	2	3	4	5	6	7
Axle Loads kips	Axle Loads X L.S.F. kips	Stress psi	Stress Ratios	Allowable Repetitions No.	Expected Repetitions No.	Fatigue Resistance Used*** percent
Trial depth 7.5 in. **M.R.*** 750 psi **k** 130 pci						
SINGLE AXLES						
30	36.0	440	0.59	640,000[a]	3,700	0.6
28	33.6	420	0.56	2,400,000[a]	3,700	0.2
26	31.2	395	0.53	11,000,000[a]	7,410	0.1
24	28.8	370	0.49	Unlimited		
TANDEM AXLES						
54	64.8	485	0.65	59,000	3,700	6.3
52	62.4	475	0.63	130,000	3,700	2.8
50	60.0	460	0.61	290,000	36,270	12.5
48	57.6	440	0.59	640,000[a]	36,270	5.7
46	55.2	430	0.57	1,600,000[a]	57,530	3.6
44	52.8	410	0.55	3,800,000[a]	179,790	4.7
42	50.4	395	0.53	11,000,000[a]	204,750	1.9
40	48.0	375	0.50	Unlimited		

Total 38.4%

* M.R. Modulus of Rupture for 3rd pt. loading.

** Cement-treated subbases result in greatly increased combined k values.

*** Total fatigue resistance used should not exceed about 125 percent.

[a] Extrapolated value.

Table D-10. Design example - 1966 PCA design curve.

CALCULATION OF CONCRETE PAVEMENT THICKNESS
(Use with Case I Single & Tandem Axle Design Charts)

Project Design Example - PCA Design Curve
Type _____ **No. of Lanes** _____
Subgrade k 100 **pci., Subbase** _____
Combined k 130 **pci., Load Safety Factor** 1.2 **(L.S.F.)**

PROCEDURE

1. Fill in Col. 1, 2 and 6, listing axle loads in decreasing order.
2. Assume 1st trial depth. Use 1/2-in. increments.
3. Analyze 1st trial depth by completing columns 3, 4, 5 and 7.
4. Analyze other trial depths, varying M.R*, slab depth and subbase type.**

1	2	3	4	5	6	7
Axle Loads kips	Axle Loads X L.S.F. kips	Stress psi	Stress Ratios	Allowable Repetitions No.	Expected Repetitions No.	Fatigue Resistance Used*** percent

Trial depth 7.5 **in.** **M.R.*** 750 **psi** **k** 130 **pci**

SINGLE AXLES

30	36.0	440	0.59	42,000	3,700	8.8
28	33.6	420	0.56	100,000	3,700	3.7
26	31.2	395	0.53	240,000	7,410	3.1
24	28.8	370	0.49	Unlimited		

TANDEM AXLES

54	64.8	485	0.65	8,000	3,700	46.3
52	62.4	475	0.63	14,000	3,700	26.4
50	60.0	460	0.61	24,000	36,270	151.1
48	57.6	440	0.59	42,000	36,270	86.4
46	55.2	430	0.57	75,000	57,530	76.7
44	52.8	410	0.55	130,000	179,790	138.3
42	50.4	395	0.53	240,000	204,750	85.3
40	48.0	375	0.50	Unlimited		

Total = 626.1%

* M.R. Modulus of Rupture for 3rd pt. loading.

** Cement-treated subbases result in greatly increased combined k values.

*** Total fatigue resistance used should not exceed about 125 percent.

Table D-11. Design example - 1966 PCA design curve.

CALCULATION OF CONCRETE PAVEMENT THICKNESS
(Use with Case I Single & Tandem Axle Design Charts)

Project Design Example - PCA Design Curve
Type _____ **No. of Lanes** _____
Subgrade k 100 **pci., Subbase** _____
Combined k 130 **pci., Load Safety Factor** 1.2 **(L.S.F.)**

PROCEDURE

1. Fill in Col. 1, 2 and 6, listing axle loads in decreasing order.
2. Assume 1st trial depth. Use 1/2-in. increments.
3. Analyze 1st trial depth by completing columns 3, 4, 5 and 7.
4. Analyze other trial depths, varying M.R.*, slab depth and subbase type.**

1	2	3	4	5	6	7
Axle Loads kips	Axle Loads X L.S.F. kips	Stress psi	Stress Ratios	Allowable Repetitions No.	Expected Repetitions No.	Fatigue Resistance Used*** percent

Trial depth 8.0 **in. M.R.*** 750 **psi k** 130 **pci**

SINGLE AXLES

30	36.0	400	0.53	240,000	3,700	1.5
28	33.6	385	0.51	400,000	3,700	0.9
26	31.2	365	0.49	Unlimited		

TANDEM AXLES

54	64.8	445	0.59	42,000	3,700	8.8
52	62.4	435	0.58	57,000	3,700	6.5
50	60.0	420	0.56	100,000	36,270	36.3
48	57.6	405	0.54	180,000	36,270	20.2
46	55.2	390	0.52	300,000	57,530	19.2
44	52.8	375	0.50	Unlimited		

Total = 93.4%

* M.R. Modulus of Rupture for 3rd pt. loading.

** Cement-treated subbases result in greatly increased combined k values.

*** Total fatigue resistance used should not exceed about 125 percent.